MODEL CALIBRATION, DRAINAGE VOLUME CALCULATION AND OPTIMIZATION IN HETEROGENEOUS FRACTURED RESERVOIRS

A Dissertation

by

SUKSANG KANG

Submitted to the Office of Graduate Studies of
Texas A&M University
in partial fulfillment of the requirements for the degree of

DOCTOR OF PHILOSOPHY

Approved by :

Chair of Committee	Akhil Datta-Gupta
Committee Members	John Lee
	Michael King
	Yalchin Efendiev
Head of Department	Dan Hill

December 2012

Major Subject: Petroleum Engineering

ABSTRACT

We propose a rigorous approach for well drainage volume calculations in gas reservoirs based on the flux field derived from dual porosity finite-difference simulation and demonstrate its application to optimize well placement. Our approach relies on a high frequency asymptotic solution of the diffusivity equation and emulates the propagation of a 'pressure front' in the reservoir along gas streamlines. The proposed approach is a generalization of the radius of drainage concept in well test analysis (Lee 1982), which allows us not only to compute rigorously the well drainage volumes as a function of time but also to examine the potential impact of infill wells on the drainage volumes of existing producers. Using these results, we present a systematic approach to optimize well placement to maximize the Estimated Ultimate Recovery.

A history matching algorithm is proposed that sequentially calibrates reservoir parameters from the global-to-local scale considering parameter uncertainty and the resolution of the data. Parameter updates are constrained to the prior geologic heterogeneity and performed parsimoniously to the smallest spatial scales at which they can be resolved by the available data. In the first step of the workflow, Genetic Algorithm is used to assess the uncertainty in global parameters that influence field-scale flow behavior, specifically reservoir energy. To identify the reservoir volume over which each regional multiplier is applied, we have developed a novel approach to heterogeneity segmentation from spectral clustering theory. The proposed clustering can capture main feature of prior model by using second eigenvector of graph affinity matrix.

In the second stage of the workflow, we parameterize the high-resolution heterogeneity in the spectral domain using the Grid Connectivity based Transform to severely compress the dimension of the calibration parameter set. The GCT implicitly imposes geological continuity and promotes minimal changes to each prior model in the ensemble during the calibration process. The field scale utility of the workflow is then demonstrated with the calibration of a model characterizing a structurally complex and highly fractured reservoir.

DEDICATION

This work is dedicated to my wife, JuYoun Han, who has been the support and motivation during the good and difficult times during my four years of Ph.D. degree period in Texas A&M University. This dissertation is not just my work. We made it together.

ACKNOWLEDGEMENTS

I would like to thank my committee chair, Dr. Akhil Datta-Gupta for all his support during my Ph.D. studies. His guidance and insightful view have been the foundation of my work. He also has provided economic support and an industry perspective through the joint industry project. Also, I want to thank all my committee members, Dr. John Lee, Dr. Michael King and Dr. Efendiev. Your comments and questions have been invaluable to look at the problem from multiple perspectives.

Thanks, also, go to my friends, colleagues and the department faculty and staff for making my time at Texas A&M University a great experience. Especially, I want to acknowledge Eric, Jiang, HanYoung and JongUk for all the valuable discussions through the different stages of my research. I want to extend my gratitude to Hopcus, Phaedra who has supported and helped MCERI students.

I would like to thank my friends: Alvaro, Satyajit, Baljit, Yanbin, Shingo, Zheng, Shusei, JeongMin, Jichao Yin, Jichao Han, DongJae, Song, ChangDong, Neha, Qing, Yip, Mohan, JungTek and all the senior students of the MCERI research group.

I also want to express my gratitude to industry coworkers; JangHak (KNOC), Xian-Huan, Zhiming, Wen (All Chevron), Andrew, Mahmut, Joaquin and Najib (All Schlumberger) for providing us good field data and constructive discussion during project and two summer internships.

Finally, thanks to my parents and parent-in-laws for their encouragement and support and to my beloved daughter, EunJae and little boy, KyungHo. You have given me all your patience and love.

TABLE OF CONTENTS

Page

Page

Page

Page

LIST OF FIGURES

Page

Page

Page

Page

LIST OF TABLES

Page

CHAPTER I
INTRODUCTION AND OBJECTIVES

Current practice of well placement in tight gas reservoirs generally involves the use of empirical correlations based on reservoir properties and analysis of past production histories and/or pressure maps from flow simulation. No rigorous procedure is available to compute well drainage volumes in the presence of permeability heterogeneity controlled by the distribution and orientation of natural fractures. The situation is complicated by the routine use of horizontal and complex wells in unconventional gas reservoirs and the presence of multistage hydraulic fractures. The computation of drainage volume will be critical to our understanding of the interaction between existing wells, potential infill locations and the estimated ultimate recovery (EUR) computations for infill wells.

We propose a rigorous approach for well drainage volume calculations in gas reservoirs based on the flux field derived from dual porosity finite-difference simulation and demonstrate its application to optimize well placement and hydraulic fracture stages. Our approach relies on a high frequency asymptotic solution of the diffusivity equation and emulates the propagation of a 'pressure front' in the reservoir along gas streamlines. The proposed approach is a generalization of the radius of drainage concept in well test analysis (Lee 1982). The method allows us not only to compute rigorously the well drainage volumes as a function of time but also examine the potential impact of infill wells on the drainage volumes of existing producers. Using these results, we present a systematic approach to optimize well placement to maximize the EUR.

We utilize the streamline-based drainage volumes to identify depleted sands and generate a reservoir 'depletion capacity' map to optimize infill well placement based on the undepleted and undrained regions. The field application clearly demonstrates a systematic approach to optimal well placement in tight gas reservoirs. Once we get the accurate drainage volume information, it's applicable to wide range of optimization target. We verified to the infill well placement and hydraulic fracture stage optimization.

This concept can easily be extended to optimal well spacing or completion. This drainage volume calculation with streamline provides general but a powerful tool even under high complex and changing well conditions.

To reduce geological uncertainty and reliable optimization plan, characterization of reservoir is imperative before forecasting in closed-loop management workflows. We propose a hierarchical history matching algorithm that is constrained to the prior geologic heterogeneity and parsimoniously updates high-resolution geologic parameters to the level that can be resolved by the available data. The hierarchical approach calibrates, in sequence, reservoir parameters characterizing global to local regions to account for the uncertainty in spatial scale of the parameters and the resolution of the data. First, a probabilistic genetic algorithm (GA) is used to assess the uncertainty in global parameters (regional permeability, pore volumes and transmissibility) that influence field-scale flow behavior, specifically reservoir energy. Results from this analysis are used to establish multiple prior models for the second stage of local or high-resolution parameter calibration to well-level observation data. Next, a novel re-parameterization method is used to considerably reduce the number of parameters for their calibration in a low-dimensional transform domain using a grid-connectivity-based transform (GCT) basis. The reduced model parameters implicitly impose geological continuity and promote minimal changes to each prior model during calibration.

To get a more rigorous history matching in global scale, we develop a novel zonation algorithm from spectral clustering scheme. The novel Spectral clustering can capture main feature of prior model by using 2^{nd} eigenvector of graph affinity Laplacian. The zoning approach from spectral clustering theory enhance speeding up global scale model calibration, which is common in hierarchical approach and standard industry practice, and then move to local fine scale calibration. At the same time, we can keep prior model's key information; facies edge, faults and channels. The proposed spectral clustering has a clear cutting edge detection power in smoothly varying high and low value regions. Hence, the proposed spectral clustering provides the optimal zonation criteria for complex reservoir history matching problems.

The suggested systematic history matching, drainage volume calculation and optimization procedures can be applied as a fast and rigorous closed-loop reservoir management process, especially in highly fractured and complex geometry systems.

1.1 Overview of Reservoir Characterization and Closed Loop Management

The closed loop reservoir management, also referred to as "smart reservoir management", is a sequential process of data assimilation and optimization (Chen and Oliver 2010; Gildin and Lopez 2011).

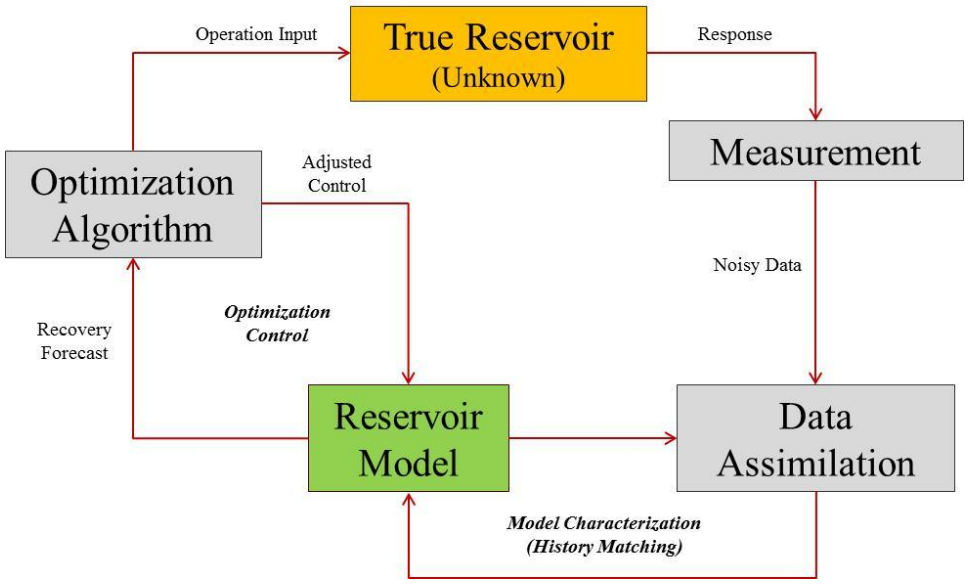

Figure 1.1. Closed Loop Reservoir Management and Control

The purpose of closed loop control in **Fig. 1.1** is to maximize the reservoir performance such as oil/gas recovery or a given financial measure. There have been many previous studies for reservoir optimization and history matching. However, the problem in the fractured reservoir management is quite difficult because of complicated flow mechanism and difficulty in both history matching and optimization compared to a non-fractured model. Hence, understanding this complex flow mechanism is a first step in closed-loop reservoir management strategy.

1.2 Fractured Reservoirs

In the low permeable porous medium, naturally generated fractures are the primary route for the fluid movement and significantly affect the real production and injection efficiency in a field. The proper modeling of naturally existing fractures and/or artificially developed hydraulic fractures is important factor in successful simulation of low permeable tight and shale gas reservoir models as well as for conventional system. Planning a field development strategy, especially in unconventional gas reservoirs, comes from estimating reservoir size and drainage capacity of current wells with proper simulation models. But in practice, the existing and induced fractures make problems more complex in production optimization and drainage volume calculation.

In the naturally fractured reservoir models, fluids exist in two systems. The rock matrix provides the storage of fluids and the fracture network provides main route for flow. If the fractures (or equivalent matrixes) are only considered to provide the main path as well as storage for gas, this system can be regarded as a single porosity single permeability system (SPSP; **Fig. 1.2 (a)**). Otherwise, the fluid flows in the reservoir through the fractures while the matrix is only connected to the fracture network. This can be regarded as a dual porosity and single permeability (DPSP; **Fig. 1.2 (b)**). Additionally, if we consider flow between matrixes as well as fractures, this system will be regarded as dual porosity and dual permeability system (DPDP; **Fig. 1.2 (c)**). The DPDP approach is the most general approach to simulate fractured reservoirs and it is reduced to the DPSP if flow between the matrix is negligible (Al-Huthali and Datta-Gupta 2004).

(a) Single Porosity Single Permeability (SPSP)

Figure 1.2. Schematics of the Different Fracture-Matrix Models

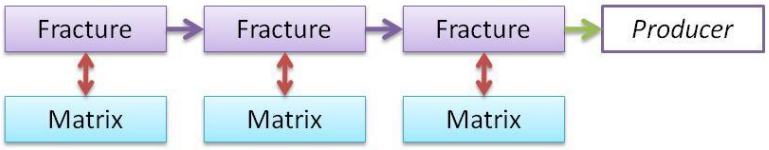

(b) Dual Porosity Single Permeability (DPSP)

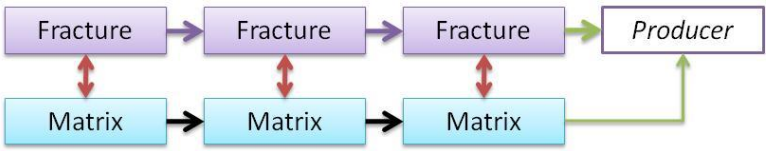

(c) Dual Porosity Dual Permeability (DPDP)

Figure 1.2. Continued

Today, many researches are focusing on optimization or history matching under SPSP models. There have been no rigorous works on drainage volume calculation under the condition of natural fractures and DPSP system. As a result, petroleum engineers mainly depend on production decline curve and/or simulated pressure distribution for estimating drainage volume and planning new infill well locations in tight gas and naturally fractured reservoirs.

In this research, we propose a closed loop management algorithm in highly fractured reservoirs; drainage volume calculation, model characterization and optimization. First in **Chapter 2**, we propose a rigorous drainage volume calculation methodology under highly fractured condition. We compute the pressure front propagation along the main flow paths (streamline trajectories) by defining a diffusive time of flight. This leads to a fast and accurate drainage volume calculation method, which allows us to identify undrained areas where we can find potential new infill well locations. We expanded this drainage volume calculation to horizontal wells, which are common in unconventional reservoirs. The calculated drainage volume in different fractured completions can provide the optimal number of fracture stages. In **Chapters 3** and **4**, we propose a new zonation algorithm and a hierarchical history matching application. The spectral clustering theory has been applied to many engineering fields for similarity grouping.

The application to reservoir zonation provides promising cutting criteria for continuous and/or fault-embedded simulation models. The systematic hierarchical approach simplifies complex history matching problems and provides guidelines in fractured reservoir model characterization.

CHAPTER II

DRAINAGE VOLUME CALCULATION, WELL PLACEMENT AND HYDRAULIC FRACTURE STAGE OPTIMIZATION: STREAMLINE APPLICATIONS TO UNCONVENTIONAL RESERVOIRS[**]

2.1 Purpose

Current practice of well placement in tight gas reservoirs generally involves the use of empirical correlations based on reservoir properties and analysis of past production histories and/or pressure maps from flow simulation. No rigorous procedure is available to compute well drainage volumes in the presence of permeability heterogeneity controlled by the distribution and orientation of natural fractures. The situation is complicated by the routine use of horizontal and complex wells in tight gas reservoirs and the presence of multistage hydraulic fractures. The computation of drainage volume will be critical to our understanding of the interaction between existing wells, potential infill locations and the estimated ultimate recovery (EUR) computations for infill wells.

We propose a rigorous approach for well drainage volume calculations in tight gas reservoirs based on the flux field derived from dual porosity finite-difference simulation and demonstrate its application to optimize well placement. Our approach relies on a high frequency asymptotic solution of the diffusivity equation and emulates the propagation of a 'pressure front' in the reservoir along gas streamlines. The proposed

---

[*] Part of this chapter is reprinted with permission from "Impact of Natural Fractures in Drainage Volume Calculations and Optimal Well Placement in Tight Gas Reservoirs" by SukSang Kang, Akhil Datta-Gupta and W. John Lee, 2011. Paper SPE 144338-MS presented at the 2011 SPE North American Unconventional Gas Conference and Exhibition, The Woodlands, Texas, 14-16 June. Copyright 2011. by the Society of Petroleum Engineers.

[*] Part of this chapter is reprinted with permission from "Optimizing Fracture Stages and Completions in Horizontal Wells in Tight Gas Reservoirs Using Drainage Volume Calculations" by Baljit S Sehbi, SukSang Kang, Akhil Datta-Gupta and W. John Lee, 2011. Paper SPE 144365-MS presented at the 2011 SPE North American Unconventional Gas Conference and Exhibition, The Woodlands, Texas, 14-16 June. Copyright 2011. by the Society of Petroleum Engineers.

approach is a generalization of the radius of drainage concept in well test analysis (Lee 1982). The method allows us not only to compute rigorously the well drainage volumes as a function of time but also examine the potential impact of infill wells on the drainage volumes of existing producers. Using these results, we present a systematic approach to optimize well placement to maximize the EUR.

We demonstrate the power and utility of our method using both synthetic and field applications. The synthetic example is used to validate our approach by establishing consistency between the drainage volume calculations from streamlines and the EUR computations based on detailed finite-difference simulations. We also present comparison of our approach with analytic drainage volume calculations for simplified cases. The field example is from one of the tight gas fields in the Rocky Mountain region. We utilize the streamline-based drainage volumes to identify depleted sands and generate a reservoir 'depletion capacity' map to optimize infill well placement based on the undepleted and undrained regions. The field application clearly demonstrates a systematic approach to optimal well placement in tight gas reservoirs.

Horizontal well technology is now considered a standard completion practice in unconventional gas reservoirs. With significant improvements in the drilling and completion technology, many tight gas and shale gas prospects have become economically viable. Optimizing location, distribution and the number of stages of hydraulic fractures is an important issue in tight gas reservoir completions, particularly for horizontal and complex wells.

A field example is shown to demonstrate the application of our approach by optimizing well completions in a horizontal well recently drilled in the Cotton Valley formation. We first apply the proposed drainage volume calculations in an existing vertical well to identify its 'region of influence' and the potential interference from the proposed horizontal well and the number of fracture stages in the horizontal well. The combined drainage volumes from the vertical and horizontal well are calculated as a function of the number of fracture stages to determine the point of diminishing return and to optimize the number of fracture stages. The results are found to be consistent with

independent analysis based on rate profiles from numerical simulation and NPV calculations.

2.2 Introduction

In low permeability gas reservoirs, natural fractures are often the primary conduit for flow in the reservoir and can significantly impact the well performance and productivity (Aguilera 2008). Proper modeling of the orientation, distribution and connectivity of the natural fractures is critical to reservoir simulation and forecasting (Cipolla et al. 2009b; Olson 2008). In particular, the understanding of the interaction between the induced hydraulic fractures and the naturally existing fractures is an important key in the successful development and exploitation of these reservoirs (Cipolla et al. 2011; Lee and Hopkins 1994; Weng et al. 2011). Planning an effective field development strategy requires estimating the drainage capacity of current wells and optimizing well placement so as to minimize the overlapping of drainage volumes of existing wells. Production decline curves have been widely used to compute drainage volumes and estimate EUR in tight gas reservoirs (Blasingame and Rushing 2005; Cox et al. 2002; Fetkovich 1980; Rushing et al. 2007). Also, pressure transient tests are commonly used in determining the well productivity and the benefits of hydraulic fracturing in tight gas reservoirs (Lee and Hopkins 1994). Whereas both decline curve analysis and pressure transient tests have played a vital role in the exploitation of tight gas reservoirs, the interpretation of such analytical tools can be considerably complicated in the presence of complex spatial heterogeneity and natural fractures. In particular, the interactions between the hydraulic fracture and natural fractures and their implications on the well drainage volumes cannot be adequately accounted for by the existing analytic methods.

Our objective in this paper is to develop a systematic procedure for well placement optimization in naturally fractured tight gas reservoirs. Towards this goal, we develop a rigorous approach to defining well drainage volumes during numerical simulation of naturally fractured tight gas reservoirs. Specifically, we will build on the concept of radius of drainage as defined by (Lee 1982). Currently there is no well-defined method

for computing the well drainage volumes from numerical simulation in gas reservoirs. A common practice is to use pressure contours to understand well drainage behavior with time. The well drainage volume is defined by following the evolution of a pressure contour level that is defined rather arbitrarily and Lee et al. (2003) define the radius of drainage as the propagation distance of 'maximum' pressure disturbance resulting from an impulse (instantaneous) source. More recently, this concept was used by Meyer et al. (2010) to examine fracture interference in the presence of multiple hydraulic fractures in horizontal wells. However, much of these previous developments have been limited to homogeneous medium. We generalize the concept of drainage radius and drainage volumes to arbitrary heterogeneous medium and completely general well conditions by first computing the reservoir flux field from numerical simulation and then, examining the propagation of the pressure disturbance along the gas streamlines.

Streamlines are trajectories or flow paths that are everywhere tangential to the local flow velocity. In fact, streamlines are simply a representation of the instantaneous velocity field. Streamlines exist whenever there is an underlying velocity field. These include compressible and incompressible flows, steady and unsteady conditions, oil and gas reservoirs (Datta-Gupta and King 2007). Although the visualization power of streamlines have been widely used to examine the swept and drainage volumes in oil reservoirs, the application of streamlines to compressible flow and particularly to gas reservoirs has been very limited.

One of the primary challenges in the application of the streamlines to gas reservoirs is the diffusive nature of the pressure equation. How can we define the concept of a propagating 'front' when the underlying phenomenon is diffusive? Kulkarni et al. (2001) generalized the streamline-based travel time approach to transient pressure conditions by introducing a 'diffusive time of flight' and rigorously computed well drainage radius during primary recovery and for heterogeneous permeability distributions. He et al. (2002) showed a good agreement between streamline-derived drainage volume calculations with decline type curve results. Kim et al. (2009) utilized the diffusive time

of flight to invert pressure response from interference test to characterize permeability distribution. The power of the method was illustrated using a field application.

Britt and Smith (2009) examine horizontal well completion and stimulation optimization for different reservoir conditions and geomechanic limitations along with risk mitigation strategies for effective horizontal well planning. They present results of design and optimization study followed by post appraisal study of the horizontal wells drilled in Arkoma basin. Meyer et al. (2010) presented analytical solution for predicting behavior of multiple transverse hydraulic fractures in a horizontal well and optimization methodology to hydraulic fracture stages considering NPV and ROI (return on investment). They also utilized the concept of radius of drainage (Lee 1982) to examine the interference between multiple transverse fractures.

Our objective in this paper is to develop a procedure for computing well drainage volumes in tight gas reservoirs. Because our approach relies on the streamlines derived from a finite difference simulator, the method is completely general and can handle any arbitrary heterogeneity and well conditions. The organization of the paper is as follows. We first highlight the main features of our approach and illustrate the steps using a synthetic example. We also validate our drainage volume calculations by comparing with analytic solutions for homogeneous medium. Next, we discuss the mathematical foundations behind the high frequency asymptotic solution of the diffusivity equation, the propagation of a 'pressure front' in the reservoir and its relationship to the concept of radius drainage as defined by Lee (1982). Finally, we demonstrate the power and utility of our method using a field application.

2.3 Approach

Our goal here is to examine the evolution of drainage volume of wells in tight gas reservoirs in the presence of natural fractures. This entails computation of well drainage volumes in the presence of arbitrary heterogeneity, well pattern and also accounting for well interactions. We build on the definition of radius of investigation Lee (1982) in terms of the propagation of a pressure pulse corresponding to an impulse source/sink.

Specifically, we generalize the concept of a propagating pressure pulse along individual streamlines in a gas reservoir. This allows us not only to compute and visualize the well drainage volumes as a function of time but also provides a mechanism to quantitatively examine the impact of well interactions on the drainage volumes and EUR. Below, we briefly discuss the major steps in our approach followed by an illustration of the procedure.

- ***Fracture Generation Using a DFN Model:*** Proper characterization of fractures is a key step in modeling naturally fractured reservoirs. A discrete fracture network (DFN) model is used to represent the fracture distribution in the reservoir. The purpose of fracture modeling is to create geological model properties which can more closely mimic the flow behavior in the real reservoir. We utilized tight and shale gas field data from previous studies (Bogatkov and Babadagli 2008; Cipolla et al. 2009a; Gale and Holder 2008) to get a representative set of fracture network model.

- ***Dual Porosity Simulation Using Finite Difference Simulator:*** We have utilized a commercial finite difference simulator (ECLIPSE^{TM}) for modeling the gas reservoir. A dual porosity model is used for the fluid movement along the hydraulic and natural fractures while accounting for the matrix-fracture interactions. All relevant physical mechanisms such as gas compressibility, gravity effects and matrix-fracture interactions are fully accounted for in the finite-difference simulation.

- ***Tracing Streamline Trajectories:*** We utilize the flux from the finite difference simulator to construct the streamlines in the fractures for the dual porosity model. The fluxes can be analytically integrated on a cell-by-cell basis to trace the streamline trajectories. The trajectory tracing is based on the method proposed by Jimenez et al. (2008). It is computationally efficient and can be used for general grid geometries including corner point cells. The streamlines are started at the

grid block centers and are traced backwards to the originating producers. Only those grid blocks having a finite gas flux will have a streamline passing through them. Because of high compressibility effects and the transient nature of the flow, the streamlines are recomputed every time step based on the updated flux field.

- ***Computing Well Drainage Volume:*** The well drainage volume is a generalization of the radius of drainage concept Lee (1982) and relies on calculating the propagation of a pressure disturbance corresponding to an impulse source/sink along the streamlines. Specifically, we utilize the concept of a 'diffusive time of flight' based on a high frequency asymptotic solution of the pressure equation (Datta-Gupta et al. 2001; Datta-Gupta et al. 2007; Vasco et al. 2000) as discussed later. It is shown that the pressure pulse propagates with a velocity given by the square root of the diffusivity. We can now extend the concept of radius of investigation to compute well drainage volumes under completely general conditions.

- ***Depletion Capacity Map:*** The well drainage volume calculations allow us to examine the interference between existing wells and also to identify the undrained regions for potential infill drilling. We define a 'depletion capacity map' for optimal well placement based on a combination of the undrained volumes and reservoir static and dynamic properties to maximize well productivity.

- ***Analysis for Various Well Completion Alternatives*.** A drainage volume analysis was carried out in the Cotton Valley field example for different well completions based on different hydraulic fracture stages being pumped in the well. The economic analysis was performed on the projections of rate profiles from the finite difference simulator and considering net gas and the lease operating

expenses. These results were compared to the drainage volumes estimated using the proposed approach for consistency check.

2.4 Illustration of Procedure

The detailed mathematical formulation for the well drainage calculations will be discussed in a later section. To start with, we illustrate our overall procedure using a section model of a tight gas field. The 3-D reservoir model consists of water-gas phase with 95×112×65 grid blocks. There are two producing wells, one near the center (well 147) and the other near the edge (well 148). The wells are separated by approximately 2,000 ft. The well 147 is first produced for 3 years; then well 148 starts producing. **Fig. 2.1** shows the matrix permeability distribution including the well locations. The wells are hydraulically fractured (x_f: 650 ft) with a fracture conductivity of 40 *md ft*.

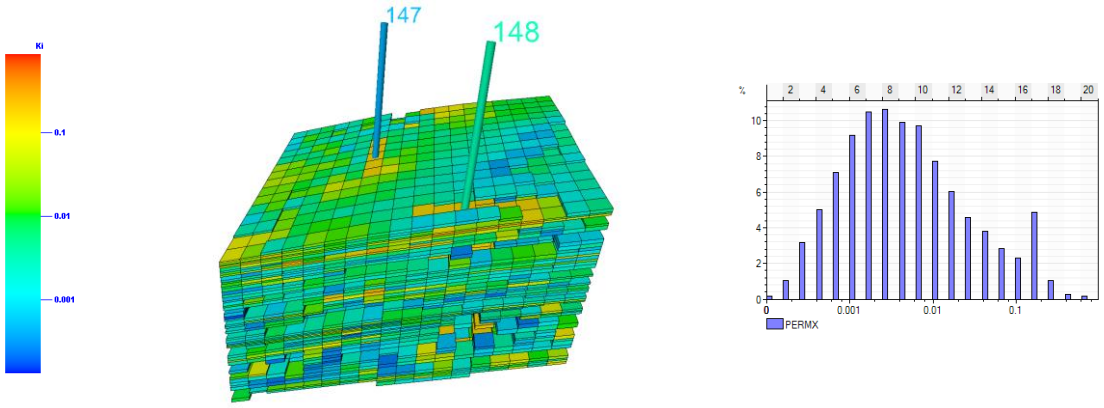

Figure 2.1. Permeability of Tight Gas Section Model

One of our objectives here is to compute and visualize the impact of natural fractures on the drainage volume calculations through dual-porosity simulation. For this, we utilize a discrete fracture network (DFN) model to generate the permeability distribution for the natural fractures. Hatzignatiou and McKoy (2000) demonstrated the use of stochastic fracture network generation based on fracture connectivity in tight gas sands. Olson and Taleghani (2009) suggested modeling parameters (apertures, fracture porosity

and effective permeability) ranges for fracture pattern generation in tight gas sands and Gale and Holder (2008) provided an observed range of fracture properties from Barnett Shale field. We utilize these previously suggested and observed ranges from field data for fracture network generation. The generated aperture range is between 3×10^{-7}~ 3×10^{-3} (ft) with a stochastic distribution. The fracture permeability and conductivity are then computed with cubic law from the aperture and permeability relationship (Bogatkov and Babadagli 2008).

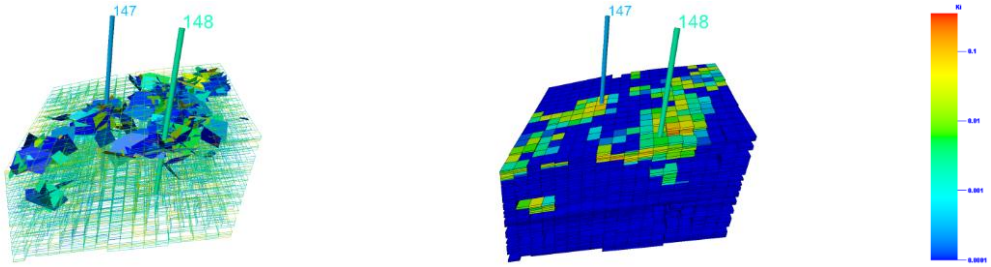

Figure 2.2. DFN Distribution with Fracture Clustering and Upscaled Permeabilities

Fig. 2.2 shows the DFN model with fracture clustering and the corresponding upscaled fracture permeability for dual porosity flow simulation. A commercial geological modeling package is used for this purpose (Petrel^{TM}). For this illustrative example, we assume that the fracture clusters follow the trend of original matrix permeability to keep direction of heterogeneity of the original single porosity model. **Fig. 2.3** shows the distribution of porosity in the matrix and in the fracture with the fracture porosity being much lower, as expected.

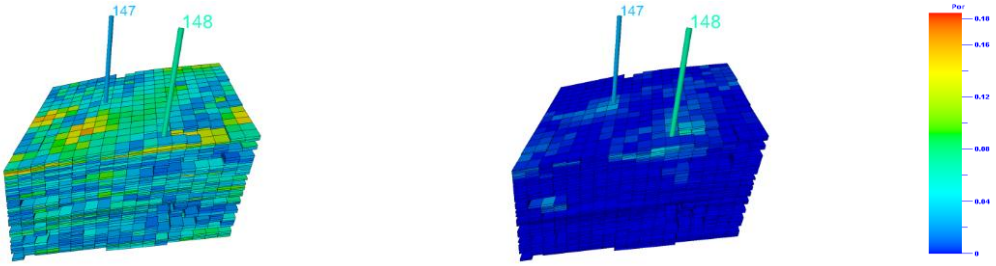

Figure 2.3. Matrix Porosity and Fracture Porosity Distribution

A dual porosity gas flow simulation is carried out with the above-mentioned fracture and matrix properties. In the dual porosity models, the gas flow is assumed to be primarily in the fractures whereas the matrix serves as gas storage. The fluxes derived from the simulator are used to trace streamline trajectories and compute the propagation of the pressure pulse along the streamlines to visualize the well drainage volumes. By thresholding the propagation time at various levels, we can visualize the evolution of the well drainage as a function of time (**Fig. 2.4a**). The drainage volume of the well at a given time is computed by summing up the pore volumes of the grid cells intersected by the streamlines. **Fig. 2.4b** shows the drained volumes mapped onto the grids. The blue regions show the drained volumes whereas the red regions are the undrained volumes which can be targeted for infill drilling.

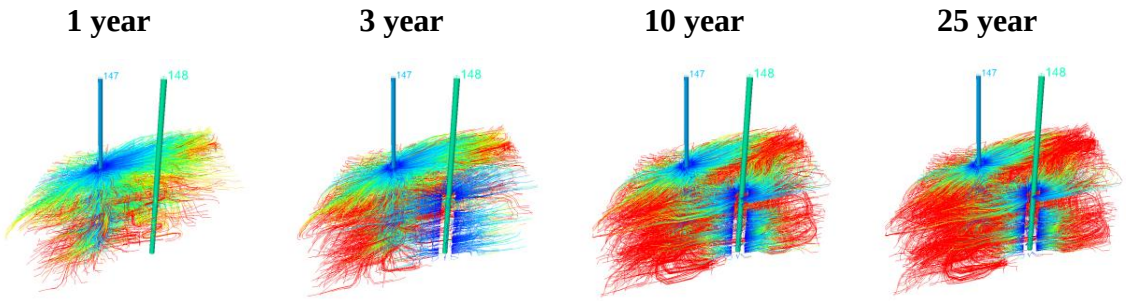

(a) Well Drainage given by Propagating Pressure Pulse along Gas Streamlines

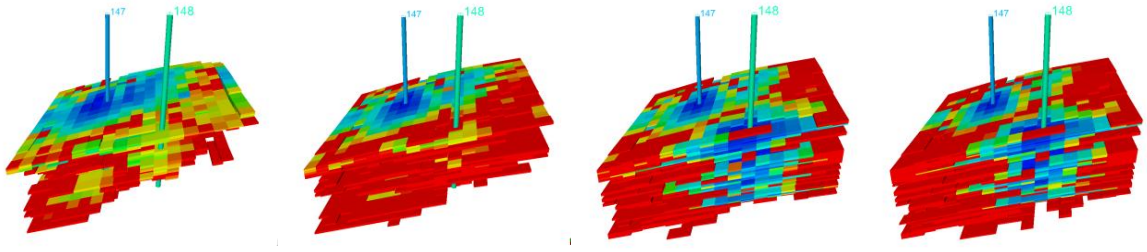

(b) Drained Volumes Computed by the Grid Blocks Intersected by the Streamlines

Figure 2.4. Gas Streamlines, Well Drainage Propagation and Drained Volumes

Fig. 2.5 shows the evolution of the drainage volumes of the two wells as a function of time including the effects of the natural fractures (NF) as discussed above. In the same plot we have shown the corresponding drainage volumes without the natural fractures, that is hydraulic fracture only. The enhanced well drainage because of the interaction of the natural fractures with the hydraulic fracture can be clearly seen in this figure. One of the powerful features of our proposed method is that we can not only visualize the evolution of the drainage volume with time but also quantitatively examine the interaction of nearby wells on the drainage volume. This is also illustrated in **Fig. 2.5(a)**. Recall that the second well came into production after three years and the impact of the second well on the drainage volume of the first well can be clearly seen here. In **Fig. 2.5(b)**, we can see approximately 30% increment in the drainage volume for this example because of the presence of the natural fractures.

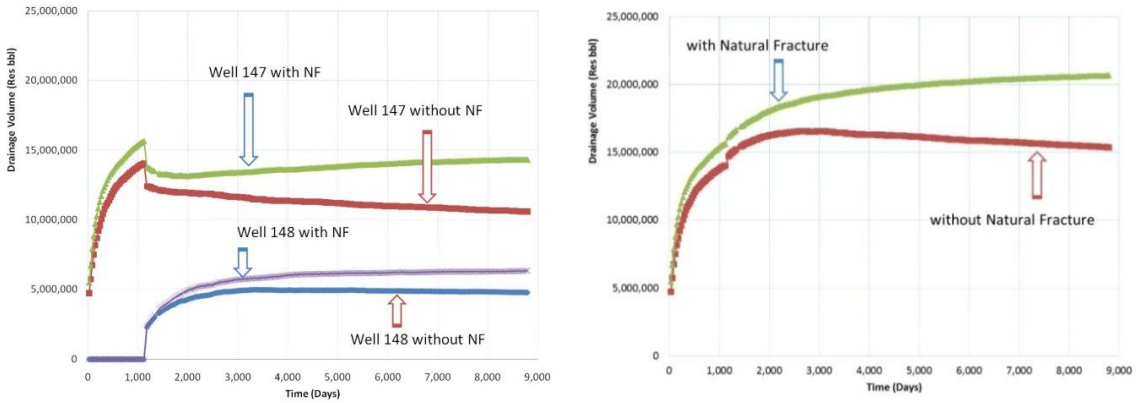

Figure 2.5. (a) Effect of Natural Fractures on Drainage Volume for Individual Wells and (b) on Total Drainage Volume

It is rather obvious that the impact of the natural fractures on the well drainage will depend upon the specific distribution of the fractures and is likely to vary significantly from case to case. To illustrate this, we generated a more dense fracture distribution as shown in **Fig. 2.6(a)**. The corresponding drainage volume evolution with time is shown in **Fig. 2.6(b)**. We can clearly see the acceleration effects on the drainage volume because of the increased fracture permeability.

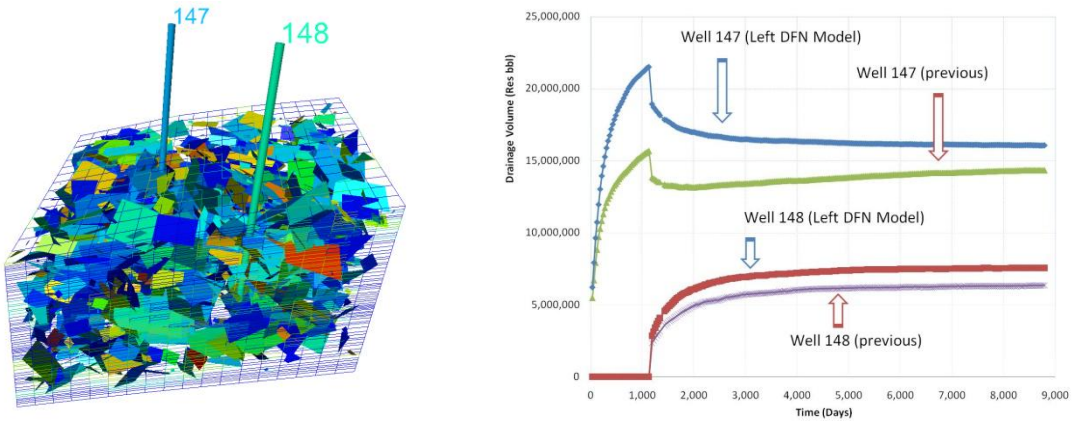

Figure 2.6. (a) High Fracture Density DFN (b) Effect of Fracture Density on the Drainage Volumes

2.5 Depletion Capacity Map and Infill Targeting

One of the objectives here is to identify undrained regions in the reservoir based on the drainage volumes of the existing wells. This will allow us to identify potential infill wells. Rather than just mapping the undrained volumes, we compute a depletion capacity index which also accounts for the reservoir properties such as permeability and pressure in the undrained regions. This is explained in more detail in the next section. The depletion capacity map shows the most productive location for the next infill well. This is illustrated in **Fig. 2.7(a)** for the two well example discussed above. The dark red areas indicate the most productive infill location for a potential third well. For comparison purposes, we carried out exhaustive simulations whereby the infill well was placed in every available grid cell and the EUR was computed. This required a total of 270 simulations for this case. The map of the computed EUR is shown in **Fig. 2.7(b)**. The similarity with the depletion capacity map is quite obvious here. However, the depletion capacity map required a single flow simulation and computation of the drainage volumes as discussed above.

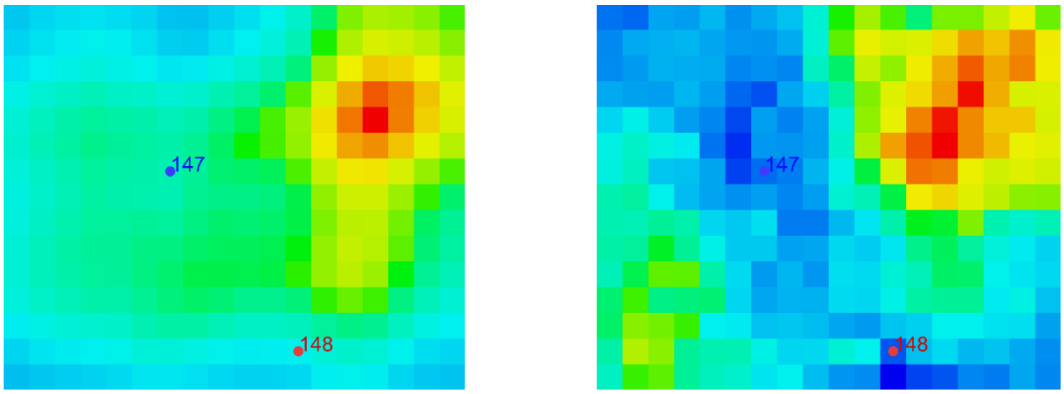

Figure 2.7. (a) Depletion Capacity Map based on Undrained Volumes
(b) EUR Map from Exhaustive Simulations

2.6 Drainage Volume Calculations: Mathematical Formulation

In this section we describe the mathematical foundations for the generalization of the radius of drainage concept (Lee 1982) using a high frequency asymptotic solution of the diffusivity equation. For clarity of exposition, we describe our formulation in terms of pressure although the same development can be made for gas reservoirs in terms of real gas pseudo pressure (Al-Hussainy et al. 1966).

The transient pressure response from a heterogeneous permeable medium can be described by the diffusivity equation

$$\phi(\mathbf{x})\mu c_t \frac{\partial P(\mathbf{x},t)}{\partial t} - \nabla \cdot \left(k(\mathbf{x})\nabla P(\mathbf{x},t)\right) = 0 \tag{2.1}$$

Using Fourier transform of **Eq. 2.1**, we obtain the following equation in the frequency domain.

$$\frac{\phi(\mathbf{x})\mu c_t}{k(\mathbf{x})}(-i\omega)\tilde{P}(\mathbf{x},\omega) = \nabla^2\tilde{P}(\mathbf{x},\omega) + \frac{\nabla k(\mathbf{x})}{k(\mathbf{x})}\cdot\nabla^2\tilde{P}(\mathbf{x},\omega) \tag{2.2}$$

The goal of the asymptotic approach is to find a solution of the diffusive pressure equation that mimics the one found in wave propagation. Asymptotic ray theory (also known as the 'ray series method') forms the mathematical basis for geometrical ray theory and has been extensively used in both electromagnetic (Virieux et al. 1994) and seismic (Červený 2005) wave propagation. The method has also proved valuable in the analysis of front propagation in general (Adalsteinsson and Sethian 1995) and many of the concepts such as ray and propagating interfaces have direct counterparts in hydrology (Bear 1972) and petroleum engineering in terms of streamlines and flood fronts (Datta-Gupta and King 2007).

The asymptotic solution for a transient pressure response assumes the following form (Datta-Gupta and King 2007; Vasco et al. 2000; Virieux et al. 1994).

$$\tilde{P}(\mathbf{x},\omega) = e^{-\sqrt{-i\omega}\tau(\mathbf{x})} \sum_{k=0}^{\infty} \frac{A_k(\mathbf{x})}{\left(\sqrt{-i\omega}\right)^k} \tag{2.3}$$

In these expansions, $\tau(\mathbf{x})$ represents the phase of a propagating wave and thus, describes the geometry of a propagating front. Also, $A_k(\mathbf{x})$ are real functions that relate to the amplitude of the wave. The advantage of this form of expansion is that the initial terms of the series represent rapidly varying (high frequency, large ω) components of the solution and successive terms are associated with lower frequency behavior. Hence, the propagation of a sharp front is described by the initial terms of the summation. To emulate the propagation of a 'pressure front', we will consider only 0^{th} order expansion or the first term in **Eq. 2.3**.

$$\tilde{P}(\mathbf{x},\omega) = e^{-\sqrt{-i\omega}\tau(\mathbf{x})} A_0(\mathbf{x}) \tag{2.4}$$

After inserting **Eq. 2.4** into **Eq. 2.2** and collecting terms with the highest order of $\sqrt{-i\omega}$, that is, $\left(\sqrt{-i\omega}\right)^2$, we obtain the equation for the front propagation in an isotropic permeable media,

$$\alpha(\mathbf{x})\cdot\nabla^2\tau(\mathbf{x})=1 \tag{2.5}$$

where $\alpha(\mathbf{x})$ is the diffusivity, given by

$$\alpha(\mathbf{x})=\frac{k(\mathbf{x})}{\phi(\mathbf{x})\mu c_t} \tag{2.6}$$

Eq. 2.5 is actually a form of the Eikonal equation which explains a variety of propagation behaviors (Kline and Kay 1965; Sethian 1999a). It is interesting and important to note that **Eq. 2.5** has a form similar to that of the streamline time of flight equation which describes the propagation of a neutral tracer (Datta-Gupta and King 2007).

$$v\bullet\nabla\hat{\tau}(\mathbf{x})=1 \tag{2.7}$$

where $\hat{\tau}(\mathbf{x})$ is the streamline time of flight and v is the interstitial velocity of a neutral tracer. By analogy with the time of flight formulation, we can see that the pressure wave fronts travel with a velocity given by $(\alpha(\mathbf{x}))^{1/2}$. In fact, we can define a diffusive time of flight for the propagation of a pressure front as follows (Datta-Gupta et al. 2001; Kulkarni et al. 2001)

$$\tau(\mathbf{x})=\int_{\psi}\frac{d\zeta}{\sqrt{\alpha(\mathbf{x})}} \tag{2.8}$$

Note that the unit of diffusive time of flight in **Eq. 2.8** is the square root of time which is consistent with the scaling behavior of diffusive flow. However, the diffusive time of flight is defined along the trajectories of a 'pressure wave front' ψ, which are given by the ray paths of the wave equation. These trajectories are not necessarily in the streamlines (Vasco and Finsterle 2004). Kim et al. (2009) has shown that for many practical applications, the pressure trajectories can be approximated by the streamlines.

2.6.1 The Pressure Wave Front

Lee (1982) defines the radius of investigation at any given time as the propagation distance of the 'maximum' pressure disturbance corresponding to an impulse (instantaneous) source. In this section, we examine the physical significance of a 'pressure front' or a 'diffusive' time of flight and demonstrate its close correspondence to the concept of the radius of investigation. The time domain solution to the 0^{th} order asymptotic expansion for an impulse source is given by the inverse Fourier transform of **Eq. 2.4**. For a 2-D medium, we obtain the following

$$P(t) = A_0(\mathbf{x}) \frac{\tau(\mathbf{x})}{2\sqrt{\pi}\, t} \exp\left(-\frac{\tau^2(\mathbf{x})}{4t} \right) \tag{2.9}$$

The above equation corresponds to the propagation of a pressure response for an impulse source in a 2-D medium. The pressure response at a fixed position, **x**, will be maximized when the time derivative of **Eq. 2.9** vanishes.

$$\frac{\partial P(t)}{\partial t} = A_0(\mathbf{x}) \frac{\tau(\mathbf{x})}{2\sqrt{\pi}} \left[-t^{-2} \exp\left(-\frac{\tau^2(\mathbf{x})}{4t} \right) + \frac{\tau^2(\mathbf{x})}{4t^3} \exp\left(-\frac{\tau^2(\mathbf{x})}{4t} \right) \right] = 0 \tag{2.10}$$

This results in the following relationship between the observed time and the 'diffusive' time of flight for a two-dimensional medium.

$$t_{\max} = \frac{\tau^2(\mathbf{x})}{4} \tag{2.11}$$

Physically, the 'diffusive' time of flight is associated with the propagation of a front of maximum drawdown or build up for an impulse source or sink. This concept is closely related to the idea of a drainage radius (Lee 1982). In fact, it is interesting to note that for a homogeneous medium with radially symmetric streamlines, **Eq. 2.11** reduces to the following.

$$t_{\max} = \frac{r^2}{4\alpha} \tag{2.12}$$

where, r is the distance travelled by the pressure disturbance along streamlines and α is the diffusivity. **Eq. 2.12** is exactly the same expression for the propagation time given by Lee (1982). To illustrate this correspondence further, we have shown in **Fig. 2.8(a)** the radius of drainage at three different times computed based on the diffusive time of flight for a single producing well in a 2-D homogeneous medium. To accomplish this, we first trace the streamlines and compute the diffusive time of flight along the streamlines as given by **Eq. 2.8**. The diffusive time of flight is then converted to physical propagation time of the pressure pulse time using **Eq. 2.11**. The evolution of the drainage volume is given by contouring the propagation time. For comparison purposes, we have also shown in **Fig. 2.8(b)** the radius of drainage based on the expression given by Lee (1982). The close correspondence between these is quite apparent from these figures.

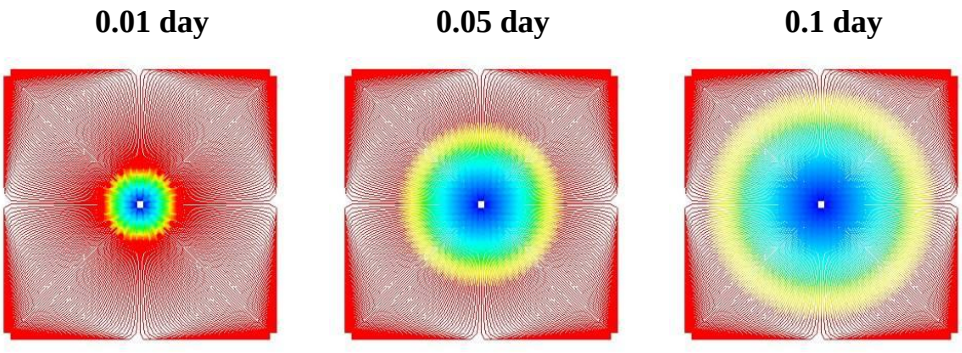

(a) Drainage Radius from the Diffusive Time of Flight

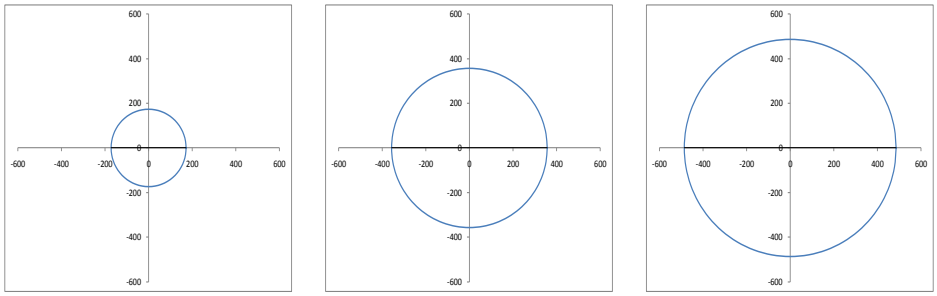

(b) Drainage Radius Computed from Lee (1982)

Figure 2.8. Comparison between Diffusive Time of Flight Radius and Analytical Solution

One of the major advantages of the asymptotic approach is that we can now extend the concept of radius of investigation to any arbitrary heterogeneous medium. This is illustrated in **Fig. 2.9** It is interesting to note that although the streamlines are recomputed based on updated flux, the streamline geometry remains remarkably similar other than their evolution with time. The well drainage volume is computed by adding up the volumes of the grid cells intersected by the streamlines at a given time.

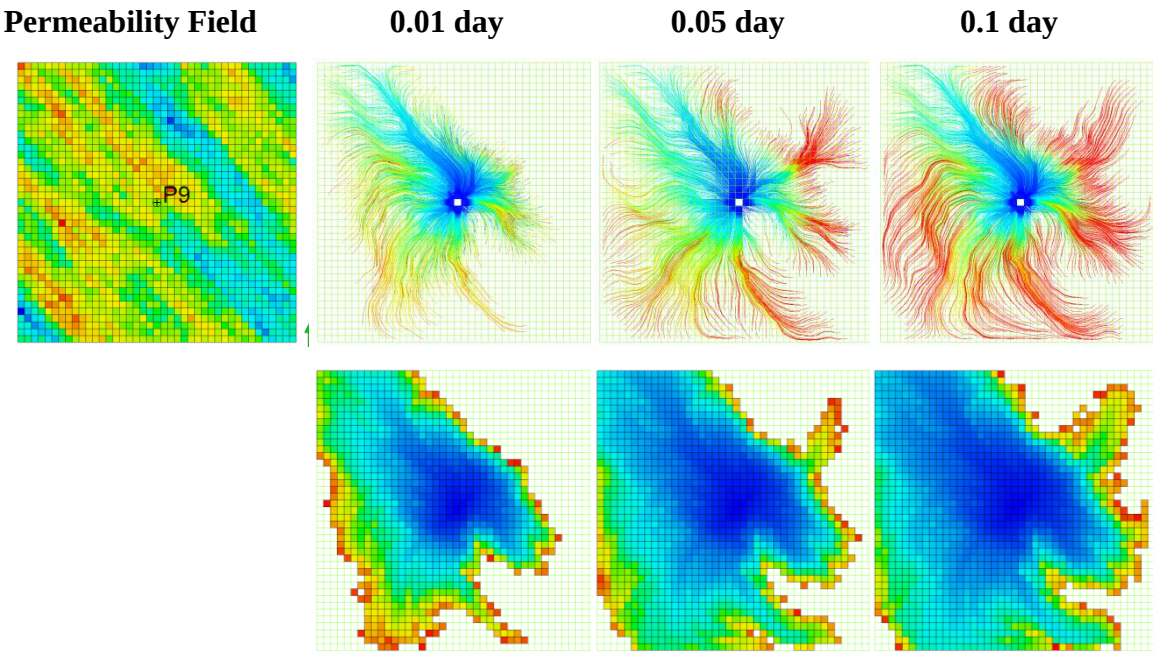

Figure 2.9. Radius of Investigation and Drainage Volume Calculations in a Heterogeneous Field.

Finally, it is worth pointing out that for a 3D medium, the time domain solution for an impulse source will be given by the following (Kulkarni et al. 2001).

$$P(t) = A_0(x)\frac{\tau(x)}{2\sqrt{\pi t^3}}\exp\left(-\frac{\tau^2(x)}{4t}\right) \tag{2.13}$$

The propagation time for the pressure 'front' will now be related to the diffusive time of flight through the following expression.

$$t_{\max} = \frac{\tau^2(\mathbf{x})}{6} \tag{2.14}$$

2.6.2 Depletion Capacity Map

One of our objectives in this paper is to optimize infill locations based on the undrained reservoir volumes. After computing the drainage volumes associated with existing wells, we can identify undrained region where the 'pressure front' has not reached. This can be seen in **Fig. 2.9** for the illustrative example with a single well in a heterogeneous permeability field. For infill locations, instead of relying solely on the undrained volumes, we define a 'depletion capacity' that includes permeability, pore volume and reservoir 'energy' as indicated by the level of pressure drop at any given time. We create a 2-D map of 'depletion capacity' by a vertical sum for the undrained cells as given by the equation below:

$$DC_{ij} = \sum_{k} \left[k_{ij} \cdot V_{ij,poro} (p_{ij} - p_{avg}) \right]_k \tag{2.15}$$

The 2-D areal map of the depletion capacity can now be used as a guide to locate potential infill locations. In the synthetic example discussed before, we have already demonstrated the close correspondence of this depletion capacity map with exhaustive flow simulations.

2.7 Field Application of Optimal Well Placement

In this section, we illustrate the application of our approach with a tight gas field located at the Rocky mountain region. The section of the field under consideration has more than 25 years of producing history and 85 production wells. The matrix permeability is shown in **Fig. 2.10(a)**. Because one of our objectives is to examine the role of natural fractures, a discrete fracture network is generated along the high matrix permeability regions. **Fig. 2.10(b)** also shows the generated DFN and upscale permeability.

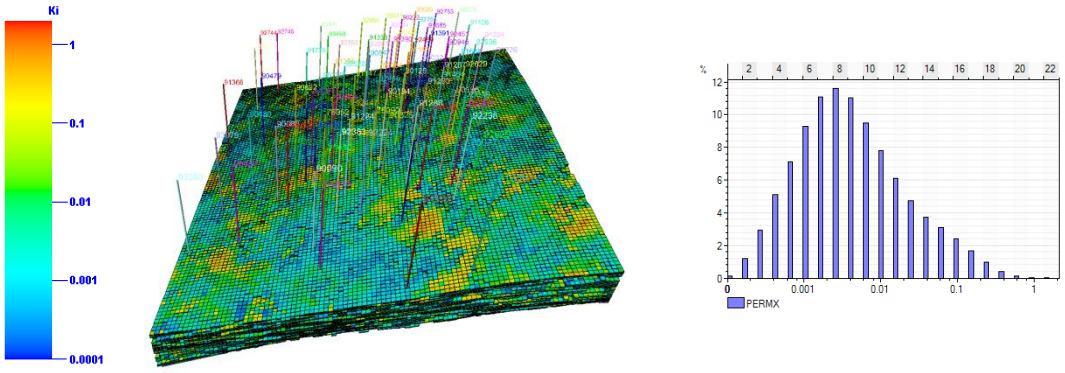

(a) Matrix Permeability Distribution

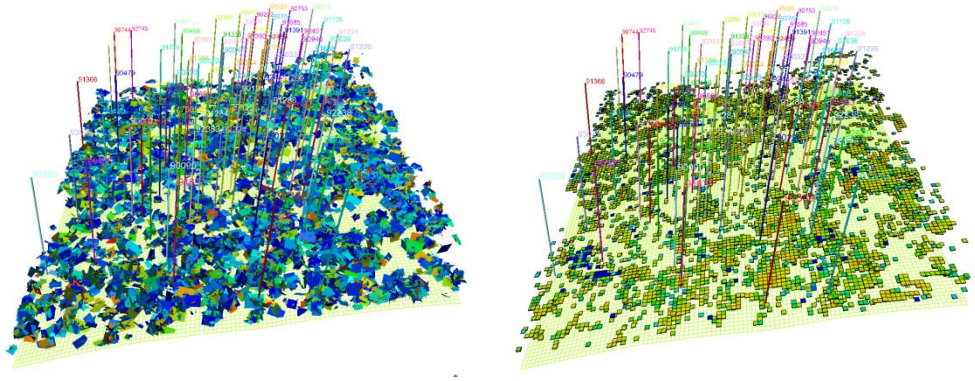

(b) Generated DFN and Upscaled Permeability Field

Figure 2.10. Field Permeability and Discrete Fracture Network (DFN) Generation

A dual porosity model is built using the matrix and fracture permeabilities and streamlines are generated based on the flux field in the fractures obtained from the dual porosity finite difference simulation as shown in **Fig. 2.11(a)**. For each simulation time, streamlines are started from the center of each grid cell and traced back to the originating producer. The diffusive time of flight is also computed along streamlines and converted to physical time required to drain the grid cell as given by **Eq. 2.14**. For computing the reservoir drained volumes, the drainage information is mapped into grid blocks as shown in **Fig. 2.11(b)**. The summation of volumes inside the drainage boundary at a given time

will be the drainage volume at that time. In **Fig. 2.11(b)**, we have illustrated the grid blocks will be drained after 35 years of production.

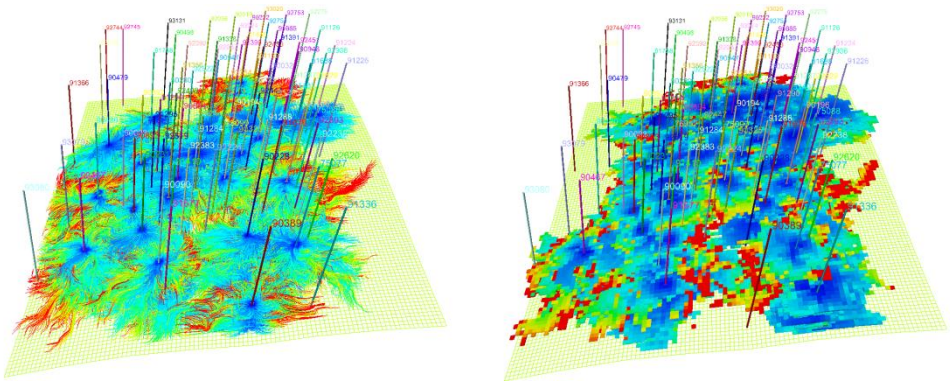

Figure 2.11. (a) Diffusive Streamline Time of Flight and (b) Drainage Grid Blocks

Because the streamlines are regenerated and drainage volumes are recomputed as a function of time, we can examine the evolution of drainage volumes of individual wells based on the streamlines originating from the well. This is shown in **Fig. 2.12**. We can see that there is a complex interference of the producing wells. In fact, we can see that the drainage volumes of some of the existing wells drop substantially when a new well is brought in. This seems to indicate that some of the new wells, at least to some extent, are 'stealing' from the existing producing well. Such interference is often not adequately accounted for computing the EUR associated with new wells.

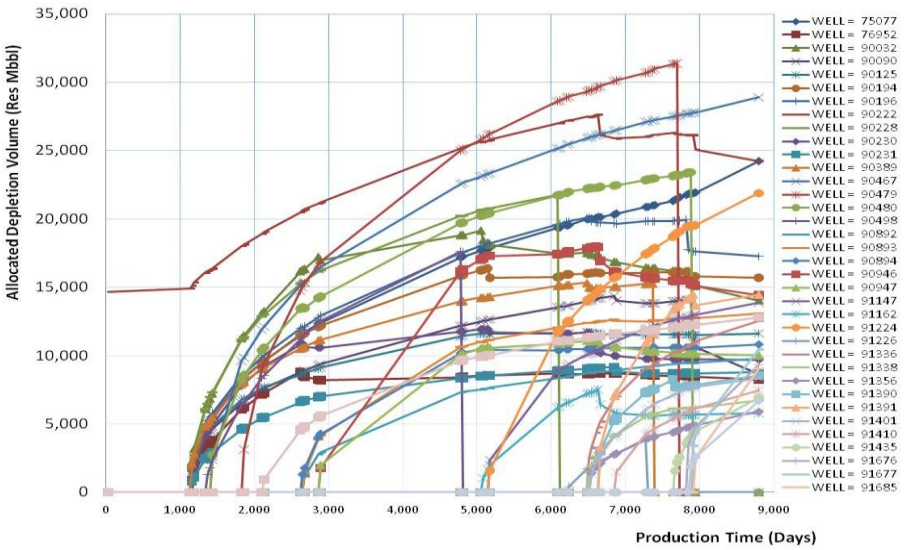

Figure 2.12. Drainage Volume in Each Well Location

Finally, as mentioned before, we can compute a depletion capacity map based on the undrained volumes and production potential in different parts of the reservoir. This is shown in **Fig. 2.13**. Such a map can greatly facilitate infill drilling decision. The red areas in **Fig. 2.13** indicate the regions that have not been drained during 35 years and are the most optimal infill target.

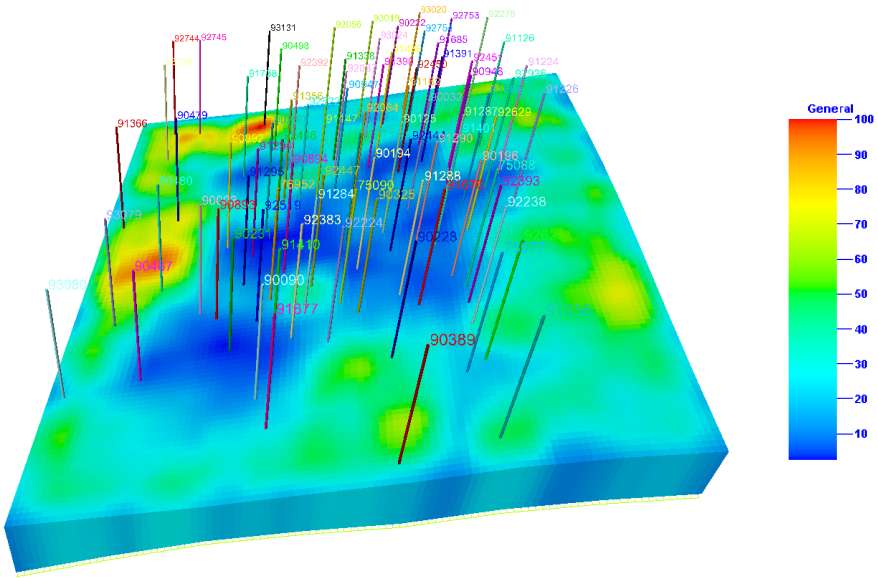

Figure 2.13. Depletion Capacity Map for Next Infill Well

2.8 Field Application of Optimal Hydraulic Fracture Stages

In this section, we discuss the field application of the concept of the drainage volumes to a tight gas reservoir in the Cotton Valley Formation. Specifically, we utilize the well drainage volumes to optimize the number of hydraulic fracture stages. We also show that the results of the drainage volume calculations to optimize the completion strategy are similar to the conclusions arrived from calculations based on the production forecast from finite difference simulator. The main advantage of the drainage volume approach is that it allows to visualize evolution of the well drainage with time and also to examine the interference between fracture stages. All these can facilitate well completion optimization and also well placement optimization based on undrained volumes in the reservoir (Kang et al. 2011).

The Cotton Valley group represents the first major influx of Clastic sediments into the ancestral Gulf of Mexico (Dyman and Condon 2006). Reservoir properties and production characteristics identified two Cotton Valley Group sandstone trends across northern Louisiana and East Texas: a high permeability blanket sandstone trend and a down-dip low permeability massive sandstone trend. The study well is located in low permeability sandstone trend in Louisiana.

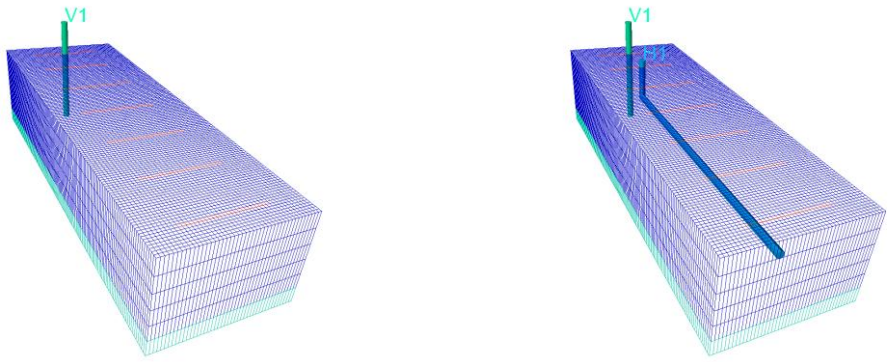

Figure 2.14. Schematic of the Two Phase Model for History Matching

An existing vertical well in the field had about two years of production history. This well was history matched by building a 3D two phase reservoir model. The schematic of

the model is as shown in **Fig. 2.14**. After three years of production of the vertical well, a horizontal well was planned. The purpose of this study is to optimize the completion strategy of the planned horizontal well while taking into account any potential interaction with the existing vertical well.

Layer 1 in the model in **Fig. 2.14** shown above is 200 ft thick with 7.6% porosity and 45% water saturation. The second layer is 40 ft thick with 11% porosity and 98% water saturation. The model was constrained to actual gas production. History matching was performed to match the model BHP and water production to the observed data in **Fig. 2.15**.

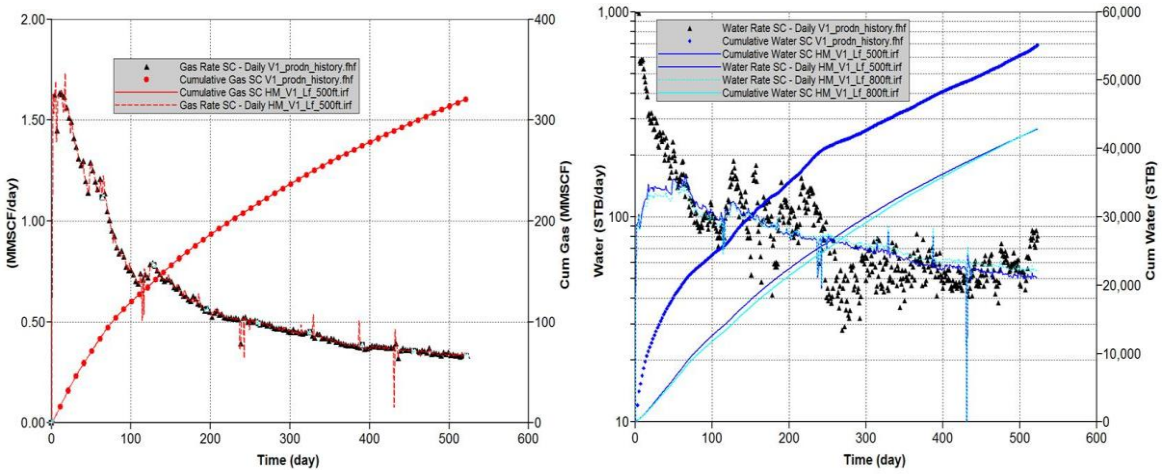

(a) Gas Production HM (V1) **(b) Water production HM (V1)**

Figure 2.15. Production Rate History Matching Results

As the produced water is a combination of the formation water and fracture fluid, Water Gas Ratio (WGR) was used as a matching parameter instead of cumulative water. The well was treated with 685 $Mgals$ of fluid and 1 $MM\ lbs$ of 20/40 white sand with tail-in of resin coated sand. The 1-ft wide hydraulic fracture was incorporated in the model (using local grid refinement) with an equivalent fracture conductivity of 0.1 inch wide hydraulic fracture created in the field conditions. The existing vertical well had an initial production of about 1.6 $MMscfd$ with a well head pressure of about 1,500 psi.

The well has a cumulative gas production of about 0.35 $Bscf$. The surface pressure data was used to estimate flowing bottom-hole pressure (FBHP) after adequately correcting for liquid loading effects. The model pressure match to calculated FBHP is shown in **Fig. 2.16**.

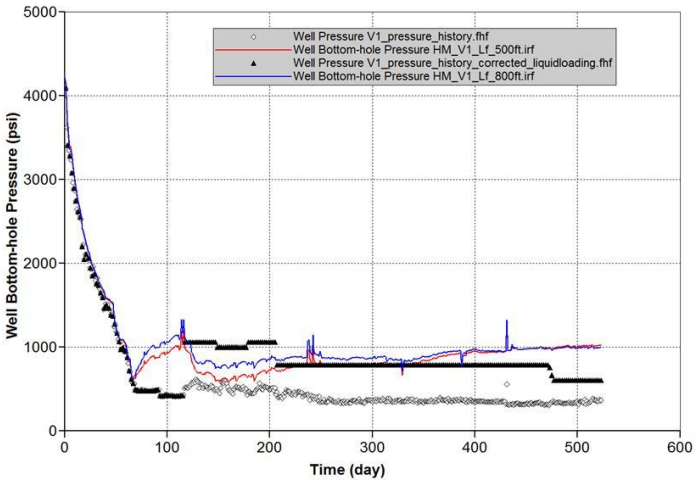

Figure 2.16. Bottom Hole Pressure History Match for Well V1

The results of the calibrated model are shown in **Table 2.1**. Two models with fracture half lengths estimate of (500 *ft* and 800 *ft*) along with permeability for gas layer and water layer are shown. This was done to get a better estimate to design the surface facilities required for producing these wells.

Table 2.1. Range of Permeability and Fracture Length from Calibrated Model (V1)

Layer	L_f **= 500** ***ft***	L_f **= 800** ***ft***
1	0.0075 md	0.0035 md
2	0.0350 md	0.0190 md

This calibrated model ($L_f = 500\ ft$) was used to estimate the drainage volumes from streamlines at the end of the history match. The planned horizontal well (H1) had a lateral length of 4000 ft. The completion strategy for the horizontal well envisaged six

(Case 1), eight (Case 2), ten (Case 3) and twelve (Case 4) hydraulic fracture stages. These hydraulic fracture stages were spaced equally. The existing vertical well along with different completion options in the horizontal well enabled examining the interference effects and helped design an optimal number of hydraulic fracture treatment stages. The forecast for the horizontal well was made with an initial production of 8 $MMscfd$ for 35 years of well life for a constant flowing BHP of 1,000 psi. Based on these forecast, DTOF was calculated for this time period and drainage volume was estimated. **Fig. 2.17** shows the drainage volume computed from DTOF at 35 years cut-off for existing vertical well (V1) and planned horizontal well (H1).

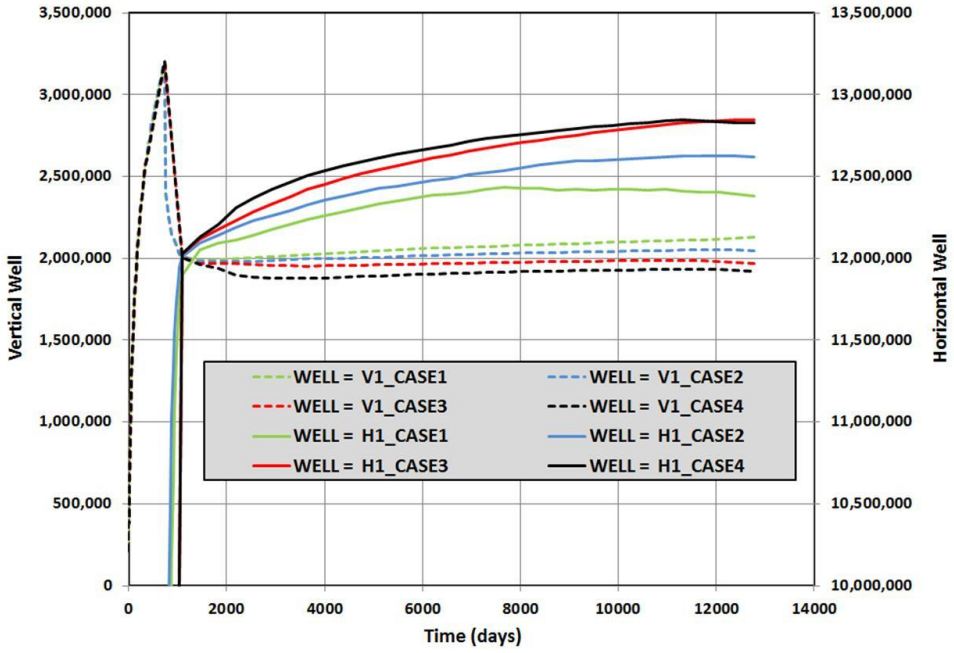

Figure 2.17. Drainage Volume (RB) based on DTOF 35 years Cut-off for Well V1 and H1

The interference between the existing vertical and new horizontal well can be seen from the plot. In particular, the drilling of the horizontal well clearly interfered with the drainage volume of the existing vertical well and we see a significant reduction in the drainage volume which is reallocated to the horizontal well. This can also be seen from

the 3-D evolution of the drainage volume along streamlines. In **Fig. 2.18** we have shown the drainage volumes at three different times corresponding to 6 and 10 stages of fractures. The gradual interference of the horizontal and vertical well drainage volumes is obvious here.

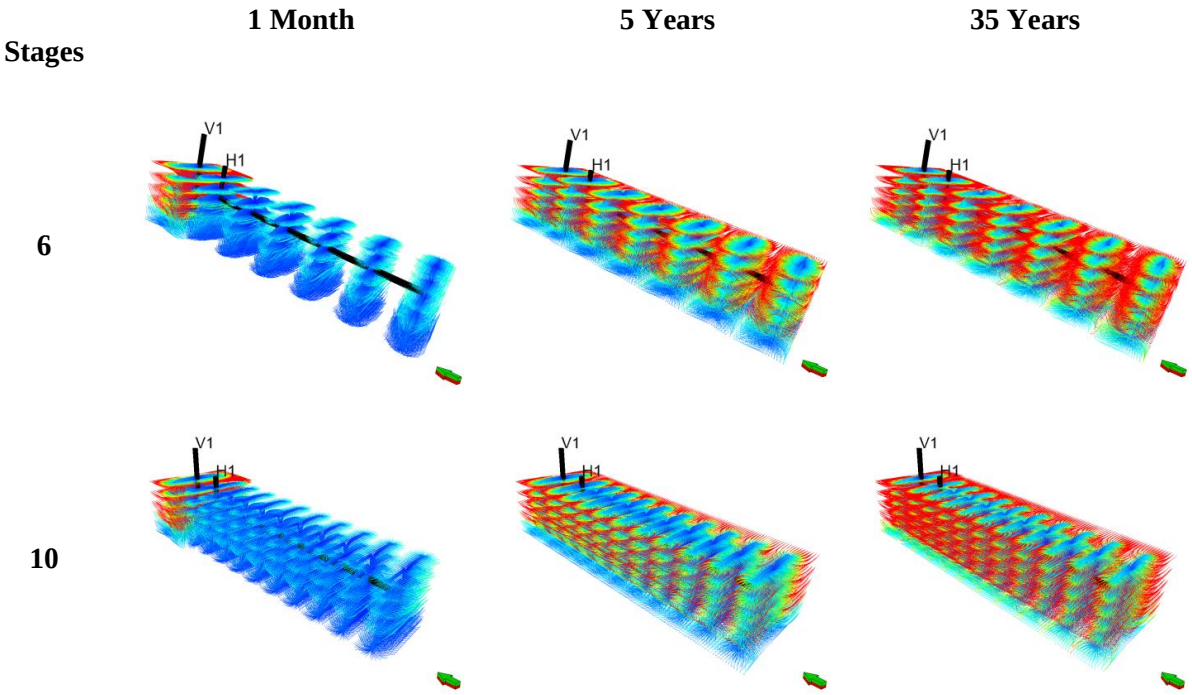

Figure 2.18. Comparison of Streamlines based on DTOF at the End of 1, 5 & 35 years for Different Completion Options

We can quantify the drainage volume by summing up the pore volumes of the grid cells intersected by the streamlines at a given time. This is shown in **Fig. 2.18** as a function of the number of hydraulic fracture stages at the end of 35 years. With increased fracture stages, we access more drainage volume until 10 stages beyond which we reach diminishing returns. This result shows that ten stage hydraulic fracture strategy is the most optimal completion that can help maximize the drainage volume.

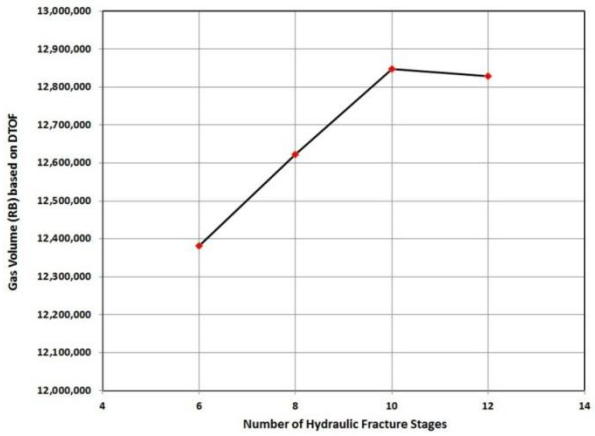

Figure 2.19. Drainage Volume for Different Hydraulic Fracture Stages for Horizontal Well (H1)

2.9 Summary and Conclusions

We have presented a systematic approach to well placement in naturally fractured tight gas reservoirs based on the well drainage volumes computed from dual porosity numerical simulation. Specifically, we have extended the radius of drainage concept (Lee 1982) to arbitrary heterogeneity and well conditions by utilizing the gas streamlines derived from dual porosity numerical simulation. This allows us to visualize the undrained regions and optimize well placement based on a single flow simulation. The results have been shown to be consistent with well placement optimization through exhaustive flow simulations.

We have also presented a systematic approach to drainage volume calculations for horizontal wells in the presence of multistage fractures. Specifically, we have extended the radius of drainage concept (Lee 1982) to arbitrary heterogeneity and well conditions by utilizing the gas streamlines derived from finite difference simulation. This allows us to optimize well completions by examining the drained volumes as a function of the number of fracture stages.

Some specific conclusions from this study are as follows.

1. Using a high frequency asymptotic solution of the diffusivity equation, the

concept of radius of drainage (Lee 1982) has been generalized to arbitrary heterogeneous medium and general flow conditions by examining the propagation of a 'pressure front' corresponding to an impulse (instantaneous) source along gas streamlines. The gas streamlines can be traced from the flux field of a finite-difference flow simulation.

2. Visualizing the well drainage is a physical and intuitive way of examining the influence of existing wells and their mutual interference. By summing up the grid cells intersected by the streamlines originating from a given well, we can quantitatively estimate the well drainage volume, its evolution with time and potential interference from wells in the vicinity.

3. We have used a discrete fracture network model to examine the role of natural fractures in the well drainage volumes. As expected, the results show that the presence of natural fractures tends to enhance the well drainage volumes and accelerate production depending upon the distribution and orientation of fractures.

4. Based on the undrained reservoir volumes and reservoir static and dynamic properties, we have defined a 'depletion capacity' map for rapid identification and optimization of infill locations in tight gas reservoirs. The power and utility of the method has been demonstrated using both synthetic and field applications.

5. We have demonstrated the use of drainage volume concept in optimizing number of fracture stages in the Cotton Valley formation. The incremental drainage volumes with the number of fracture stages indicate that eight to ten hydraulic fracture stages indicate the most optimal completion strategy for the horizontal well studied from the field example.

CHAPTER III
A MODEL SEGMENTATION FROM SPECTRAL CLUSTERING: NEW ZONATION ALGORITHM AND APPLICATION TO RESERVOIR HISTORY MATCHING

3.1 Purpose

Proper characterization of reservoir is an important step for optimization and field management. A purpose of this research is proposing a novel zonation criterion in the history matching stage. Typically we apply a multiplier in the large scale field model and it has been subjective to choose the parameter multiplicative region. Many industry practices have applied a box multiplier near the well region or on the geological key features; fault or flow barrier. Many cases applied a single multiplier over whole reservoir field. This box multiplier approach might improve matching simulation to observation, but it violates prior model's important features and disengaged geologic continuity between different region boundaries. That has been a key issue in history matching process for geologists and reservoir engineers. It is also clear that this broken links, between the prior and update model's static key features, will decrease forecasting and optimization reliability.

Our goal in the paper is minimizing static feature's loss by proposing reasonable zonation criteria. In other words, by using proposed zonation, we will be able to keep main features of the prior model. At the same time, we can ensure improved history matching quality after history matching step.

Zonation is a technique that partitions the reservoir region based on certain criteria. In that sense, graphic partitioning provide a good decision gauge to segment regions while keeping prior model's main heterogeneous and/or connectivity features; such as high or low permeable channel and barrier. For this purpose, we introduce graphical partitioning for reservoir segmentation based on grid properties and/or connectivity. The heterogeneity and connectivity are closely related to flow dynamics of a reservoir.

For history matching, we integrate genetic algorithm (GA) for calibrating reservoir models. We demonstrated the strength and applicability of proposed zonation in reservoir history matching problem, with both synthetic example and the Brugge field example. This zonation approach from spectral clustering theory can enhance speed up of global scale model calibration, which is common in hierarchal history matching approach and in industry practice. At the same time, we can keep prior model's main information. Another advantage of spectral clustering is its adaptability to every grid properties, even dynamic data at certain time.

The proposed spectral clustering has a clear edge detection power in smoothly varying high and low valued regions. Hence, the proposed approach will provide potential zonation criteria for reservoir history matching problems.

3.2 Introduction

The clustering or grouping algorithm is defined as "minimize the similarity between groups and maximize the similarity within a group". A graph partitioning from spectral theory provides a fast way to decompose a domain for local grouping. As a matter of fact, the spectral clustering has been used in various engineering fields; supercomputing, machine learning, logistics, internet shopping, social network service and more. Because of that, spectral clustering algorithm has profound theoretical background and is comparatively easy to implement in new area.

The spectral clustering is an algorithm that partitions an affinity matrix with eigenvectors of a graph. Pothen et al. (1990) showed that the 'second' smallest eigenvalue will be positive if the graph G is connected. The corresponding second eigenvector relates to the vertex and edge connectivity of a graph. Hagen and Kahng (1992) applied the ratio cut partitioning and clustering for VLSI circuit design. They adopted the spectral 'ratio cut' clustering to minimize the number of inter block signals. Shi and Malik (2000) proposed a new clustering algorithm, 'normalized cut' and compared with 'ratio cut' using some sample images. They examined the relationship with 'normalized cut' and other eigenvector based partitioning algorithm. The

'normalized cut' algorithm can balance between 'finding clumps' and 'finding splits'. Wang and Siskind (2003) proposed an improved 'ratio cut' algorithm in image segmentation. They proposed a new cost function to minimize for optimal clustering. von Luxburg (2007) introduced and summarized the underline background theory in a tutorial paper. She also proposed many new algorithms in the spectral clustering area (Von Luxburg 2010; von Luxburg et al. 2011). Buhler and Hein (2009) proposed the spectral clustering by using graph p-Laplacian. They proved that their Laplacian construction is at least equal or better than normal square Laplacian (also called standard cut). Recently, Hein and Bühler (2010) proposed a novel spectral clustering based on the Laplacian. They generalized a non-linear standard graph Laplacian and verified capturing key feature in a graph image. **Fig. 3.1** shows how the spectral clustering generates segmentation on a sample image. Briefly, it captures the main features of image and cut the edge based on optimization criteria from image pixel information. The spectral clustering theory has been extensively applied and verified in other industries with its theory and applications.

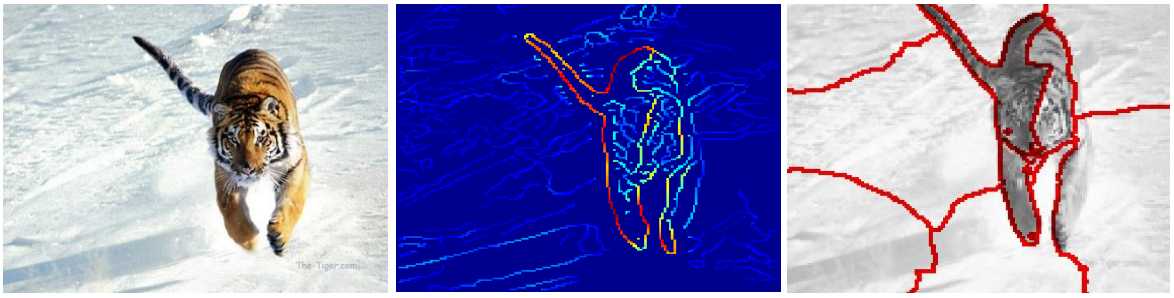

(a) Original Image (b) Computed Edges (c) 10 Clusters

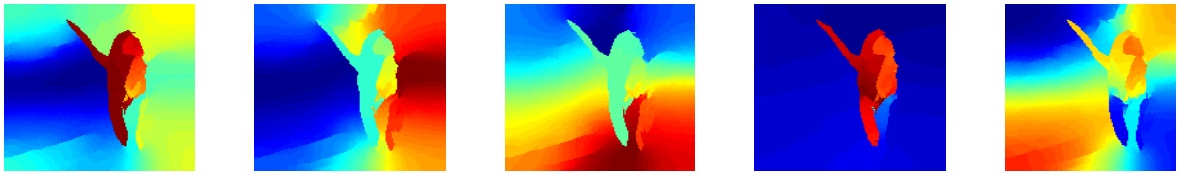

(d) Leading Eigenvectors (2nd to 6th from left)

Figure 3.1. Illustration of Spectral Image Clustering

In the reservoir history matching field, various zonation algorithms have been proposed for partitioning reservoir models. Huang et al. (2001) proposed cluster analysis for constructing fluid flow zones from seismic attributes. They used the spatially dense set of geophysical attributes to create spatial zones. Agunwoke et al. (2004) suggested the reservoir flow zonation based on similar geologic, physical property from well logging data. They applied a statistical approach based on geologic litho-stratigraphic correlation using gamma ray and resistivity logs. Brun et al. (2004) proposed the 'Gradzone analysis' to impose geological constraints during the gradient based history matching process. They generated the 'Gradzone' based on spectral analysis of the second derivative (Hessian) matrix from the objective function. Cominelli et al. (2007) proposed a gradient-based multiscale parameterization method. They used the multiscale zone as history matching parameter. D'Windt (2007) proposed a hybrid approach to compute permeability based on Carman-Kozeny equation. His suggested an approach for defining 'flow zone indicators' for identifying rock types. Most of these zonal approaches attempt to reduce the size of model parameter or dimension of history matching problems with certain proposed grouping or categories. Recent work of Bhark et al. (2011a) introduced a 'ratio cut' for reservoir modeling application. This zonation algorithm concept from spectral clustering can be found in their work. In this paper, we expand this spectral zonation algorithm and verify the applicability for the reservoir history matching problems.

3.3 Approach

Our proposed research consists of the following steps: (1) construct adjacency based Laplacian to capture spatial variability in subsurface properties (2) use graph partitioning techniques to create zonation and find cutting edges (3) apply the partitioning with history matching algorithms. The graphic cut from the model geometry and/or heterogeneity is not arbitrary and derived from optimization with graphic cutting metric.

- ***Construct Affinity Laplacian*** We construct affinity Laplacian from the prior connectivity and/or heterogeneity information (Bhark et al. 2011a). The connectivity strength between grid points should be defined based on geometry and heterogeneity. In this paper, we introduce three different ways to define the affinity. Grid Connectivity Laplacian (GCL) is based on pure connection between the adjacency grids. Adjacency Based Laplacian (ABL) is constructed with model heterogeneity and Euclidean distance. These two Laplacian are mostly used on graphic partition algorithm. A new Prior-weighted Connectivity Laplacian (PCL) is also proposed in this paper. This Laplacian has both connectivity and prior information, which are important key factors in reservoir flow dynamics.

- ***Model Segmentation from Spectral Clustering*** From eigenvalue decomposition of the affinity matrix, the leading eigenvectors can be attained. The 'second' eigenvector, more exactly 'eigenvector corresponding to smallest positive eigenvalue', will be used for spectral clustering. The reason of using 'second' vector is described more details in the mathematical formulation section. The segmented zones represent the dissimilar facies or disjointed region in the subsurface domain.

- ***Deciding clustering algorithm and number of Segments*** The spectral clustering itself is a heuristic approach. Also, there are many algorithms in the spectral clustering area and there will return similar but different zones. Note that we use the clustering to propose history matching zonation, not just for clustering itself. In other words, we should decide in meaningful zones for history matching. It requires some experiments and deciding the number of segments is a trade-off between history matching computation time and resolution. We also illustrate various zonation results to explain these issues.

- ***Application to History Matching*** Once we segmented the reservoir model, we can calibrate prior model with respect to dynamic observation or seismic data, which is a routine process in history matching practices. We can use gradient based optimization approach (Conjugate Gradient or L-BFGS) or derivative free methods (EnKF or GA), which are very popular and have been applied in many history matching cases. Our selected algorithm is the well-known evolutionary optimization, Genetic Algorithm (GA), to find optimal zonal multiplier for history matching.

From the image clustering theory (Hagen and Kahng 1992; Shi and Malik 2000; von Luxburg 2007), the 'second' eigenvector, or 'the smallest positive eigenvalue and its corresponding eigenvector' represent model partitioning. With this second vector, we can suggest an optimal reservoir model zonation for the next stage. This approach is particularly applicable when we use a hierarchal history matching approach (Massonnat et al. 2002; Yin et al. 2010). Our segmentation method can propose optimal multiplicative zonation in the global history matching stage with low resolution. Then, we can further calibrate with local fine scale algorithm, for example, streamline assisted history matching (Vasco et al. 1999) or reparameterization approach (Bhark et al. 2011a).

3.4 Illustration of Procedure

We illustrate using a simple 5 spots synthetic example to verify our proposed algorithm. In this model, there is a water injection well in the middle (I1) and four producing wells at each corner as in **Fig. 3.2**. In this history matching problem, our objective function is reducing water cut misfit between observation data and calculated response from the finite difference simulator by calibrating gird block permeability (k_x).

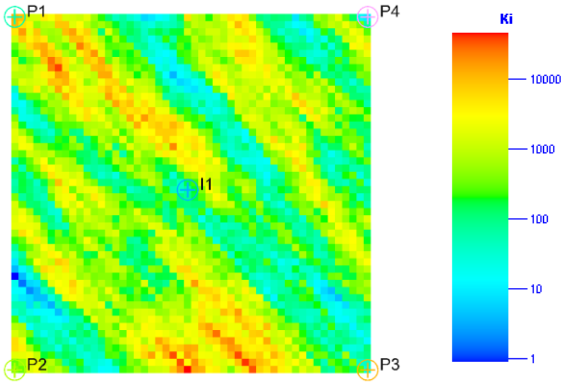

Figure 3.2. Initial Model with Heterogeneous Permeability Field

3.4.1 Construction of the Affinity Laplacian Matrix and Computing the Second Eigenvector

First step is constructing the affinity Laplacian based on grid property and/or connectivity. **Fig. 3.3** illustrates the leading eigenvectors from an eigenvalue decomposition of the Laplacian. Note that the first eigenvalue is always zero and its corresponding eigenvector is a constant because the graph Laplacian are always positive semi-definite (von Luxburg 2007). Among these leading eigenvectors, the 'second' eigenvector, shown inside the box will be used for spectral clustering.

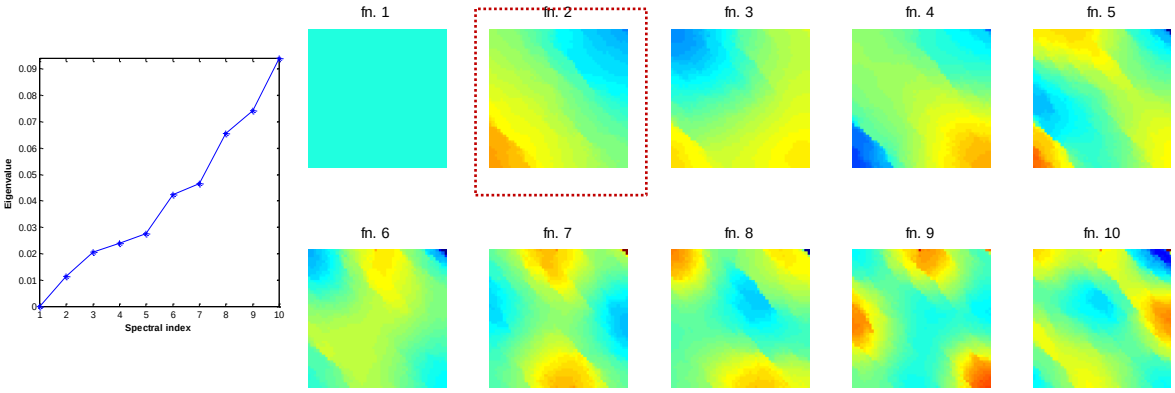

Figure 3.3. Leading Eigenvalue and its Corresponding Eigenvectors; Increasing Order

3.4.2 Model Segmentation from Spectral Clustering

By using the second eigenvector, the optimal partitioning can be achieved (Weiss 1999) and this is illustrated in **Fig. 3.4**. If we compare **Fig. 3.2** and **Fig. 3.4**, the segmented pieces represent the main heterogeneity trends. This is a key advantage that we can obtain from spectral clustering. We can preserve main heterogeneity features, which come from the underlying geostatic and petro-physical analysis. What we attempt to preserve the features during the history matching process.

In **Fig. 3.4**, one more important point to note is the way to do sub-partitioning from fewer to more segments, i.e. from the segments 2 to 3 or 4. It will subdivide it in existing segment to generate new segments by 'bi-partitioning' (Shi and Malik 2000; Wang and Siskind 2003). This is how the spectral clustering works, and we will discuss it more details in the mathematical formulation section.

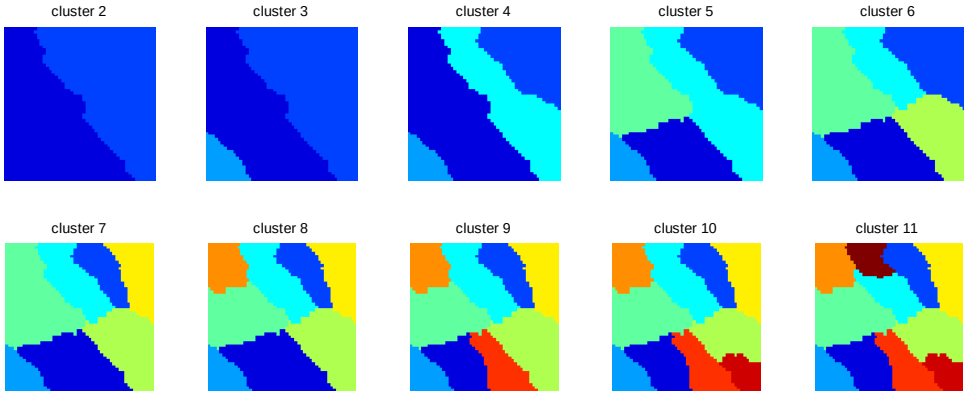

Figure 3.4. Segmented Model (Ratio cut)

3.4.3 Application to History Matching

In this section, we utilize the generated segments for history matching. To verify the robustness of our proposed zonation, we compared our zonation with box-type multipliers, common in manual history matching as shown in **Fig. 3.5**. In both cases, we use 4 multiplier zones with Genetic Algorithm (GA) for history matching. The specified population size is 20 and the GA is run until 4th generation in both cases.

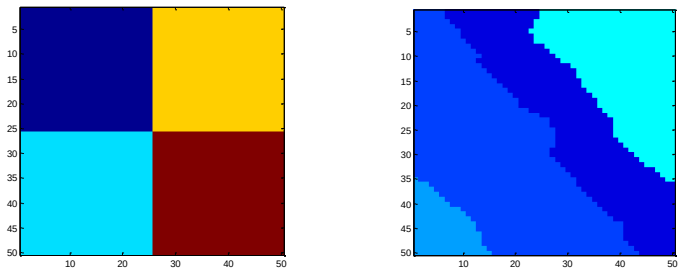

Figure 3.5. Tested History Matching Segmentations; Box Type (Left) and Proposing (Right)

The Genetic Algorithm (GA) is an evolutionary algorithm for both constrained and unconstrained optimization. The GA mimics the process of natural evolution: inheritance, mutation, selection and crossover. After several stages of evolution, this algorithm returns an improved population compared to the initial population and best fitting solutions. **Fig. 3.6** illustrates the best fitting solution from both proposed zonal history matching and the conventional box type segmentation in **Fig. 3.5**.

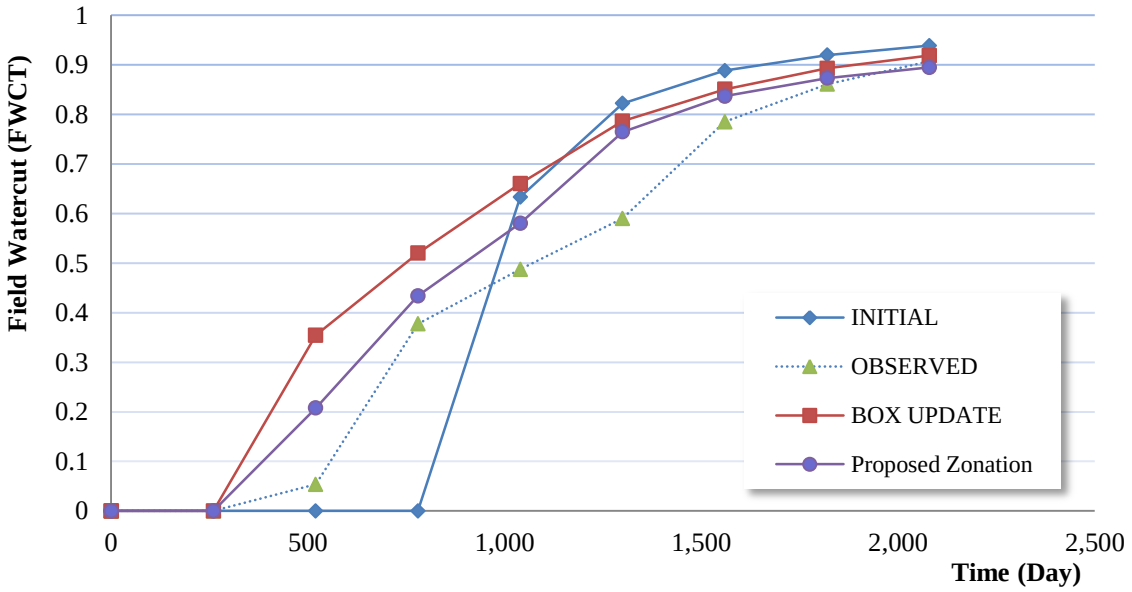

Figure 3.6. Updated Field Watercut Response after Genetic Algorithm (GA)

It is quite obvious that we can get better solution after GA optimization in both cases. Although, the proposed spectral zonation gives closer fitting solution in **Fig. 3.6**, it is difficult to tell which one is better because different number of population or generation make difference in the GA. But if we compare the final history matching quality as in **Fig. 3.7**, it is quite evident why our approach is providing more reasonable zoning criteria. Even box type multiplier can fit the dynamic response but it loses the prior model's main heterogeneity trends (**Fig. 3.7**; upper). Also, we need to change a lot from the original permeability; see the ΔPerm Field. Such discontinuity of the original model's main feature is quite often observed in the manual history matching results. From this example, it is clear that the new proposed algorithm can provide better zonal criteria for history matching.

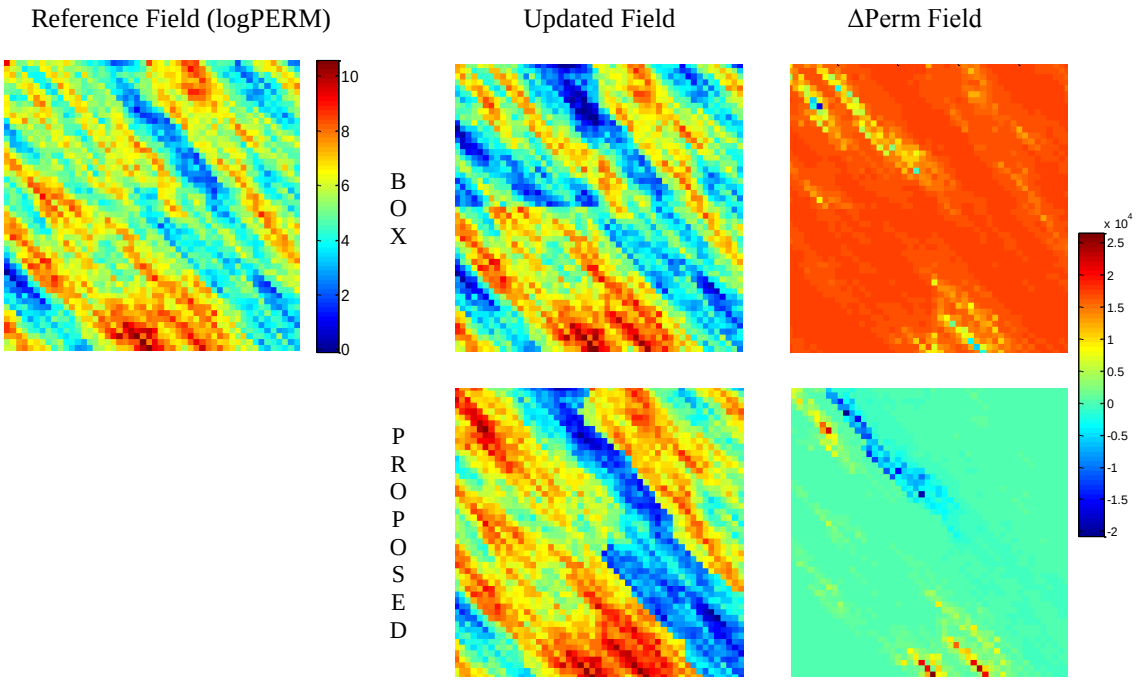

Figure 3.7. Compare History Matching Results

3.5 Mathematical Formulation

A graph G is defined as $G = (V, E)$, where V notates the vertex and E denotes the edge, can be separated into two subgraph $(C, \bar{C})$ set by simply drawing a cutting edge on the graph. The degree of dissimilarity of these segmented graphs can be computed as a 'cut' function, defined as the total weight of the edges that has been removed after the segmented in **Eq. 3.1** below.

$$cut(C, \overline{C}) = \sum_{u \in C, v \in \overline{C}} w(u, v) \tag{3.1}$$

The optimal segmentation is finding the 'optimal cut' of a graph *G*, where the generated edge minimizes this 'cut' value between two clusters. The procedure is : (1) constructing an affinity Laplacian matrix based on point connectivity (2) decomposing the Laplacian with eigenvalue decomposition (3) segmenting domain from the second eigenvector, known as Fiedler vector (Fiedler 1973), with graphic optimization algorithm.

3.5.1 Constructing Affinity Laplacian

The affinity Laplacian (L) is always symmetric and positive semidefinite, is defined as

$$L = D - W \tag{3.2}$$

In this formulation, *D* is the degree of affinity, *L* is Laplacian of system (also, called as Kirchhoff operator) and *W* is the connectivity weight matrix (or conductance matrix) between grid points, where matrix component $w_{ij} \geq 0$. The degree matrix *D* is a diagonal matrix, which defines the degree sum of connectivity strength (d_i) between one point (i) and others ($j \neq i$) as in **Eq. 3.3**.

$$d_i = \sum_{j=1}^{n} w_{ij} \tag{3.3}$$

We propose three different ways to formulate the connection weights (also called Affinity) between the grid points; Grid Connectivity based Laplacian (GCL), Adjacency Based Laplacian (ABL) and Prior-weighted Connectivity Laplacian (PCL).

Grid Connectivity based Laplacian (GCL)

The spectral mesh has been proposed in the field of machining learning and computer vision (Wu 2005; Zhang et al. 2010). This mesh grid construction has been applied to identify connectivity based parameterization (Bhark et al. 2011b; Bhark et al. 2011c). The generated Laplacian is used for reparameterization using leading eigenvectors for parameterization, not spectral clustering. As in **Eq. 3.4** below, the constructed Laplacian has immediate neighboring information on each matrix entry and this construction is powerful in complex geometry models including unstructured grids.

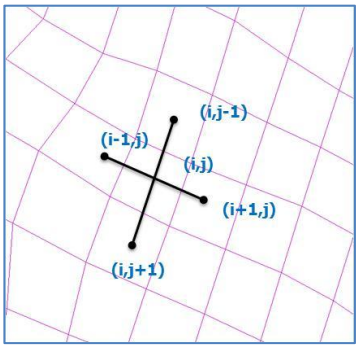

$$a_{ij} = \begin{cases} 1 & \text{if neighboring} \\ 0 & \text{otherwise} \end{cases} \tag{3.4}$$

Adjacency Based Laplacian (ABL)

The adjacency based measure is defined as the product of two exponential functions, which provide similarity measure of paired grid block i and j as in **Eq. 3.5** below (Bhark et al. 2011a; Shi and Malik 2000). First term of **Eq. 3.5** measure the distance between block *i* and *j*, second term is the corresponding property difference (permeability, porosity, pressure and so on). The adjacency beyond the Euclidean distance limit '*r*' is

always zero. Note that both the distance and property have value of one if two points are located at the same coordinate or have the same property value. Also, each term diminishes very fast if the difference is increasing due to the exponential form.

$$a_{ij} = \exp\left(\frac{-\left\| f_i - f_j \right\|_2^2}{\sigma_P}\right) \times \begin{cases} \exp\left(\dfrac{-\left\| x_i - x_j \right\|_2^2}{\sigma_I}\right) & if \ \left\| x_i - x_j \right\|_2 < r \\ 0 & else \end{cases} \quad (3.5)$$

In **Eq. 3.5**, variables σ_p and σ_I are defined as free parameters in spectral theories (Weiss 1999). There is no rigorous formulation but several proposals to select those two parameters and Euclidean cut off distance r. In fact, the spectral clustering performance is heavily dependent on the proper combination of these free parameters. Previous work of Bhark et al. (2011a), select these three parameter indirectly. They picked parameters such that two terms are 'similar' far from a point, where the parameters can be regarded as 'correlation thresholds for the property difference and distance between cell pairs and both zero beyond distance *r*'. Fischer and Poland (2004) proposed two different selection methods: manual using distance histogram or context-dependent similarity. Shi and Malik (2000) recommended to set the values between 10 to 20 percent of the parameter or distance range.

An interesting point is that if we select two free parameters as big numbers, the calculated adjacency is approaching very fast to the GCT affinity value ($a_{ij} = 1$) and will lose heterogeneity and/or distance measure. So, a proper combination of two free parameters as well as the cut off distance plays an important role to capture the prior information.

Our proposed approach is using variogram to select these three parameters. First, the Euclidean distance cut off 'r' is calculated from the 'range' of variogram analysis (Gringarten and Deutsch 1999) as shown in **Fig. 3.8**.

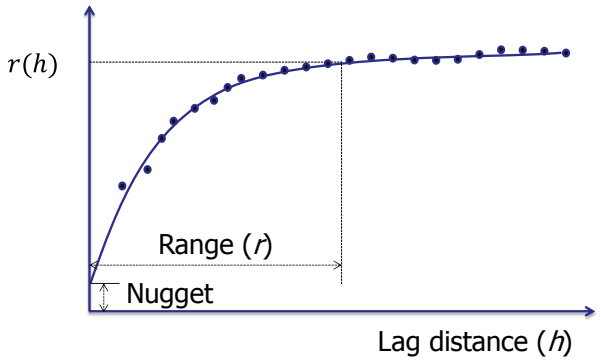

Figure 3.8. Variogram Model and Range (*r*)

Once we decide the cut off distance, we can easily decide the distance parameter σ_I. If we take a negligible value (ε, for example 0.001) at the boundary (r), the free parameter for distance (σ_I) can be calculated as in **Eq. 3.6**;

$$\sigma_I = -\frac{r^2}{\ln(\varepsilon)} \tag{3.6}$$

The free parameter for property σ_P can be calculated initially from the range of grid property value as in **Eq. 3.7**. This is an experimental formulation and comparable to suggestion of Shi and Malik (2000).

$$\sigma_P = S_p \sqrt{range(f_i)} \quad where \;\; S_P = 0.01 \sim 0.02 \tag{3.7}$$

In **Eq. 3.5**, we use different measures with L_2 norm but different order of definition is possible, i.e. L_1, L_3, L_4 and so on with new free parameters. Basically, higher order norms emphasize more the difference of grid property and/or connected distance. Ideally, the optimal combination for free parameters in this 'Gaussian kernel' type function is to determine variables σ_P and σ_I such that both exponential terms diminish to similar insignificant values (ε) near the range (r).

Prior weighted Connectivity Laplacian (PCL)

We propose a new affinity Laplacian construction as in below **Eq. 3.8**. This new formulation has both grid connectivity from GCL and prior model's heterogeneity as in ABL. In other words, the PCL formulation can capture faulted geometry, which is missing in ABL and can include prior heterogeneity, which is missing in GCL. The two free parameters in the formulation (**Eq. 3.8**) can be decided by the same approach as with ABL construction even though there is no distance cut off 'r' term in **Eq. 3.8**.

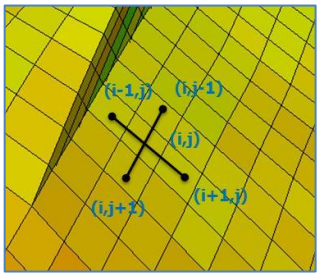

$$a_{ij} = \exp\left(\frac{-\left\| f_i - f_j \right\|_2^2}{\sigma_P}\right) \times \begin{cases} \exp\left(\dfrac{-\left\| x_i - x_j \right\|_2^2}{\sigma_I}\right) & \textit{if neighboring} \\ 0 & \textit{else} \end{cases} \quad (3.8)$$

This simple example illustrates how we construct the affinity Laplacian matrix in the simple 9 (3×3) grid data points as in **Fig. 3.9**. The lines between data points show the weighted connectivity and its strength (a_{ij}) from **Eq. 3.4, 3.5** and **3.8**.

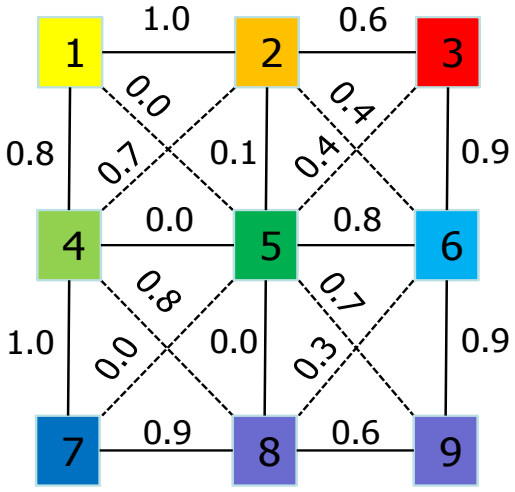

Figure 3.9. Discrete Grid Points (3×3)

The constructed Laplacian in **Fig. 3.10** illustrate the information captured from the same data points in **Fig. 3.9** by different definition of affinity. Note that diagonal term in each matrix (d_i) is the sum of the non-diagonal entries. PCL has the same matrix entry points as in GCL and have same weight as in ABL matrix between adjacency points. Only ABL takes diagonal connection in the affinity construction. Also in ABL, points between non-diagonal (for example, 1 to 6 or 1 to 9) can have non-zero connectivity values if Euclidean distance is inside the cut off 'r' and there exists a connectivity value from **Eq. 3.5**.

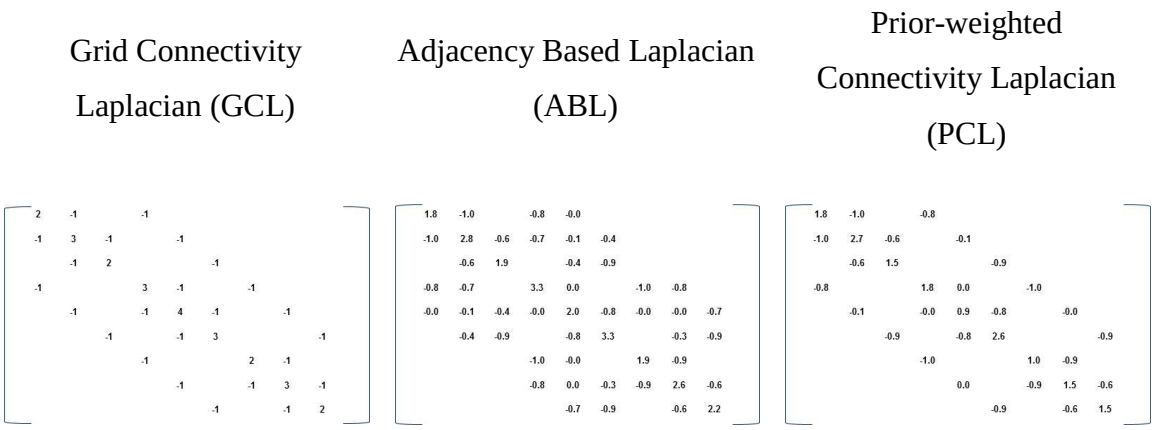

Figure 3.10. Affinity Laplacian Matrix Construction

We illustrate how different affinity constructions affect the second eigenvector and corresponding segmentation results from the model in **Fig. 3.11** (heterogeneous 9-spot synthetic model, **Fig. 3.2**); the grid connectivity Laplacian (GCL) performs cutting based on equal weigh on each grid. Both adjacency based Laplacian (ABL) and prior-weight connectivity Laplacian (PCL) take into account the model heterogeneity in the generated segments. An interesting point in **Fig. 3.11** is that the GCL clustering provides exactly the same clusters as in the box zones in **Fig. 3.5** (left), where we assumed that we don't have any prior knowledge and do a blind cutting.

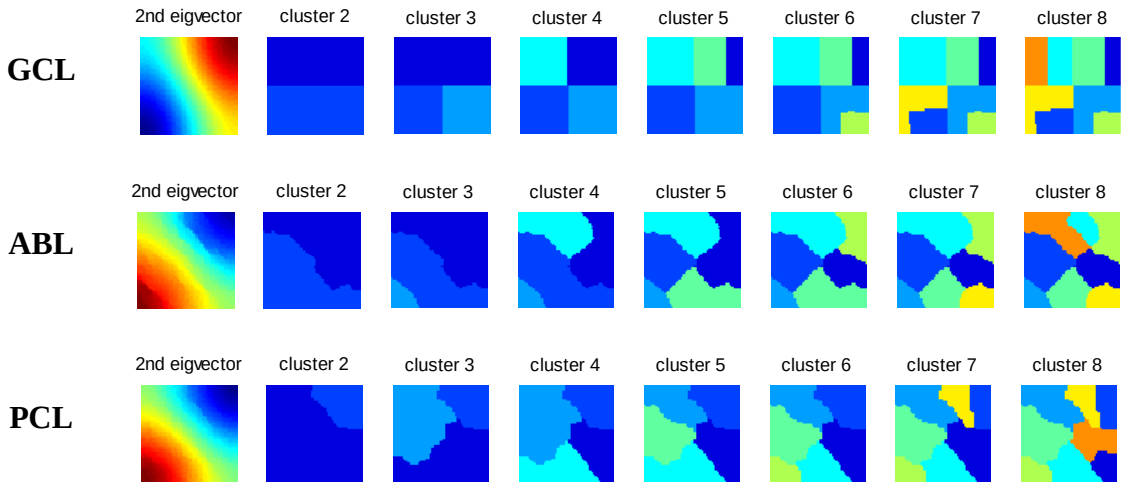

Figure 3.11. Second Eigenvector and Segmentation Results (Ncut) from Different Affinity Laplacian

3.5.2 Graphic Cut Algorithm

The fundamental concept of graph partitioning is solving a minimum cut problem. To get the optimal solution in this NP hard (von Luxburg 2007), Non-deterministic Polynomial-time hard in computational complexity theory, minimization problems. The spectral relaxation of 'ratio cut' (Hagen and Kahng 1992) and 'normalized cut' algorithm (Shi and Malik 2000) have been suggested and used as standard graphic partitioning criterion. Under the baseline of these two main frame works, many improved algorithms have been proposed (Buhler and Hein 2009; Fischer and Poland 2004; Hein and Bühler 2010; Wang and Siskind 2003). In this section, we explain the basic idea of two representative partitioning and their improvement by using Cheeger Constants (Cheeger 1970).

Explaining 'graphic cut algorithm' is related to graphic theoretic language. So, we first clarify some important definitions. The notation $|A|$ is the size of A defined by its number of vertices and $vol(A)$ is the size of A by summing over the weights of all edges attached to the vertices.

Ratio Cut (Rcut)

The ratio cut algorithm is to find a 'cut', which is relaxed by the vertices between clusters (Hagen and Kahng 1992). The size of a subset *C* in a graph *G* is measured by its number of vertices $|C|$;

$$Rcut(C,\overline{C}) = \frac{cut(C,\overline{C})}{|C|} + \frac{cut(C,\overline{C})}{|\overline{C}|} \tag{3.9}$$

Normalized Cut (Ncut)

The size of clustering is measured by the weights of its cutting edge (Shi and Malik 2000). The normalized cut is relaxed by the weight of edges between clusters. The main difference between 'ratio' cut and 'normalized' cut is using un-normalized Laplacian (ratio cut) versus the normalized one (see next section for detail).

$$Ncut(C,\overline{C}) = \frac{cut(C,\overline{C})}{vol(C)} + \frac{cut(C,\overline{C})}{vol(\overline{C})} \tag{3.10}$$

Ratio Cheeger Cut (RCC)

The Cheeger constant is a measurement of 'bottleneckedness' in a graph (Cheeger 1970). The baseline of Cheeger Constant is defining isoparametric inequality in a Riemannian geometry. Hein and Büehler (2010) proved that the Cheeger cut is at least as good as standard spectral clustering with expensive of computation time, which is explained with the Cheeger inequality (Amghibech 2003). They solve the nonlinear eigen problems (Cheeger Cut) with Inverse Power Method (IPM). In the Ratio Cheeger Cut (RCC), the balanced cut is optimized by the minimum cardinality of the clusters;

$$RCC(C,\overline{C}) = \frac{cut(C,\overline{C})}{\min\{|C|, |\overline{C}|\}} \tag{4.11}$$

Normalized Cheeger Cut (NCC)

The Normalized Cheeger Cut (NCC) is optimized by the minimum volume of clusters. Recall that volume is summation of degree in a grid (Buhler and Hein 2009; Hein and Bühler 2010). From spectral theory, 'normalized cut' is statistically more consistent than 'ratio cut' (von Luxburg 2007) and 'Cheeger cut' performs at least equal to 'standard' cut or better in most cases (Hein and Bühler 2010). Hence, NCC is recommended for first trial among the four cutting algorithms.

$$NCC(C,\bar{C}) = \frac{cut(C,\bar{C})}{\min\{vol(C), vol(\bar{C})\}} \tag{3.12}$$

We illustrate the segmentation results in **Fig. 3.12** from the same 'second' eigenvector. Also, grid property (permeability) field is the same as **Fig. 3.2**. It is obvious that different algorithm returns different relaxation cut as illustrated in **Fig. 3.12**.

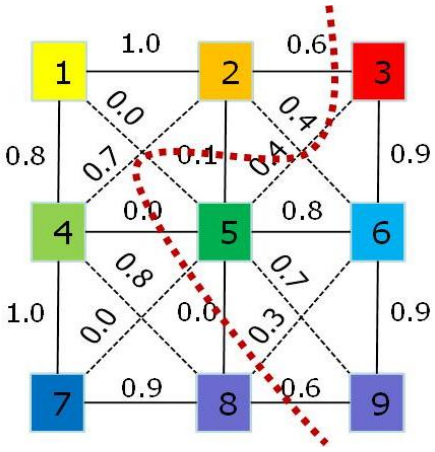

$$Rcut = \frac{cut(C,\bar{C})}{|C|} + \frac{cut(C,\bar{C})}{|\bar{C}|} = \frac{2.0}{5} + \frac{2.0}{4} = 0.9$$

$$Ncut = \frac{cut(C,\bar{C})}{vol(C)} + \frac{cut(C,\bar{C})}{vol(\bar{C})}$$

$$= \frac{2.0}{1.8+2.1+3.3+1.9+2.6} + \frac{2.0}{1.9+2.0+3.3+2.2} = 0.384$$

$$RCC = \frac{cut(C,\bar{C})}{\min\{|C|, |\bar{C}|\}} = \frac{2.0}{4} + \frac{2.0}{4} = 1.0$$

$$NCC = \frac{cut(C,\bar{C})}{\min\{vol(C), vol(\bar{C})\}}$$

$$= \frac{2.0}{1.9+2.0+3.3+2.2} + \frac{2.0}{1.9+2.0+3.3+2.2} = 0.426$$

(a) Calculation Illustrations

Figure 3.12. Second eigenvector and Segmentation results by Different Clustering Algorithms (using Adjacency Based Laplacian)

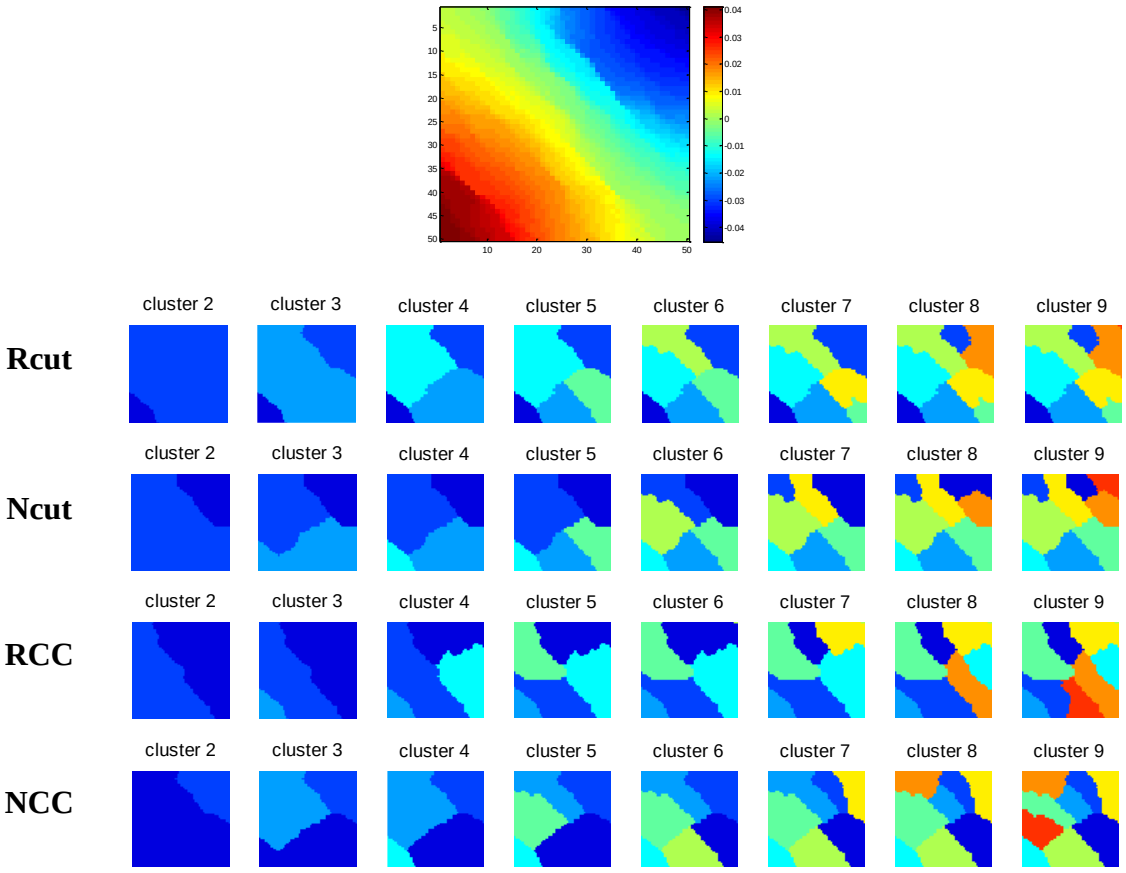

(b) Cutting Results from Different Algorithms

Figure 3.12. Continued

You may raise a question: "which algorithm is better one?" or "How many clusters do we have to use for history matching?". The selection of algorithm and number of optimal clustering will be discussed in the 'nature of graph partitioning' section.

3.5.3 Optimal Partitioning with Second Eigenvector

For the graph partitioning, we use the 'second' eigenvector of the affinity Laplacian, constructed from the connectivity definition. The reason why we use the 'second' eigenvector can be clarified with both physical and mathematical explanations (Shi and Malik 2000; von Luxburg 2007). Note that K-means clustering, also used in many

clustering problems, is different from spectral clustering and it will not use 'second' eigenvector (Fischer and Poland 2004).

Physical Explanation

A physical analogy is provided by comparing a spring-mass system (Shi and Malik 2000) or vibration of a string as in **Eq. 3.13**. We can relate graphic nodes as physical nodes and graph edges as moving part of string inside the node as in **Fig. 3.12**. Imagine that if we shake this string with a strong oscillation frequency, the stationary nodes will not move at steady state and will divide the region into subpieces as in **Fig. 3.13**. In the equation, x is a location in a string, y is magnitude of vibration, t is time of a certain moment, μ is linear mass and T is acting tension on each side of the string.

$$\frac{\partial^2 y(x,t)}{\partial x^2} = \frac{\mu}{T}\frac{\partial^2 y(x,t)}{\partial t^2} \tag{3.13}$$

From general solution of this wave equation with fixed ends, where f_n is vibration frequency, L_s is length of the string and n_m is nth mode;

$$y(x,t) = y_m \sin\left(\frac{n_m \pi}{L_s} x\right)\cos(2\pi f_n t) \tag{3.14}$$

The steady solution of **Eq. 3.14** can be derived by plugging into **Eq. 3.13**;

$$y_k\left(\frac{n_m \pi}{L_s}\right)^2 \sin\left(\frac{n_m \pi}{L_s} x\right)\cos(2\pi f_k t) = y_k (2\pi f_n)^2 \left(\frac{\mu}{T}\right)\sin\left(\frac{n_m \pi}{L_s} x\right)\cos(2\pi f_k t) \tag{3.15}$$

Eq. 3.16 below satisfies the steady state of string vibration with non-trivial terms of k^{th} harmonic mode;

$$\left(\frac{T}{\mu}\right)y_k = \left(\frac{2 f_k L_s}{n_m}\right)^2 y_k \tag{3.16}$$

The amplitude component y_k gives the steady state displacement of the fundamental vibration in each k^{th} harmonic mode, which is eigenvector of a system. We also can derive harmonic frequency f_k that relates the energy (f_k^2) to sustain each vibration mode, where it minimized if *k* is smallest in **Eq. 3.17**;

$$f_k = \frac{n_m}{2L_s}\sqrt{\frac{T}{\mu}} \tag{3.17}$$

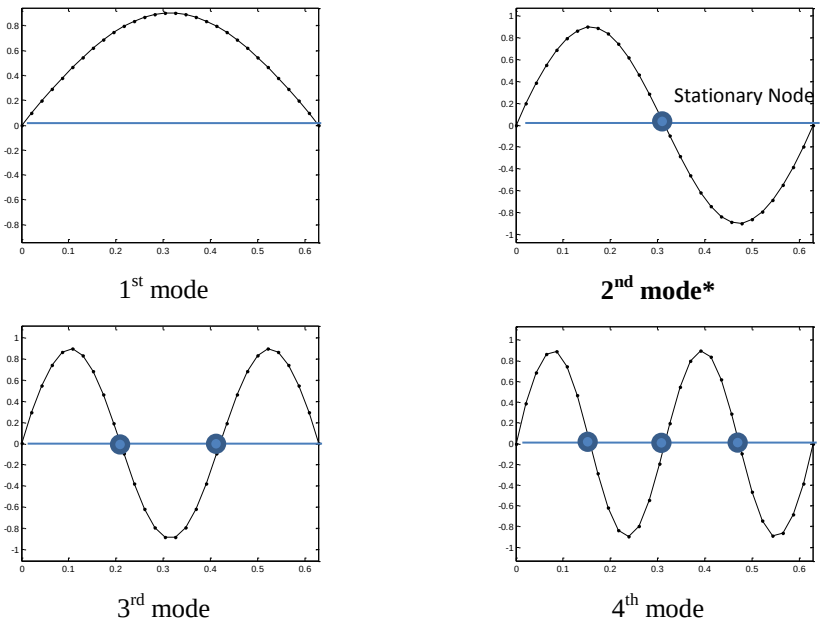

Figure 3.13. Fundamental Vibration Modes of Sting Problem; Leading Eigenvectors

Therefore, the first mode is constant and the second eigenvalue is the first steady state solution, to divide the zone as in **Fig. 3.13**. Physically, it requires the minimal energy to sustain segments or least effort to divide. In other words, finding graphic cutting edge is

a process to find "minimal effort" stationary node to divide the system. Note that 'second' eigenvector always divide the system into 'two' pieces which is called bipartitioning. This is how the spectral clustering works in most of partitioning algorithms.

Mathematical Explanation

In **Eq. 3.1**, we define the 'cut' function for measuring the degree of dissimilarity between two pieces. Fiedler (1973, 1975) proved and applied the algebraic connectivity theory from second eigenvector (called Fiedler vector) of non-directed graphs. Hagen and Kahng (1992) provide the mathematical bipartition for 'ratio cut' algorithm. Shi and Malik (2000) also prove that second eigenvector offer optimal 'normalized cut'. It is an important spectral property of eigenspectrum. If the graph *G* is connected, the second eigenvalue (λ_2; also called algebraic connectivity) is positive ($\lambda_1 = 0 \leq \lambda_2 \leq \cdots \leq \lambda_n$) and first eigngenvector is a constant (Pothen et al. 1990) as already shown in **Fig. 3.3**.

Finding optimal clustering can be proved by solving relaxation of simple balanced 'ratio' cuts (von Luxburg 2007) as in **Eq. 3.18**;

$$\min_{C,\overline{C}} cut(C,\overline{C}) \quad where, \quad |C| = |\overline{C}| \tag{3.18}$$

If we choose clustering $f = (f_1, f_2, \ldots, f_n)'$ such that

$$f_i = \begin{cases} 1 & if \quad x_i \in C \\ -1 & if \quad x_i \in \overline{C} \end{cases} \tag{3.19}$$

Here, we transformed the real value problem into discontinuous indicator vector space (von Luxburg 2007). From **Eq. 3.1**, we can rearrange as;

$$cut(C,\overline{C}) = \sum_{u \in C, v \in \overline{C}} w(u,v) = f'Lf = \frac{1}{2}\sum_{i,j} w_{ij}\left(f_i - f_j\right)^2 \tag{3.20}$$

We have already imposed condition that $|C| = |\bar{C}|$ from **Eq. 3.18**, which leads to **Eq. 3.21** for optimal condition;

$$\sum_i f_i = 0 \tag{3.21}$$

The above **Eq. 3.21** indicate that

$$f\vec{1} = 0 \quad or \quad f \perp \vec{1} \tag{3.22}$$

The vector f as defined in **Eq. 3.19** is orthogonal to the constant identity vector $\vec{1}$. Also, from same definition in **Eq. 3.19**, norm of vector f;

$$\|f\|^2 = \sum_{i=1}^{n} f_i^2 = |C| + |\overline{C}| = n \tag{3.23}$$

The optimal clustering, which is solving minimization problem as derived in **Eq. 3.20** from **Eq. 3.18**, can be rewritten from **Eq. 3.20**, **3.22** and **3.23** ($1/2$ is a scale factor and can be discarded) ;

$$\min_{C \subset V} f'Lf \quad subject\ to \quad f \perp \vec{1},\ f_i = \pm 1\ and\ \|f\| = \sqrt{n} \tag{3.24}$$

By Rayleigh Quotient (also known as Rayleigh-Ritz theorem), it can be immediately proved that the solution of this problem is given by the second eigenvector of Laplacian (L). Recall that 'second' means the smallest non-zero eigenvalue and its corresponding eigenvector (Weiss 1960). So, we can approximate the optimal solution by the second eigenvector in 'ratio cut' relaxation problems.

The optimal 'normalized' cut is also easily proved by same approach from the comparable one (**Eq. 3.18** with **Eq. 3.25**);

$$\min_{C,\bar{C}} cut(C,\bar{C}) \;\; where, \;\; vol(C) = vol(\bar{C}) \tag{3.25}$$

We can derive the imposed conditions as $(Df)\vec{1} = 0$, $f'Df = vol(C)$ (von Luxburg 2007). Recall that D has been defined as degree of affinity in **Eq. 3.2**.

$$\min_{C \subset V} f'Lf \;\; subject \; to \;\; Df \perp \vec{1}, \; f_i = \pm 1 \; and \; f'Df = vol(V) \tag{3.26}$$

Now, we substitute f with normalized vector $g = D^{1/2}f$ in **Eq. 3.26** and $L_{sym} = D^{-1/2}LD^{1/2}$;

$$\min_{C \subset V} g'L_{sym}g \;\; subject \; to \;\; g \perp D^{1/2}\vec{1}, \; f_i = \pm 1 \; and \; \|g\| = \sqrt{vol(V)} \tag{3.27}$$

Consequently, we also arrive at the standard Rayleigh Quotient type formulation as in **Eq. 3.27**. The relaxation solution g is given by the second eigenvector of normalized Laplacian (L_{sym}). Now, we can see that 'ratio' cut leads to un-normalized clustering as in **Eq. 3.24** while relaxing 'normalized' cut leads to normalized solution in **Eq. 3.27**. Hence generally speaking, the 'normalized' cut is more statistically consistent than 'ratio' cut (von Luxburg 2007).

3.5.4 Nature of Graph Partitioning

We already see that different affinity construction and relaxation algorithm will lead to different segmentation. There are also many more affinity construction and algorithms that we cannot illustrate in this paper. Even, a small change in selecting free parameters will induce quite different segmentations. It is almost impossible to recommend one single method for reservoir model segmentation. Instead, we will explore the true nature of graph partitioning and will derive 'tentative' answer to select cutting algorithm and number of segments for history matching.

3.5.5 Recursive bipartitioning and Hierarchical Approach

The fundamental idea of getting more clusters is bipartitioning inside the subdomain using its ‘new’ second eigenvector. It is a recursive and hierarchical divisive approach. After initial partitioning of the graph into two pieces, reapply the same procedure to the sub graphs as in **Fig. 3.14**. The new number of groups is controlled by imposing threshold to the objective function. If we require odd number of segments, the clustering algorithm compares and chooses a piece such that sub partition makes overall ‘cut’ value minimum.

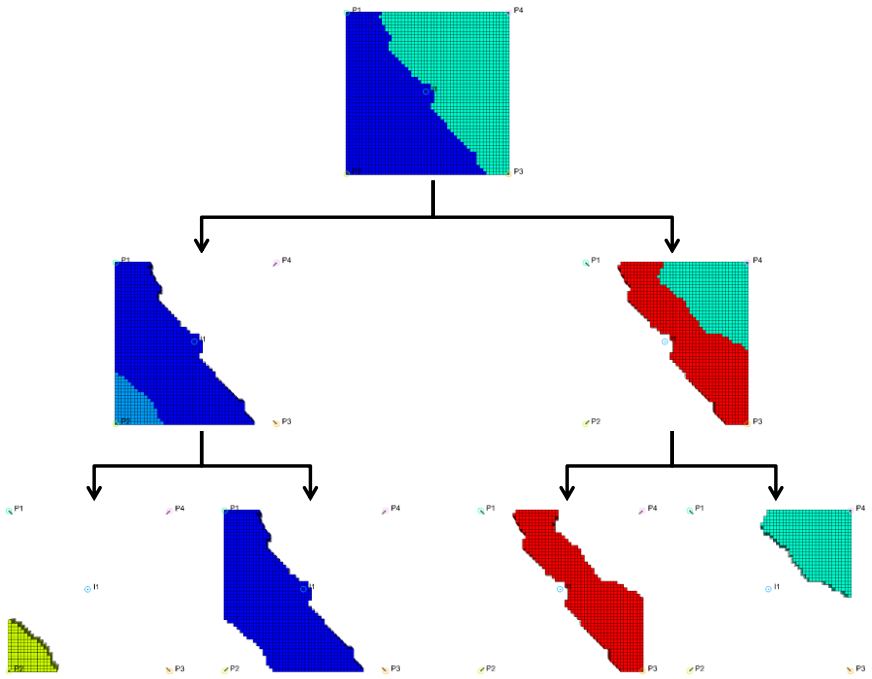

Figure 3.14. A Hierarchal Bipartitioning

One important observation in **Fig. 3.14** is that sub-partitioning will not change the previously generated cutting edge. Hence, more numbers of segmentation will ‘always’ make higher degrees of freedom.

3.5.6 Facies Edge Detect

The strength of spectral clustering is detecting the clear edge of a group for both continuous and discontinuous medium. To verify this important property of our approach, we test with a very simple 3 facies field in **Fig. 3.15**.

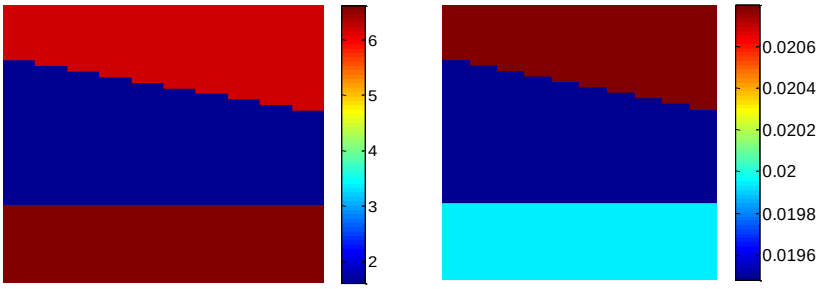

Figure 3.15. Log-Permeability in 3 Different Facies (Left) and Second Eigenvector of Adjacency based Construction (Right)

The ABL affinity Laplacian is constructed from **Eq. 3.5** and decomposed into eigenspectrum. The eigenvector in **Fig. 3.15** (right) has exactly same distribution as the original facies. From this second vector, we get clustering with ratio cut. **Fig. 3.16** shows how it recaptures the facies in this example. Other algorithms can also successfully detect the facies boundary edge. This is the main underlying idea to use spectral clustering for reservoir model segmentation.

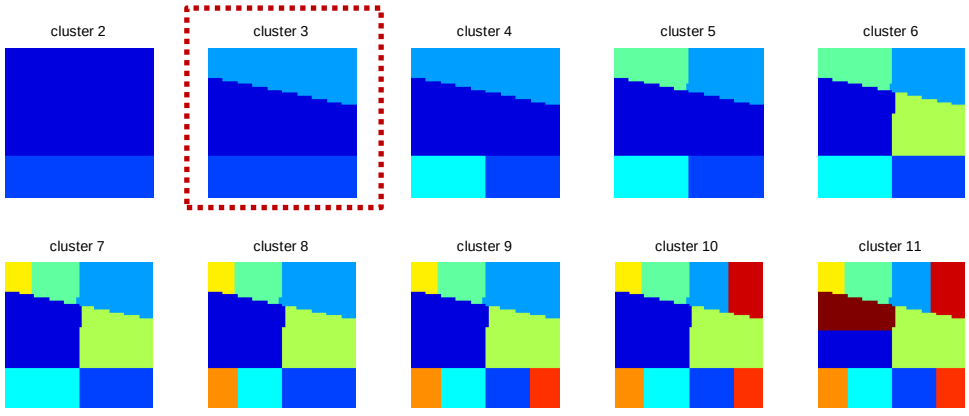

Figure 3.16. Segmented Zone from Ratio Cut and Facies edge detection (ABL)

3.5.7 NP hardness and Heuristic Approach

The clustering has no ground truth and is naturally an unsupervised problem in itself. This makes it hard to find optimal clustering in real problems. Also, the graph partitioning is a well-known NP hard (non-deterministic polynomial-time hard) problem (Wang and Siskind 2003). The clustering results at some parts of the space may affect a completely different region. Hence, one important property of spectral clustering is that algorithm requires a heuristic approach and trials to get good segmentations.

3.5.8 A Good Segmentation; Algorithm Point of View

Getting a good segmentation starts from choosing a proper affinity Laplacian. The adjacency based Laplacian (ABL) leans toward capturing model heterogeneity. The grid connectivity Laplacian (GCL) has advantageous in complex and faulted geometry but takes no prior heterogeneity into account. Prior-weighted connectivity Laplacian (PCL) is standing in the middle as in **Fig 3.17**.

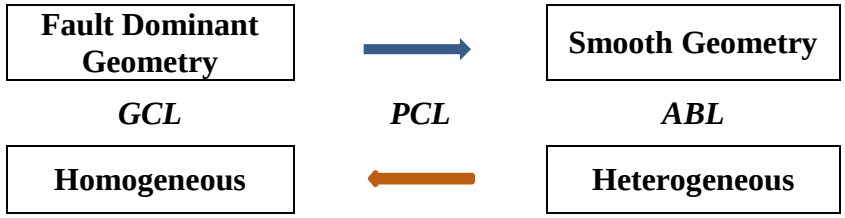

Figure 3.17. Relationship between Affinity Laplacian and Geological Models

Exploring the two free parameters (σ_I, σ_P) and cut off distance (r) is also important issue to get a connected graph. In **Fig 3.18**, we illustrate the exponential diminishing behavior of two 'Gaussian Kernel Function' from **Eq. 3.5** (σ_P, $\sigma_I = 0.1, 1, 10, 100$, r = 1.5). The previous work of Bhark et al. (2011a) showed how various parameters affect the eigenspectrum.

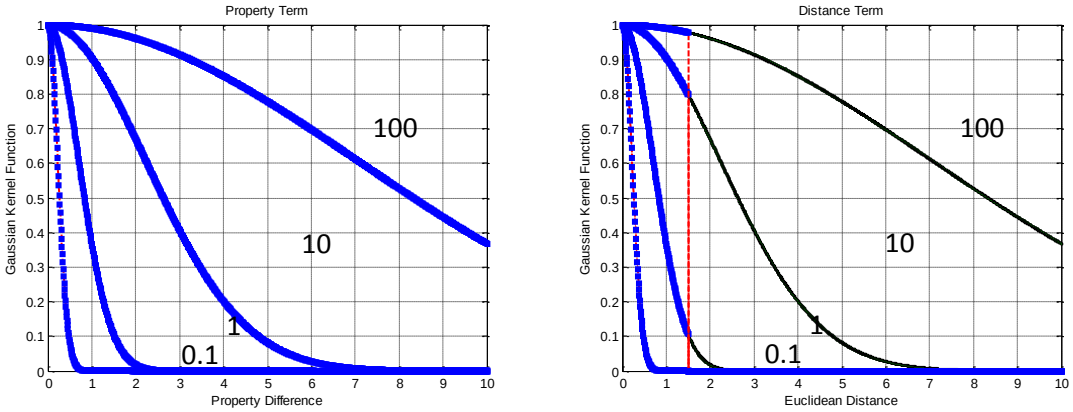

Figure 3.18. Diminishing Behavior of Adjacency Measures

The role of scale factor (S_P) or the property parameter (σ_P) is examined in **Fig. 3.19** (r = 170ft, σ_I = 4.1837E3, ABL, NCC). For small scale factor (S_P = 0.005), the second eigenvector looks less variable (upper left; looks homogeneous but it isn't) but finds sharper cutting edges. Larger scale factors miss prior heterogeneity and result in wide and stable clustering (S_P = 0.10) with little prior features.

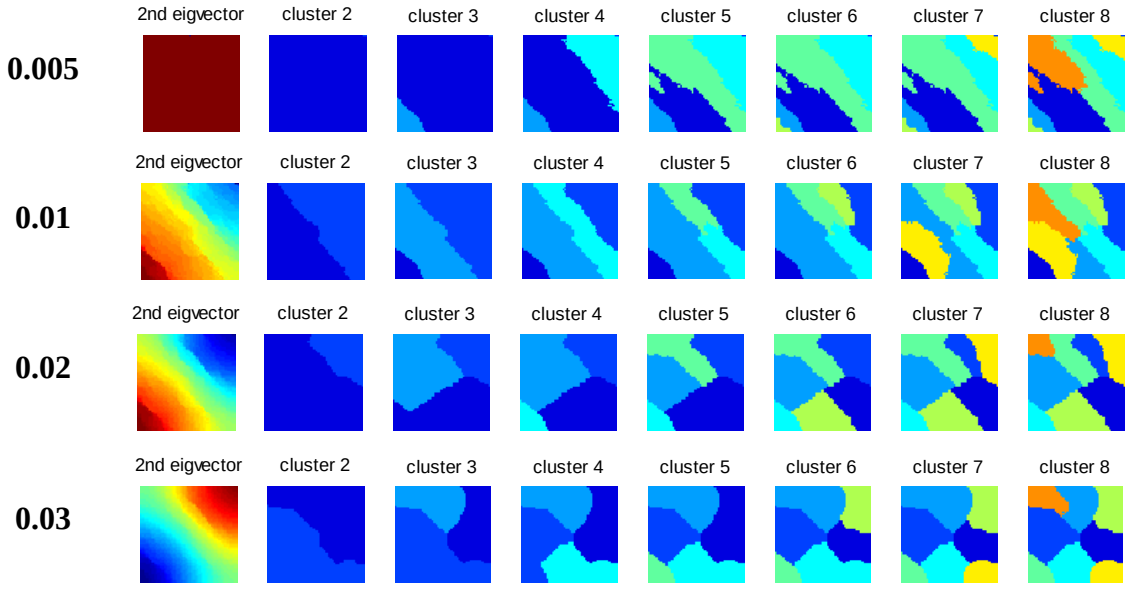

Figure 3.19. Effect of Scale Factor in Eq. 5 on Second Eigenvector and Clustering

Figure 3.19. Continued

Also, we explore the cut off distance (r) and the computed parameter (σ_I) from **Eq. 3.6**. Note that a value (ε) in **Eq. 3.6** equal to 0.001 throughout the paper. The grid block size is uniform with 32.8 ft in this model and minimum '*r*' should be bigger than that for a connected graph *G*.

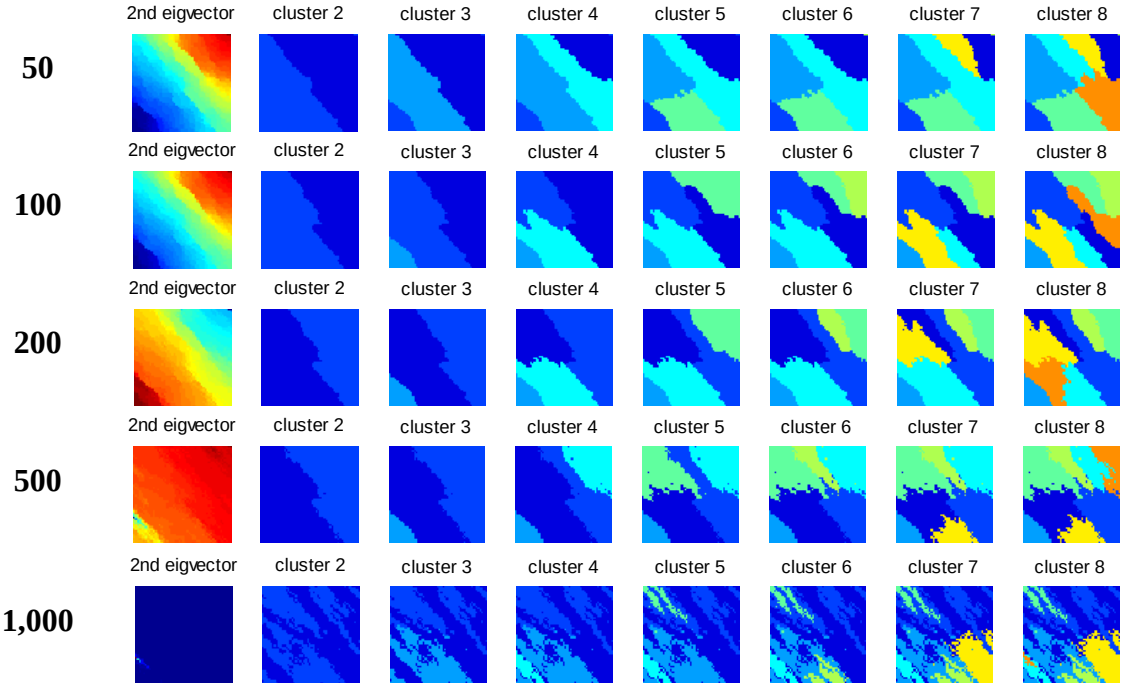

Figure 3.20. Effect of Cut off Distance (*r*) in Eq. 4.6 on Second Eigenvector and Clustering

In the smaller cut off range, we get clearer cutting edge. If we apply bigger cut off criteria (r = 1,000 *ft*), the edge becomes indistinguishable due to wider diagonal terms in affinity Laplacian as in **Fig. 3.21**. This causes 'mixing' between different zones.

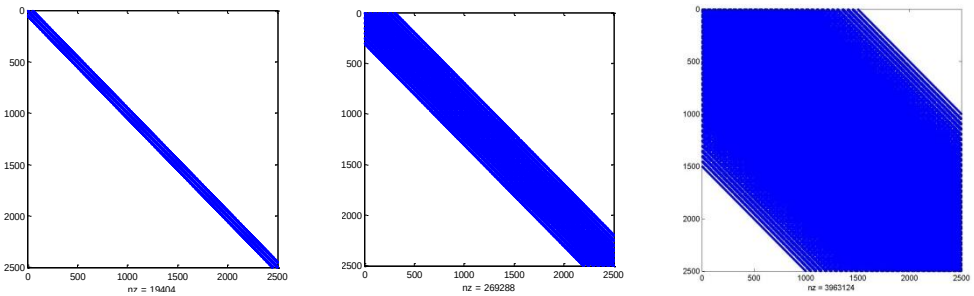

r = 50 r = 200 r = 1,000

Figure 3.21. Constructed Adjacency Based Laplacian (ABL) Matrix

As we illustrate in **Fig. 3.19** and **3.20** (r = 170*ft*, $\boldsymbol{S_P = 0.01}$, ABL, NCC), the optimal relaxation of a graph is heavily dependent on two free parameters (σ_P, σ_I) and cut off distance (r) in the adjacency based Laplacian (ABL). Comparatively, grid connectivity based Laplacian (GCL) is free of that dependence. From the spectral image theory point of view, there is no rigorous guideline to choose the type of affinity Laplacian and free parameters. There are some the guideline for this important points (Igor and Jan 2004; von Luxburg 2007) but there are not extensively tested for many different cases. In the reservoir engineering application, we provide a general guideline for affinity Laplacian in **Fig. 3.17** and **Eq. 3.6** and **3.7** for initial free parameters selection.

The other point, we need to address, is deciding the number of clusters for history matching. This is an old issue in spectral clustering theories (Igor and Jan 2004; von Luxburg 2007). There has been several methodology for suggesting optimal number of clustering: stability analysis (Hur et al. 2002), the gap statistic (Tibshirani et al. 2000), an Information-theoretic approach (Still and Bialek 2003) and the eigengap heuristic analysis (von Luxburg 2007). Those approaches are useful to estimate optimally relaxed segmentation in spectral theory point of view. We also can refer to those algorithms for our decision. But, our segmentations are generated for history matching purposes. Hence, deciding the number of segmentation should reflect the computation power and history matching algorithms after segmentation. Again, this decision is a trade-off between computation time and degree of freedom for the next stage. Recall that spectral

clustering is a hierarchical approach and 'always' give higher degrees of freedom in higher number of segmentation.

The most important key point to get good clustering is that segmented pieces should be "meaningful" zones for history matching. This should be decided by geologic and engineering considerations.

3.6 History Matching: Genetic Algorithm (GA)

We adapt the method genetic algorithm, one of the well-developed evolutionary algorithms in reservoir history matching. Experimental design, genetic algorithm and response surface are used for calibrating geological features of initial reservoir model. The strengths of genetic algorithm are its wide flexibility in choice of parameters as well as construction of objective function. The objective function to optimize with GA is constructed as logarithmic summation of data misfits as in **Eq. 3.28**;

$$O(m) = O(m_1, m_2, ..., m_N) = \sum_{j=1}^{N_{objective}} \ln\left(\sum_{i=1}^{N_{Well}} \left| Obs_i - Sim_i \right| \right) \tag{3.28}$$

3.6.1 Field Application: Brugge

In this section, we apply our model segmentation approach to a field example. We choose the Brugge reservoir model in **Fig. 3.22**, a SPE benchmark case. This Brugge reservoir model has been widely used to evaluate closed-loop reservoir management strategy developments (Alhuthali 2009; Peters et al. 2010) and history matching algorithm verification (Bhark et al. 2011a; Vallhs and Naevdal 2009).

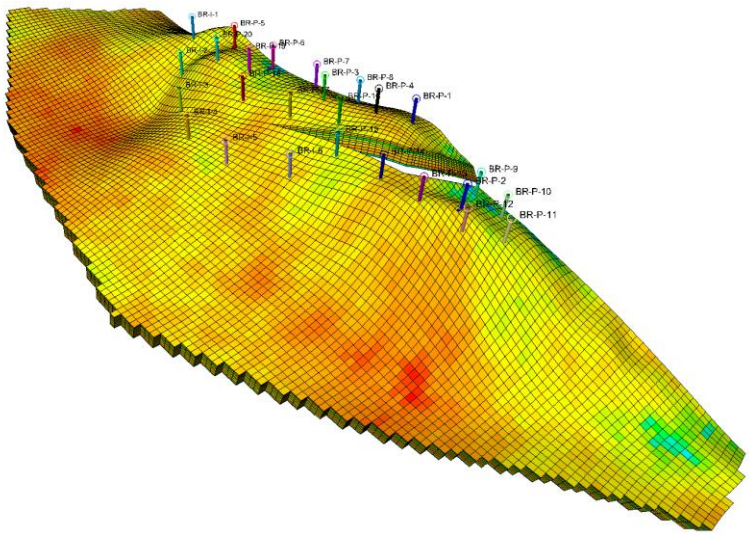

Figure 3.22. Brugge Reservoir Model

3.6.2 Field Descriptions

The Brugge reservoir model is developed by TNO and includes multiple high resolution prior permeability fields with unknown level of uncertainty. This reservoir is replicating a North Sea Brent type field with 44,355 active corner point grids. The wells consist of ten peripheral water injectors and twenty producers in the up structure. Production data are provided for 10 years: well water production rate (WWPR), well oil production rate (WOPR) and bottom-hole pressure (BHP). One realization of the prior permeability with nine layers is illustrated in **Fig. 3.23.** We used this realization for history matching from 104 realizations provided by TNO. This black oil model is targeted for characterizing oil flow dynamics; therefore, gas productions are not taken account. The boundary condition for producers is liquid rate control (LRAT) mode and injectors are under bottom hole pressure control (BHP). In this field application example, we will update permeability distribution by matching WWPR, WOPR and BHP at each producers.

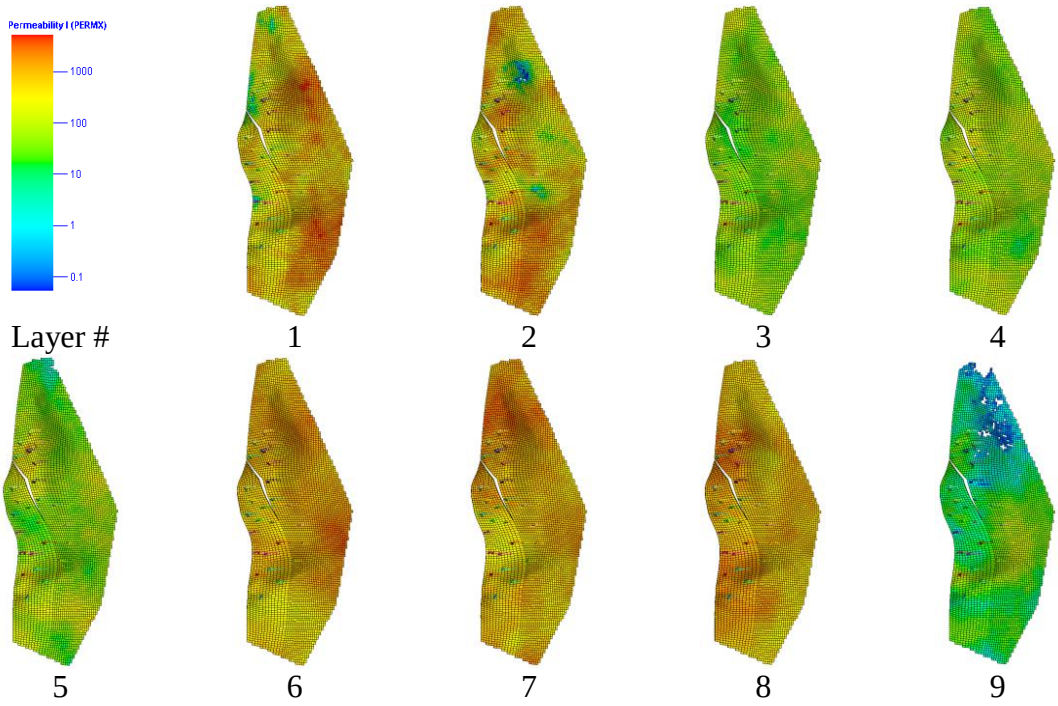

Figure 3.23. Permeability Distribution in Each Layer

3.6.3 Spectral Decomposition (Model Segmentation) in of the Permeability Field

For spectral decomposition, the affinity Laplacian is constructed based on adjacency (ABL) as in **Eq. 3.5**. This ABL construction is more attractive in smoothly varying permeability fields as in **Fig. 3.23** (see also suggestion in **Fig. 3.17**).

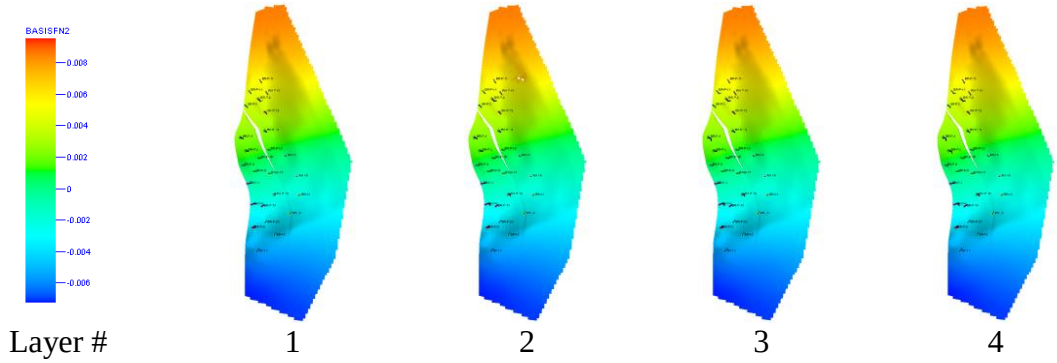

Figure 3.24. Second Eigenvector (ABL)

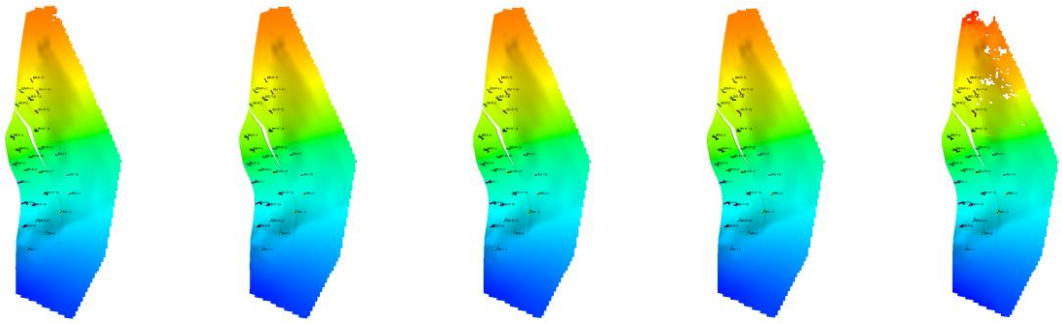

5 6 7 8 9

Figure 3.24. Continued

The spectral clustering is based on the second eigenvector (**Fig. 3.24**: $S_P = 0.055$, r = 2,000 *ft*). The generated segmentation zones from the Normalized Cheeger Cut (NCC) are illustrated in **Fig. 3.25**. This segmentation pieces are representative of different heterogeneity regions. A comparison with Ratio Cut (Rcut), Normalized Cut (Ncut) and Ratio Cheeger Cut (RCC) are discussed later.

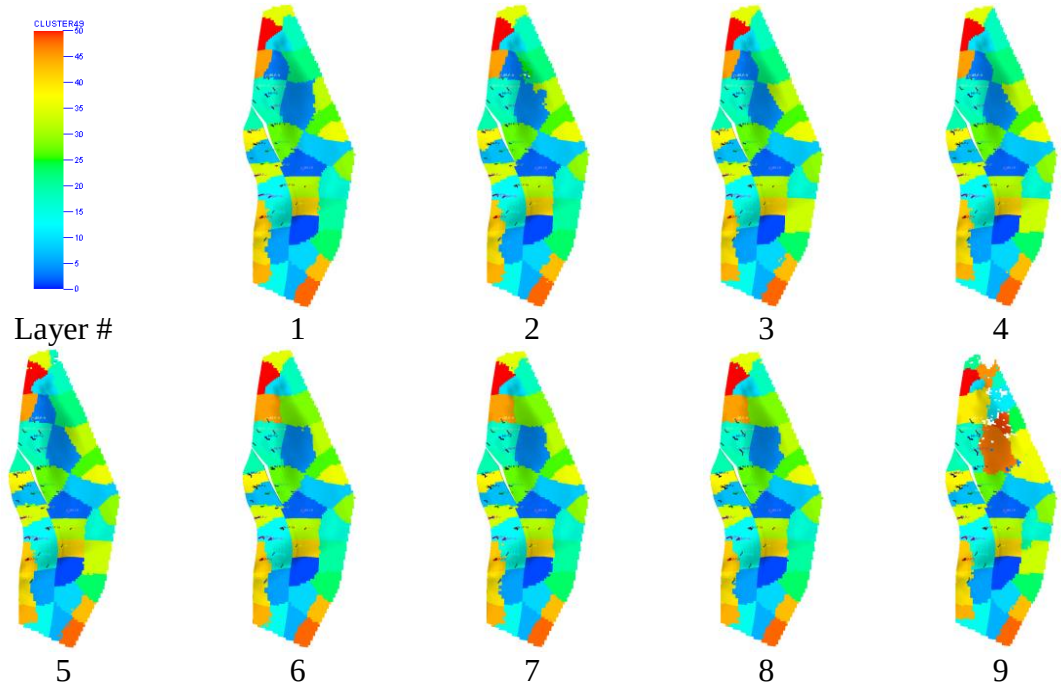

Figure 3.25. Segments from Normalized Cheeger Cut (NCC): 50 Zones

3.6.4 History Matching Results

In the history matching problem, our update parameter is now reduced to the number of segmentations instead of number of grids. As we previously mentioned, choosing the number of segmentation should be based on the computation capability for simulation and the type of application. Recall that selecting the number of cluster is a 'trade-off between computation power and the degree of freedom".

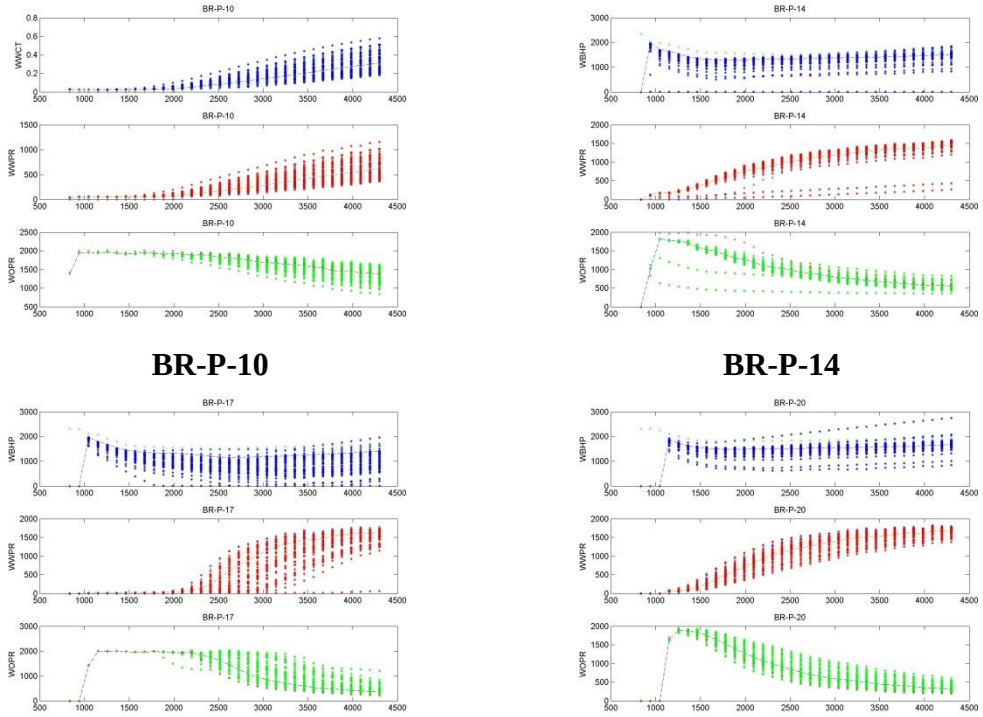

Figure 3.26. Genetic Algorithm Populations (WBHP, WWPR and WOPR); circle: Observed, line: Initial and dot: updated

Fig. 3.26 illustrates how the genetic algorithm works during the history matching process. We use a population size of 50 and 5 generations for the objective function optimization. The genetic algorithm performs evolution with inheritance, selection, mutation and cross over. The final best history matching results are shown in **Fig. 3.27**.

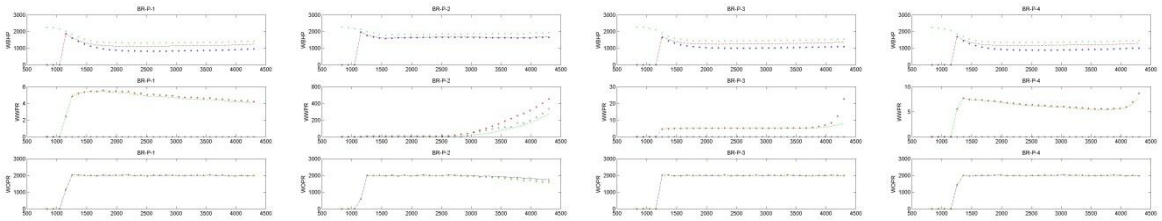

BR-P-1 **BR-P-2** **BR-P-3** **BR-P-4**

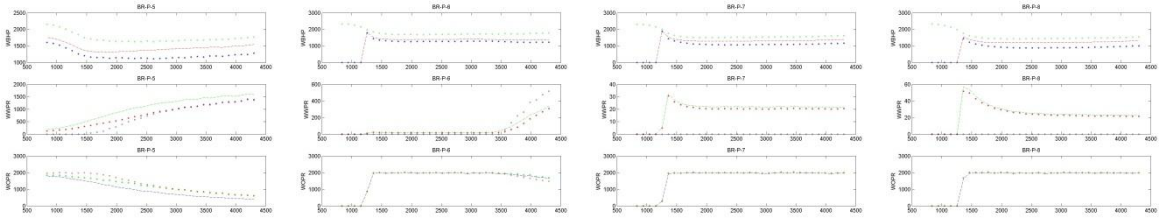

BR-P-5 **BR-P-6** **BR-P-7** **BR-P-8**

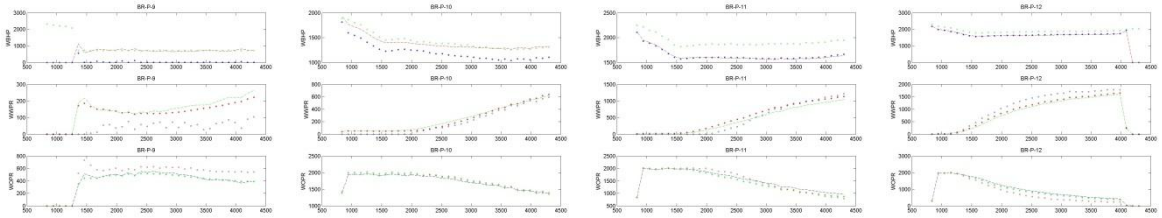

BR-P-9 **BR-P-10** **BR-P-11** **BR-P-12**

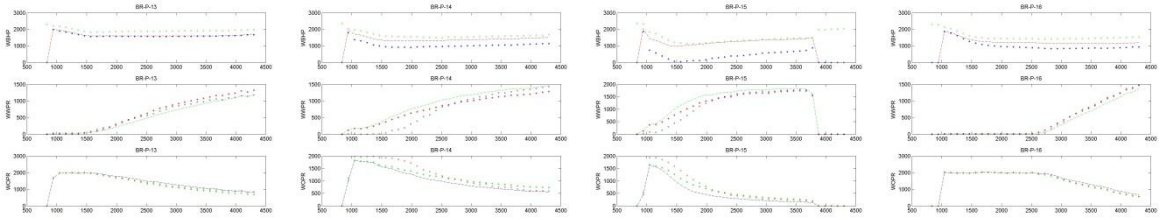

BR-P-13 **BR-P-14** **BR-P-15** **BR-P-16**

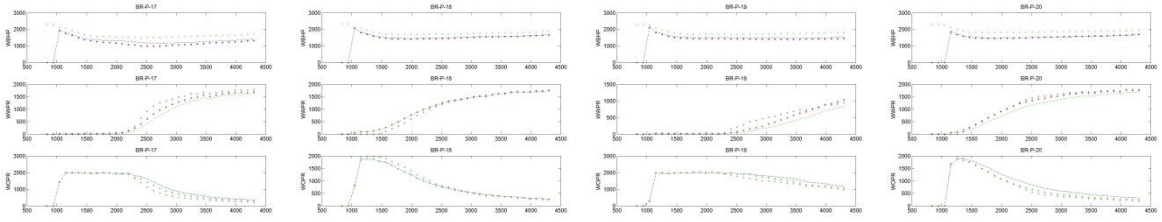

BR-P-17 **BR-P-18** **BR-P-19** **BR-P-20**

Figure 3.27. Updated Dynamic Response (WBHP, WWPR and WOPR); circle: Observed, line: Initial and dot: updated

At the end of history matching, we can achieve match to the dynamic response as in **Fig. 3.27**. The updated permeability field in **Fig. 3.28** shows that we can preserve the main features of the prior permeability field after the updates.

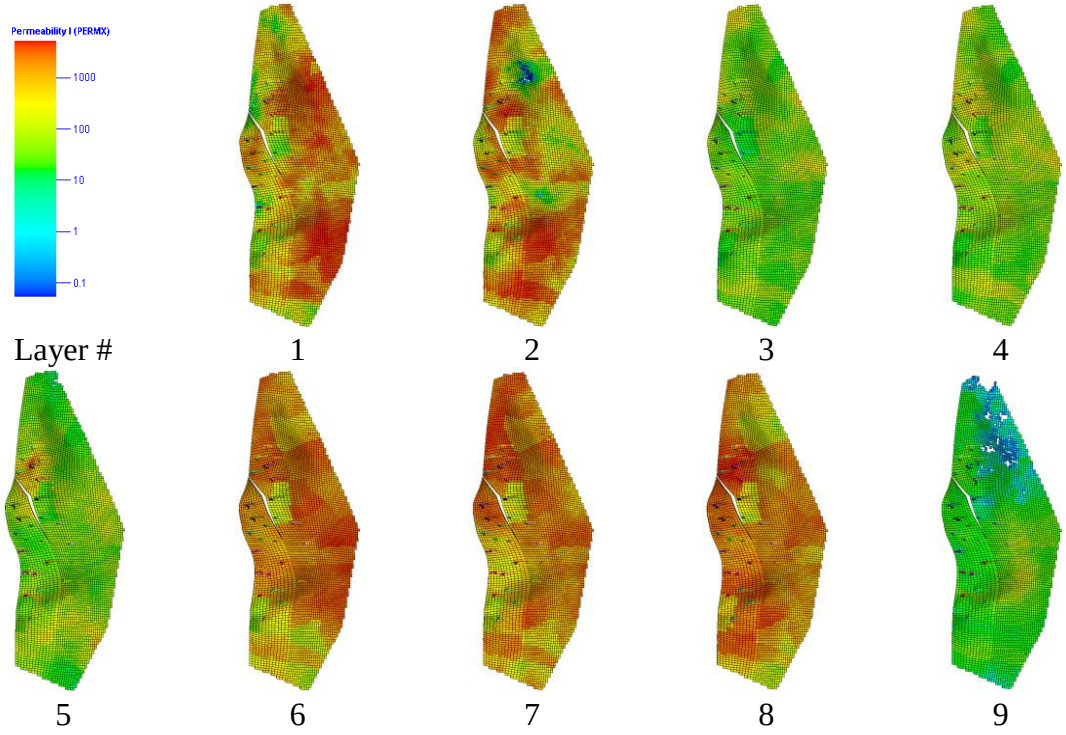

Figure 3.28. Updated Permeability Distribution in Each Layer

3.6.5 Segmentation Experiments

In this section, we compared different segmentation algorithms with the same free parameters and cut off criteria. Also, we explore clustering from different Laplacian in the same parameters.

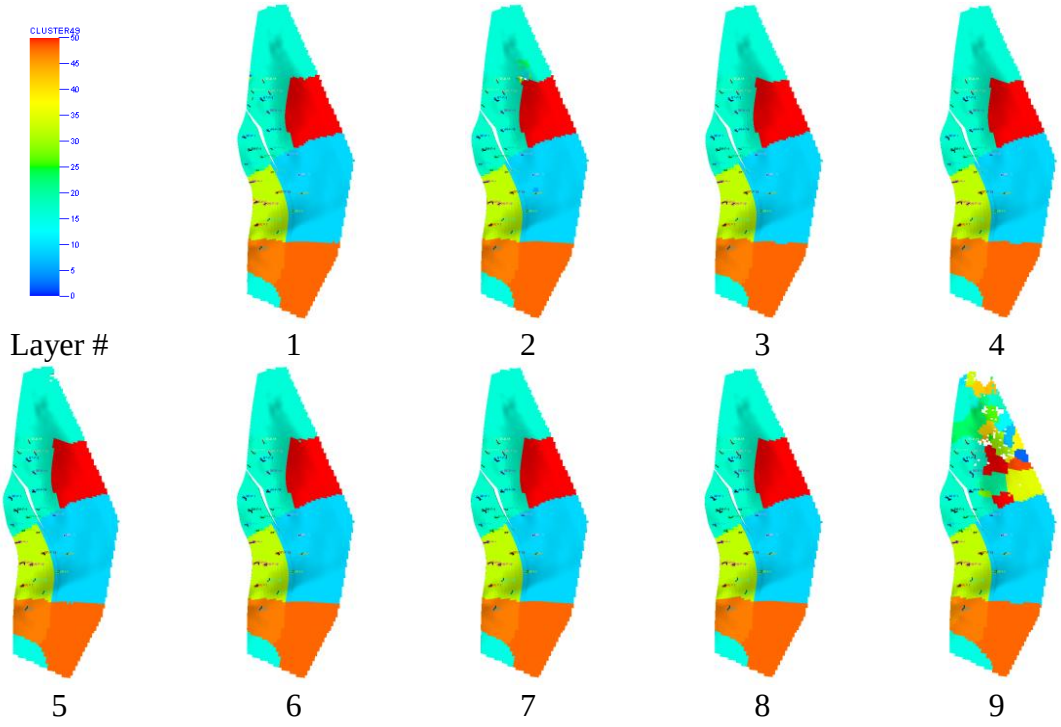

(a) Ratio Cut (Rcut)

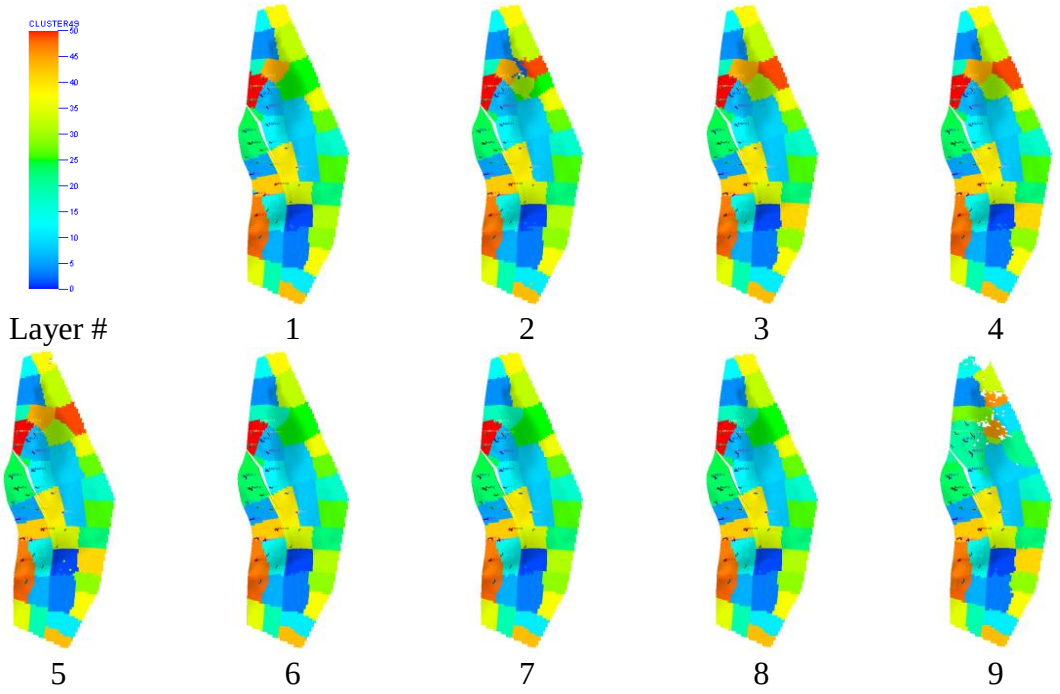

(b) Normalized Cut (Ncut)

Figure 3.29. Segmentation from Different Cutting Algorithms: 50 zones

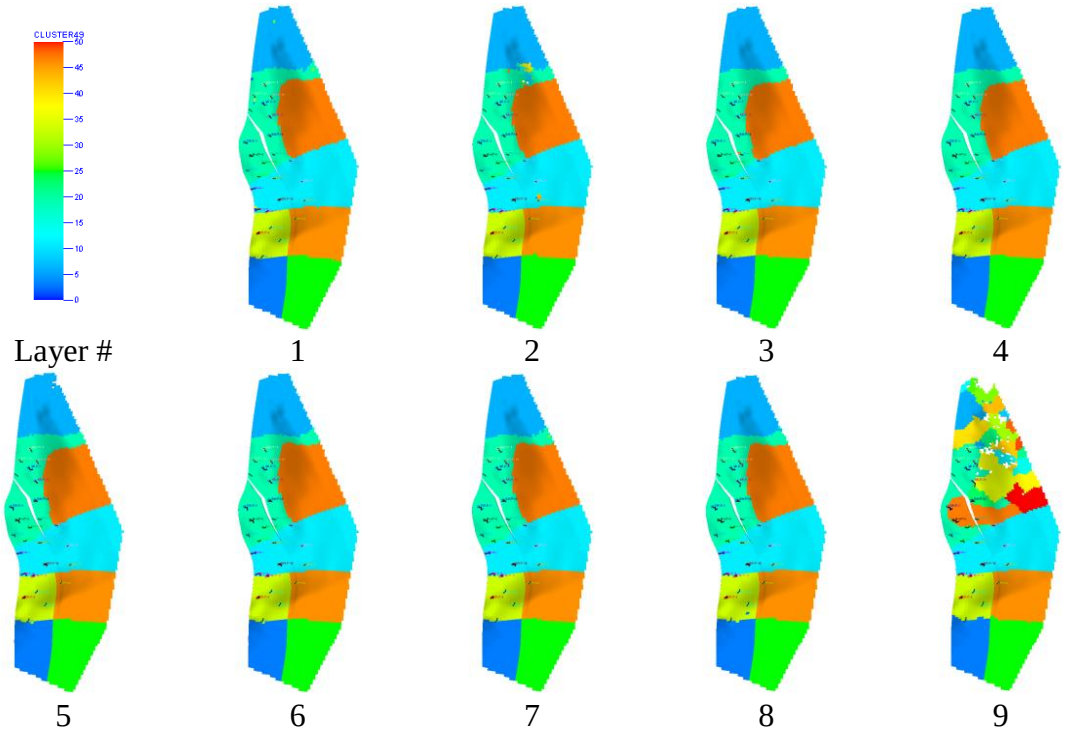

(c) Ratio Cheeger Cut (RCC)

Figure 3.29. Continued

The 'ratio' cut in **Fig. 3.29(a)** and **(c)** shows a noticeable difference with 'normalized' cuts (**Fig. 3.25** and **Fig. 3.26 (b)**) using the same affinity Laplacian. Most of segmentations are located around the low permeability region in **Fig. 3.23**. Basically, 'ratio' and 'ratio Cheeger' cuts focus on "Finding strong connection". But 'normalized' and 'normalized Cheeger' cuts show more "balanced behavior" as in **Fig. 3.29**. Also, 'Cheeger' cuts seem to take into account more heterogeneity than 'standard' cuts (compare **Fig. 3.25** and **3.29(b)**).

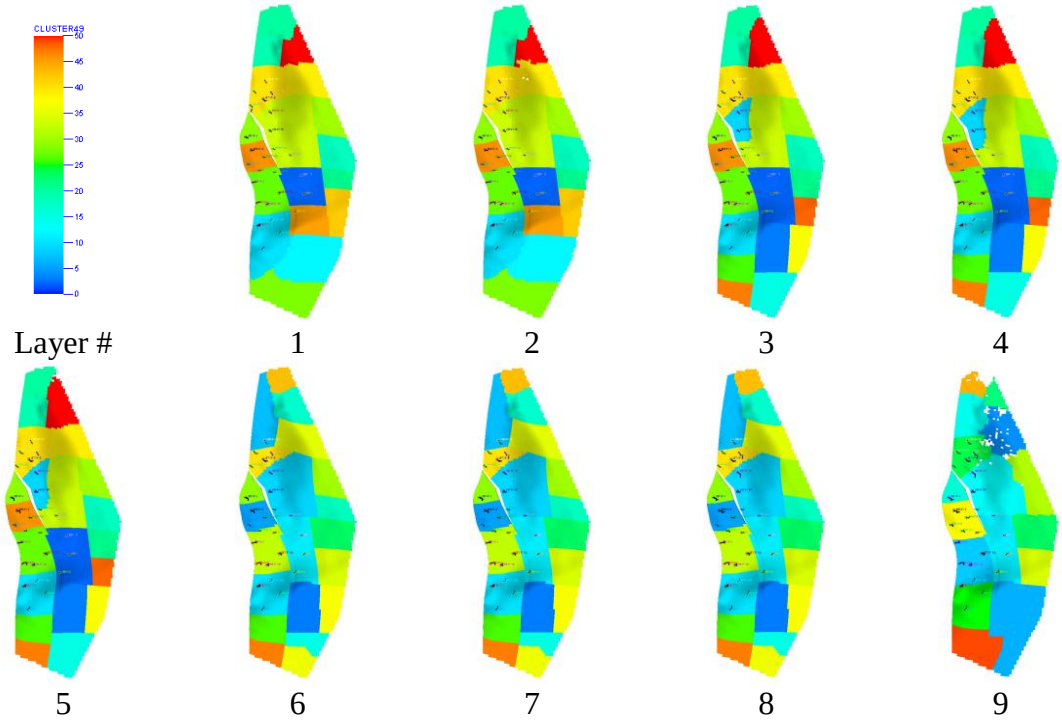

(a) Prior-weighted Connectivity Laplacian (PCL): Normalized Cheeger Cut (NCC)

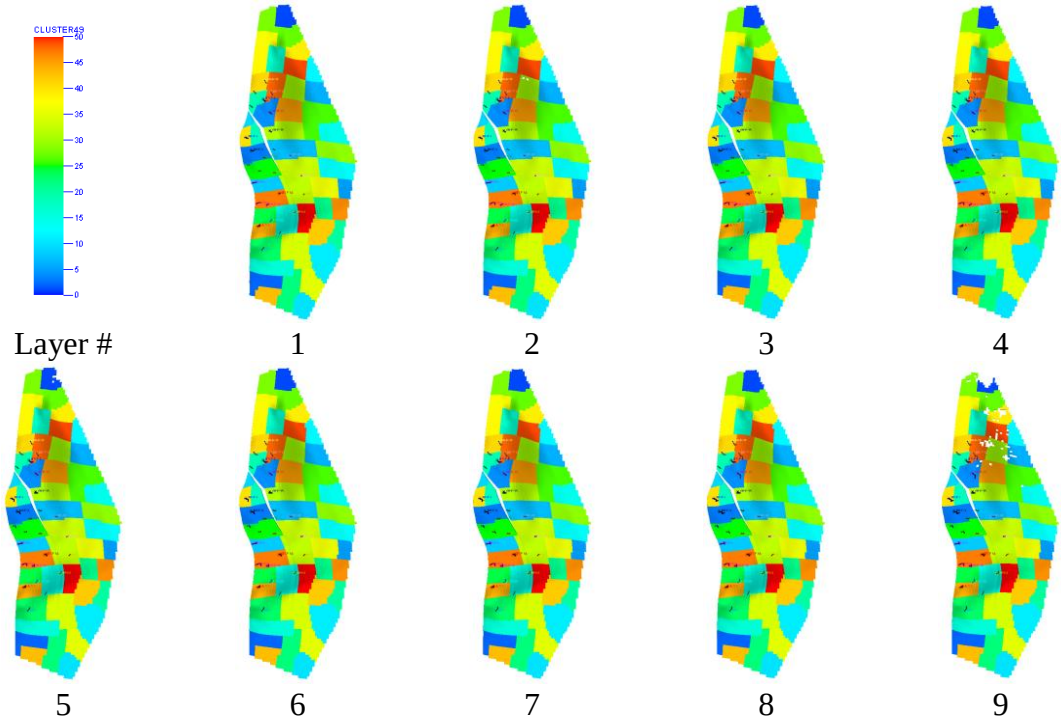

(b) Grid Connectivity Laplacian (GCL): Normalized Cheeger Cut (NCC)

Figure 3.30. Segmentations from Different Affinity Laplacian

More interestingly in **Fig. 3.30**, the Prior-weight Connectivity Laplacian (PCL) is showing features between ABL and GCL as expected (compare **Fig. 3.25** and **3.30(b)**). But the Grid Connectivity Laplacian (GCL) shows less variability (almost constant) in z-direction. Because the grid dimension of *x* (139) and *y* (48) directions are comparatively bigger than the *z* direction (9), the grid connectivity is more dominant in the *x*-*y* plain.

3.7 Summary and Conclusions

We propose a new model segmentation technique from the spectral clustering theory. The suggested approach is verified with both synthetic and the Brugge SPE benchmark model. The new zonation algorithm provides more consistent criteria for history matching compared to the common industry practice; box multipliers.

The procedure is to (1) construct Affinity Laplacian to capture spatial variability in subsurface properties; (2) use graph partitioning techniques to create zonation and find cutting edges; (3) apply partitioning with history matching algorithm. The graphic cut from the model geometry and/or heterogeneity is not arbitrary but is satisfied by optimization with graphic cutting metric.

1. The proposed zonation algorithm can preserve the major features of the prior model after history matching because the generated zonation is based on the model heterogeneity and/or connectivity information. We illustrate that spectral clustering approach can potentially capture different facies in the reservoir.

2. We propose three different Affinity Laplacian constructions and four different graph cutting algorithms. Basically, there is no ground truth in spectral clustering. So, it is not possible to say which one is the best or the worst. But we can arrive at some general conclusions from image clustering problems: ‘normalized’ cut is more statistically stable than ‘ratio’ cut. Also, ‘Cheeger’ cut shows at least as good or better performance than ‘standard’ cut. Hence, ‘Normalized Cheeger Cut’ is a good starting point for segmentation.

3. The spectral clustering problem is a NP-hard and heuristic approach. As we demonstrated, we can generate different cutting with combinations of Laplacian and cutting algorithms. Even wider choices are available with free parameter and cutting range. We inherited these properties in our proposed segmentation. Hence, we require some initial experiments and experience with different combination of cutting algorithms and Laplacian. Also, the two free parameters and cut off range heavily impact the clustering.

4. Through human interventions and heuristics, the spectral clustering provides a good guideline for automatic zonation criteria. This is more attractive when we do hierarchical history matching; which is essential for history matching problems for full-field model with decades of production history. We can adapt this zonal concept for global stage history matching and then further calibrate with fine scale approach.

CHAPTER IV
A HIERARCHAL MULTISCALE MODEL CALIBRATION WITH SPECTRAL DOMAIN PARAMETERIZATION: APPLICATION TO A STRUCTURALLY COMPLEX FRACTURED RESERVOIR

4.1 Purpose

A hierarchal history matching algorithm is proposed that sequentially calibrates reservoir parameters from the global-to-local scale in consideration of parameter uncertainty and the resolution of the data. Parameter updates are constrained to the prior geologic heterogeneity and performed parsimoniously or only to the spatial scales at which they can be resolved by the available data. In the first step of the workflow, a genetic algorithm (GA) is used to assess the uncertainty in global parameters (i.e., regional permeability, pore volumes and aquifer strength) that influence field-scale flow behavior, specifically reservoir energy. To identify the reservoir volume over which each regional multiplier is applied, we have developed a novel approach to heterogeneity segmentation from spectral clustering theory. The ensemble of model realizations identified using GA, then reduced via cluster analysis to establish for the second stage of local or high-resolution parameter calibration to well-level observation data. At this stage we parameterize the high-resolution heterogeneity in the spectral domain using the Grid Connectivity based Transform (GCT) to compress the dimension of the calibration parameter set. At the same time, the GCT implicitly imposes geological continuity and promotes minimal changes to each prior model in the ensemble during calibration.

We apply the proposed calibration workflow to a structurally complex and highly fractured reservoir located offshore in Peru. The reservoir is modeled as dual porosity and single permeability (DPSP). First, the field water and gas production are matched using the GA with zonal multipliers for fracture porosity and shape factor (‘sigma’). Next, well-by-well production history is matched by locally calibrating the most uncertain fracture network property, fracture permeability distribution, which is reduced using the GCT parameterization to improve the ill-posedness of the problem. The final

updated model is found to be geologically realistic and is being used for field development strategies.

4.2 Introduction

Reservoir model calibration to field production data, commonly known as dynamic data integration or history matching, is an essential component of successful field development planning and optimization. The history matching of high-resolution geological models is typically an ill-posed inverse problem because the numbers of observed data are considerably less than the number of calibrated reservoir parameters, which themselves are often strongly correlated. This leads to non-unique and potentially unstable parameter solutions despite an acceptable history matching of the data. However, if the history matching problem is structured relative to the resolution of the data and appropriately constrained, then together with assisted history matching algorithms a geologically consistent and close-to-optimal calibration solution can be achieved. For this purpose, we propose a hierarchal history matching algorithm that is constrained to the prior geologic heterogeneity and parsimoniously updates high resolution geologic parameters to the level that they can be resolved by the available data.

The hierarchal approach calibrates, in sequence, reservoir parameters that characterize global-to-local regions while accounting for multiscale parameter uncertainty and the resolution of the data. As the first component of the workflow, a history matching of the coarse-scale genetic algorithm (GA) is applied to characterize the uncertainty in global parameters including regional permeability, porosity and transfer function between matrix and fracture, that influence field-scale flow behavior and reservoir energy. Rather than using box-type or manually defined multiplier regions, we introduce a novel method of model segmentation based on a spectral analysis of the reservoir grid connectivity, which is an important key factor in reservoir flow dynamics. This zonal segmentation technique assists in the definition of regional multiplier boundaries in consideration of prior model heterogeneity and its connectivity. An eigenspectrum

analysis is then used to parse the ensemble of calibrated models resulting from the GA analysis into a smaller set of prior models for the second stage of local or high resolution parameter calibration to well observation data.

In this second workflow component, a heterogeneity parameterization technique is used to characterize the high-resolution calibration parameters in a low-dimensional, spectral transform domain using the Grid Connectivity-based Transform or GCT. This compact representation of the model parameters implicitly imposes geologic continuity and promotes minimal changes to each prior model during the calibration updates to match well production data. The calibration of each prior model itself is performed using an iterative least-squares method; therefore, each model is deterministically history matched and parameter uncertainty is assessed from the ensemble of final models. To improve the computational efficiency of this conceptual approach, the basis parameter sensitivities at each model update steps are derived from a semi-analytical streamline based formulation. Such that all sensitivities are computed via a single forward simulation and streamline tracing.

The development of the proposed history matching workflow builds on the strengths and limitations of more recent hierarchical approaches to the integration of dynamic data into reservoir description, beginning with those based on a GA then local model calibration. The genetic algorithm has many applications so far in reservoir history matching. Schulze-Riegert et al. (2002) applied to complex history matching problem. They applied genetic algorithm and arbitrary zonal multiplier for history matching. Cheng et al. (2008) provide a robust flow chart for a structured history matching approach listing dominant global and local parameters. They applied a GA for history matching and determined probabilistic reservoir models using proxy models of history match error for model filtering and optimization. Yin et al. (2010) applied a GA to update global reservoir parameters, followed by a streamline-assisted history matching of finer scale heterogeneity. (Bhark et al. 2011c) applied the GCT parameterization to calibrate field-scale permeability trends (GCT) using a quasi-Newton method and then a

streamline-assisted calibration of local or grid-cell scale permeability at spatial scales finer than the data could resolve using the global parameterization.

In this paper, a focus is placed on the calibration of fractured reservoirs. We demonstrate that in addition to permeability and porosity heterogeneity, which are the parameters typically calibrated in automatic history matching (AHM) workflows, that the proposed methods of connectivity based segmentation and parameterization, applied within a hierarchical approach, are applicable to fracture properties as well. The characterization of fractured geologic properties has long been studied. Warren and Root (1963) investigated flow behavior in naturally fractured reservoir models and defined fracture flow with two parameters, the absolute permeability and the effective porosity. They proved that with these two parameters, much of the fracture storage capacity and matrix-fracture interaction could be represented. Massonnat et al. (2002) illustrated the importance of characterizing the fracture network in a fractured carbonate reservoir. They examined the connection from the fracture network to the flow network. Then they conclude that fracture aperture distribution is a strong factor for assessing fracture properties rather than fracture distribution. A more recent study by Jabbari and Zeng (2011) suggest a third parameter description for fractured reservoirs; an elasticity parameter similar to Poisson's ratio and Young's modulus should be included to account for stress sensitive natural fracture system. They described fractured reservoir with fracture storage capacity, matrix-fracture interaction and combined effect of both matrix geomechanic and fracture apertures.

From these previous descriptions of fractured reservoirs, we define the fracture parameters of interest for calibration; fracture porosity, fracture permeability and a shape factor (σ) which characterizes matrix-fracture interface area per unit volume (Kazemi et al. 1976). All of which are typically of large uncertainty in dual porosity finite difference models. It should be noted that the analysis methods applied during the proposed workflow are relevant to fractured reservoir modeling. Kang et al. (2011) investigated the effect of natural and hydraulic fracture network for drainage volume calculation in tight gas reservoir.

Previously, there have been several attempts to integrate dynamic data for fracture characterization. Al-Huthali and Datta-Gupta (2004) presented a general dual porosity and dual permeability formulation for streamline simulation in naturally fractured reservoirs. They explained the domain flow mechanism in dual systems. Al-Harbi et al. (2005) use the streamline sensitivity for fine scale Model Calibration in the fractured reservoir. They used the streamline derived sensitivities in conjunction with a dual porosity finite difference simulator for fine scale model update. They characterized the fracture permeability based on streamline derived sensitivity in local grid.

In this paper, we focus on characterizing fracture properties in the complex structured geometry with a hierarchical approach. To explain our approach, the mathematical formulations, together with a hierarchical workflow are presented first. We then apply the proposed calibration workflow to a highly complex and fractured reservoir field. The field is modeled as dual porosity and single permeability (DPSP) and located offshore in Peru. In this field example, the global dynamic data (total field water production) misfit is successfully reduced at first along the field wise using the genetic algorithm (GA); updating aquifer property, shape factor and fracture porosity with zonal multipliers. Average reservoir pressures are also considered with observation data in this stage. The well-by-well production history is then matched by calibration of the uncertain local fracture properties; fracture permeability, which is updated using the GCT parameterization and improved the ill-posedness of the problem.

4.3 Approach

This section explains the individual components of the proposed hierarchical workflow from a conceptual viewpoint. The mathematical formulation behind each step is presented in the following section. In brief summary, there are two primary hierarchical components. The first uses a GA to calibrate the reservoir model at the global or coarse scale using regional property multipliers, where region geometries are defined using a novel model segmentation technique. Other global parameters, e.g., those that characterize aquifer strength, are included in the calibration based on the outcome of a

parameter sensitivity analysis. These selected parameters are subsequently applied in an experimental design for construction of a proxy model of the data misfit response surface (Yin et al. 2010). The response proxy is required for reduction of the computational expense of the GA-based calibration which executes inheritance, selection, mutation and crossover of the parameters during their evolution or updating. At termination of the GA an ensemble of globally calibrated reservoir models is defined, so a cluster analysis is used to select a small subset that approximates the range of variability of the complete set. In the second hierarchical component, each of the (now prior) heterogeneity models from the first component is calibrated at the local scale. To reduce the number of high-resolution parameters, they are compressed in a low-dimensional transform domain in which the calibration is performed. The sensitivities of the production data to the transform parameters, which drives a gradient-based inversion approach, are efficiently computed using a streamline-based technique. The production data misfit is accordingly characterized using the generalized travel time (GTT) approach (Al-Huthali and Datta-Gupta 2004), which also exploits the efficiencies of a streamline-base characterization of model heterogeneity as described below. The combined approaches of spectral parameterization and GTT data misfit reduce the dimensionality and non-linearity of the inversion, expediting data misfit reduction and reducing the occurrence of local minimum convergence. These steps are now altogether reviewed, referring to the field application as appropriate.

- ***Initial Model Response and Parameter Sensitivity Analysis*** A proper history matching workflow must start from a conceptual understanding of the prior geologic model and its static and dynamic uncertainties. In the fractured field model presented, the San Pedro field at offshore Peru, the primary uncertainties are hydraulic continuity across the main faults, static and dynamic fracture properties and aquifer strength. To understand the influence of these properties on production behavior, particularly in the presence of complex flow geometries and changing field conditions, we utilize two approaches. First, and more

qualitatively, we use streamline simulation to visualize and quantify fluid movement. With individual phase streamlines, i.e., individually tracing water, oil or gas flux trajectories as opposed to tracing the total fluid flux trajectories, the individual phase production source and flow paths are easily identified. For example, in the San Pedro modeling application, water phase streamlines are used to identify the level of aquifer support, which is suspected to be strong, from a source in the bottom layer of the reservoir model. Second, and more quantitatively, we apply the complete set of global parameters in a sensitivity analysis to identify the 'heavy hitters' that are to be applied in the first step of the hierarchical calibration. The sensitivity analysis is efficiently computed using an analytical proxy of the production data misfit surface, which itself is constructed via an experimental design with a proficient Latin hypercube sampling.

- ***Model Segmentation from Spectral Clustering*** To characterize static heterogeneity related to fracture properties for the global calibration, a novel model segmentation technique based on the theory of graph partitioning is applied to identify regional multiplier domains over the complete grid volume. These regions rely on the grid geometry structure to indicate a natural partitioning rather than applying traditional box-type multiplier regions. When the grid geometry, relative to its cell connectivity structure, is characterized in a specific Laplacian operator or matrix, then the eigenvector corresponding to the second smallest (non-zero) eigenvalue represents the grid grouping based on heterogeneity and connectivity. This eigenvector, in turn, can be applied in a spectral clustering algorithm to partition the domain (Pothen et al. 1990). We take advantage of this property and propose an optimal model zonation for history matching relative to a graph cut metric, which quantifies any piecewise continuous partitioning of the grid cells. In this field application, we apply the graphic "normalized cut" for model segmentation.

- ***Global Parameter Calibration*** To complete the first stage of the hierarchical history match, a GA is used to identify the reservoir parameter combinations that match the observed field water production and average reservoir pressure, both of which are considered to represent global drive mechanisms and energy. These data are shown particularly sensitive to aquifer strength. At each generation of the GA, a proxy of the individual data misfit terms is used to efficiently select an ensemble of models. Each model is added to the accepted population of that generation if the data misfit is reduced. At the termination of each generation, each proxy surface is updated to include the latest simulation results, each corresponding to a new and unique parameter combination, before moving on to the next generation. This sequence is continuously repeated until a maximum number of generations are reached or until the data misfit can no longer be reduced. At termination of the GA, a small subset of the ensemble at the last generation is selected using a cluster analysis. The cluster reproduces the statistical uncertainty of the complete ensemble and yields a small number of prior reservoir models that are applied in the next stage of local parameter calibration. **Fig. 4.1** presents a flow chart of the first hierarchical workflow components.

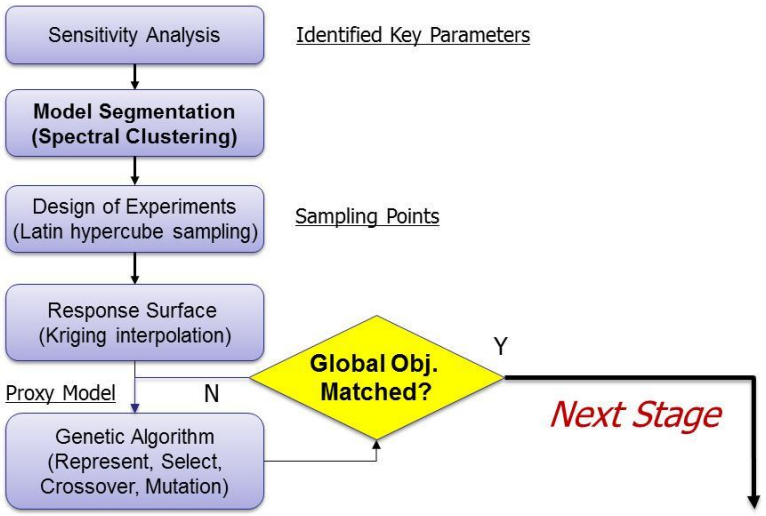

Figure 4.1. Global Stage Model Update

- ***Spectral-Domain Parameterization of High-Resolution Reservoir Properties*** The second hierarchical workflow component involves calibration of the fracture properties at high resolution, or at the scale of individual grid cells. To address the intractable inverse problem of their individual identification from the well production data, each fracture property field is characterized in a low dimensional transform domain for the history matching. For this the GCT parameterization (Bhark et al. 2011c) is applied to linearly map a spatial property field, at grid cell resolution, to a spectral domain in which the dominant modes of the property can be identified and calibrated. However, note that we have elected to apply a domain-scale multiplier field in lieu of each of the calibrated property fields for the parameterization. This permits the retention of all prior model features through the calibration, which are assumed constructed from multiple data sources and their modification only when warranted by the production data. Regardless of whether a multiplier field or the reservoir property itself is calibrated, the transformation to the spectral domain is achieved by multiplication of the spatial property with the orthogonal GCT basis. The basis is itself constructed from the grid connectivity structure such that each mode or basis vector represents a harmonic of the grid structure that is characterized by a modal frequency. Therefore, when characterized in the transform domain, the spatial property is decomposed as the linear combination of GCT coefficients, where each coefficient corresponds to the amplitude of an associated modal frequency. When only the coefficients corresponding to the dominant modal frequencies are calibrated, the estimable parameter dimension is considerably reduced, typically to less than one percent of the original dimension in the spatial domain. A secondary benefit of the GCT parameterization is the enforcement of spatial continuity or smoothness in the calibration updates.

- ***Transform Parameter Sensitivity Calculation*** An iterative sensitivity-based algorithm is applied to deterministically calibrate each of the prior reservoir

models output from the first stage of the hierarchical workflow. Accordingly, for the calibration of each model, the sensitivity of the well production responses to a perturbation in each of the fracture model parameters is required. However, the production data misfit in this second local component of the workflow is characterized by the GTT approach, or by a single time shift per well response that maximizes the cross-correlation between the observed and simulation fractional flow profiles. Further, the fracture property field is parameterized by a small set of GCT coefficients. Despite the parameterization of both the model input parameters and production response metrics for definition of a less ill-posed calibration problem, formulation of the sensitivity matrix remains a computationally expensive task. To mitigate this expense, a streamline-derived sensitivity technique is used to efficiently define the complete sensitivity matrix at each model update, requiring only a single forward simulation. As an additional contribution of this paper, we expand the Generalized Travel Time (GTT) sensitivity formulation for consideration of the GCT coefficients as opposed to high-resolution grid cell parameters. This extension is straightforward and requires only an additional vector-matrix multiplication (see **Eq. 4.18**). Once computed, the derived GCT coefficient sensitivities are applied to minimize the GTT misfit using a sparse equations solver with a least-squares optimization algorithm (LSQR).

- ***Local Parameter Calibration in the Transform Domain*** At the termination of each LSQR calibration step, the GCT coefficients, which again characterize fracture property multiplier fields, must be transformed back to the spatial domain or to the grid for their inclusion in flow simulation. This requires only a vector-matrix multiplication between the GCT coefficients and the transpose of the GCT basis because the basis vectors are pairwise orthogonal. The resultant simulation output is used to check if the updated parameters improve the production data misfit. At some step in the iterative minimization, the data misfit

or objective function will converge to a minimum, likely a local minimum. If the data misfit is unsatisfactory at this point, then additional basis vectors can be appended to the GCT basis and the minimization re-started from previous updated point. These new basis vectors correspond to higher modal grid frequencies, or to finer scales of spatial information in the calibrated multiplier field. Therefore, an outer iterative loop to the LSQR minimization is defined that consists of adding increased levels of spatial resolution to the multiplier fields via the addition of successively higher-frequency GCT basis vectors to the parameterization. This multiscale loop enables the calibration of simple and coarse heterogeneity to complex high-resolution heterogeneity. A flow chart of this workflow, or for the second component of the hierarchical history matching workflow, is illustrated in **Fig. 4.2**.

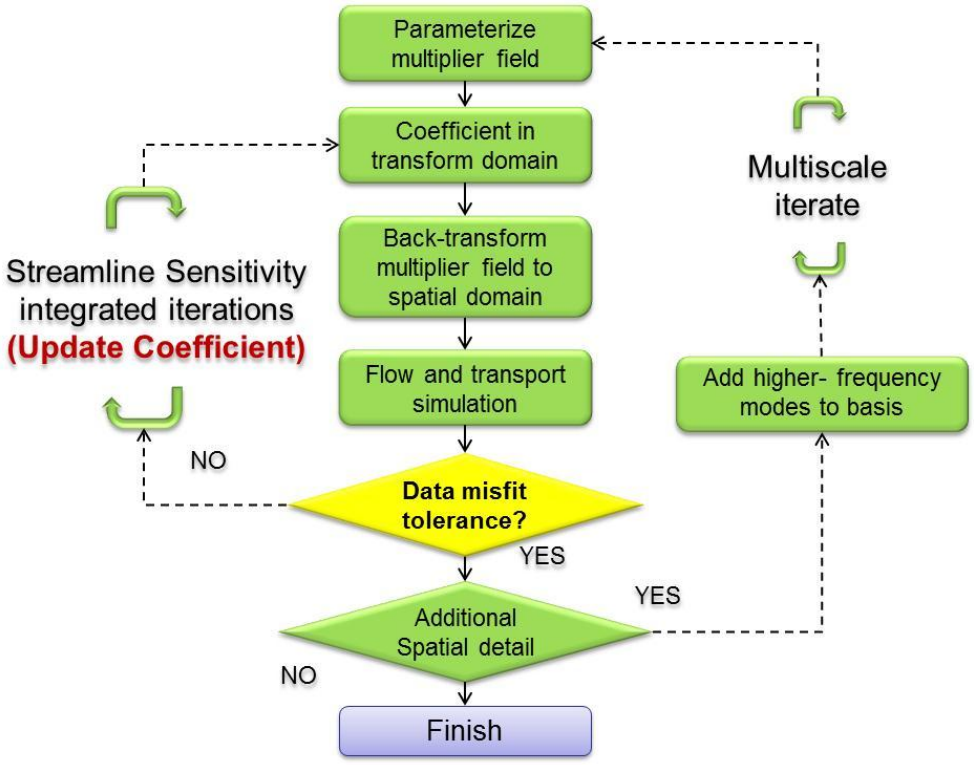

Figure 4.2. Local Stage Model Calibration

4.4 Mathematical Formulation

This section describes the mathematical formulation behind individual steps of the history matching workflow. Only those steps, in either the coarse or local-scale components of the hierarchical workflow, requiring mathematical details are presented. The intent of this section is not to review the complete workflow but to provide details only when warranted.

4.4.1 Genetic Algorithm

The approach of global parameter estimation in the coarse-scale component of the hierarchical workflow is adapted from Yin et al. (2010). This involves the steps of experimental design, response surface characterization via proxy modeling, and data misfit reduction using a proxy-based GA. The data misfit objective function is constructed as the summation of the natural logarithm of the individual data misfit components;

$$O(m) = O(m_1, m_2, ..., m_N) = \sum_{j=1}^{N_{objective}} \ln\left(\sum_{i=1}^{N_{Well}} \left| Obs_i - Sim_i \right| \right) \tag{4.1}$$

where $O(m)$ is objective function to optimize during GA evolution and m_i represent individual history matching parameter. Obs_i and Sim_i represent any type of dyanamic response data misfit, e.g., well pressure, well production rate, etc. The logarithmic summation of each objective function component, which corresponds in Eq. 1 to the summation of data misfit at an individual well, is equivalent to normalizing each data type for the difference in magnitude across different types of sources.

The GA-based history matching is achieved by minimizing the objective function while maximizing the fitness of genomes, where the latter become the measure of an objective function. We further incorporate a stretching of the fitness function with the 'heat-bath algorithm' to facilitate, or relax, the selection criteria for those models that are

passed on to the next generation (Sen et al. 1995). The selection probability of an individual model m_i is given by

$$P(m_i) = \frac{\exp(-f(m_i)/T_n)}{\sum_i \exp\left(-f(m_i)/T_n\right)} \tag{4.2}$$

In **Eq. 4.2**, $O(m_i)$ is the objective function of model m_i that is to be minimized by maximizing fitness $\exp(-O(m_i)/T_n)$ and T_n is a control parameter that corresponds to temperature in simulated annealing (SA). The heat-bath algorithm accelerates convergence and requires fewer simulations for reduction of the objective function, both of which properties are important to reduce the large computational expense of the GA, particularly with field-scale models (Yin et al. 2010).

4.4.2 Connectivity Based Graph Laplacian

The spectral graph *G* is defined as a set of data set $[x_1, x_2, \dots, x_n]$ in a domain with vertex $V = [v_1, v_2, \dots, v_n]$ and edges *E*, that is connectivity a_{ij} between v_i and v_j. The graph Laplacian $\boldsymbol{L}$ is used to calculate the number and connected strength of a given graph *G*. The graph Laplacian $\boldsymbol{L}$ is constructed simply as $\boldsymbol{L} = \boldsymbol{D} - \boldsymbol{W}$, where $\boldsymbol{W}$ is the grid weighted adjacency matrix and $\boldsymbol{D}$ is the degree matrix in **Eq. 4.4**. For an N number of data set, $\boldsymbol{W}$ is the $N \times N$ matrix constructed as **Eq. 4.3**;

$$w_{ij} = \begin{cases} 1 & if\ neighboring \\ 0 & otherwise \end{cases} \tag{4.3}$$

and the entry of degree matrix $\boldsymbol{D}$, defined as diagonal matrix, equal to the degree of each corresponding vertex.

$$d_i = \sum_{j=1}^{N} w_{ij} \tag{4.4}$$

Such that each non-zero diagonal element of ***D*** is equal to the row sum of *W*. Accordingly, the Laplacian is constructed only once, prior to the history matching workflow, using grid connectivity information and is independent of the prior parameter heterogeneity. **Fig. 4.3** depicts the two-point connectivity structure, corresponding to a 5-point stencil in two dimensions, used to define Laplacian *L*. The graph Laplacian must represent 'connected' graph *G*, which means all the data should have at least one connectivity to the rest.

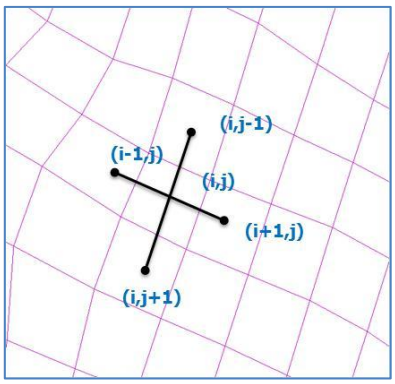

$$L_{i,j} = \begin{cases} d_i & i = j \\ -w_{ij} & otherwise \end{cases} \tag{4.5}$$

Figure 4.3. Construction of Connectivity Laplacian

The same graph Laplacian will be used for global and local scale update; clustering for global and reparameterization for local update. Note that the clustering in the global stage will do spatial grouping based on 'second eigenvector' of Laplacian (von Luxburg 2007) and the reparameterization is to transform history matching parameters into frequency domain with 'leading eigenvectors'. This is important to understand that we can use the same graph Laplacian for different stage of hierarchical history matching. How it is possible? The leading eigenvectors of graph Laplacian, corresponding from lowest eigenvalues, represent the dominant eigenspectrum of a system (Bhark et al.

2011c). Especially, the second eigenvector, corresponds to lowest positive eigenvalue, provide the algebraic connectivity of a connected graph (Fiedler 1973).

4.4.3 Spectral Domain Decomposition: Model Segmentation for Global Update

For the global stage update, we propose the new zoning algorithm from spectral clustering theories. The spectral cutting criteria, such as 'ratio cut' and 'normalized cut', has been applied in many engineering problems; MRI image analysis (Szu-Hao et al. 2009), remote sensing (Wem et al. 2010) and circuit design (Hagen and Kahng 1992), because of its profound mathematical theory and easy to implement in new area. The utility of spectral clustering is defining similarity measure between data points such that maximize similarity in a same cluster and minimize similarity between different clusters. This fundamental idea of spectral clustering enables us to construct zonal groups with similar grid properties or electrofacies.

We want to reemphasis that the region boundaries are not selected manually but are deterministically defined from an optimal partitioning of the prior fracture property field relative to a partitioning metric known as 'cut' criteria. In this application we apply a specific cut algorithm, defined as the optimization approach is to generate a partition C and its complement $\bar{C}$ which minimizes the value of **Eq. 4.6**, where x_i and x_j are data points in a set.

$$cut(C,\overline{C}) = \sum_{x_i \in C,\ x_j \in \overline{C}} w(x_i, x_j) \tag{4.6}$$

The optimal clustering of a connected graph is that minimize this cut value as **Eq. 4.6**. The summation of weighted affinity provides zoning criteria for optimal spatial zones. This is corresponding to define the clustering as "finding a partition of the graph such that points in different clusters are dissimilar and within a group are similar to each other" (von Luxburg 2007).

Now, how we find the optimal value? This is related to clustering algorithms. We suggest a novel 'ratio cut' and 'normalized cut' partitioning for balanced clustering in the zonation of a reservoir model. In fact, there are many clustering algorithm but most of them are based on those two clustering idea. Before we explain algorithms, we need to define two different ways to measure the size of a subcluster in **Eq. 4.7**.

$$\begin{aligned} |C| &: \textit{the number of vertices in subcluster } C \\ vol(C) &: \textit{the sum of weighted affinity in subcluster } C \end{aligned} \tag{4.7}$$

The minimum of Ratio Cut is shown to define the optimal partitioning of the data characterized by the affinity matrix (Hagen and Kahng 1992). The ratio cut is clustering based on number of vertices;

$$Rcut(C,\overline{C}) = \frac{cut(C,\overline{C})}{|C|} + \frac{cut(C,\overline{C})}{|\overline{C}|} \tag{4.8}$$

In **Eq. 4.8**, the optimal partitioning identifies regions that have maximum similarity within regions (numerator) balanced by the condition of equal size or number of data (denominator) (von Luxburg 2007). In easy speaking, if we have a data set with size of *n*, we can minimize *Rcut*(ratio cut measure) by equally dividing with *n*/2.

Shi and Malik (2000) proposed a new partition criteria, 'normalized cut', for measuring the goodness of an image partitioning. The normalized cut is measured by the weight of its edges. This cut measure is minimized by equal weighting. The main difference between 'ratio' cut and 'normalized' cut is using un-normalized Laplacian for ratio cut and normalized cut use normalized Laplacian (von Luxburg 2007).

$$Ncut(C,\overline{C}) = \frac{cut(C,\overline{C})}{vol(C)} + \frac{cut(C,\overline{C})}{vol(\overline{C})} \tag{4.9}$$

The ‘normalized cut’ leads to normalized spectral clustering, which is statistically stable, while relaxing ‘ratio cut’ leads to unnormalized spectral clustering. These two spectral clustering algorithms provide ‘balanced’ cutting criteria even in complex geometry, regarded as connected graph.

The approximate solution to the minimization of cut, or alternatively to the minimum of the Rayleigh quotient (solve eigenvalue problem with iterative approximation), is achieved by the eigen decomposition of the affinity Laplacian L. In the form of **Eq. 4.5** is always positive semi-definite and, therefore, has real non-negative eigenvalues with a smallest eigenvalue always equal to zero (von Luxburg 2007). The zero eigenvalue corresponds to a constant eigenvector, and then the next eigenvector corresponding to the second eigenvalue indicates an optimal partitioning of the heterogeneity information embedded in L. If mapped onto the simulation grid, the second eigenvector depicts spatial features, potentially including edge information, related to similar and dissimilar regions of the prior model, where again the term ‘similar’ is defined relative to the adjacency graph metric in **Eq. 4.3**.

4.4.4 Reparameterization for Local Update

The parameterization of high-resolution reservoir properties, or in this application fracture properties defined at each grid cell, is performed using the Grid Connectivity-based Transform or GCT (Bhark et al. 2011c) in **Eq. 4.5**. As described, a spatial fracture property field is mapped to a spectral domain via the GCT basis vectors, each of which corresponds to a modal shape of the grid structure and is associated with a modal frequency. Several such basis vectors are shown mapped onto the grid in the application below. The basis in its entirety is constructed as a subset of the eigenvectors of a grid connectivity matrix, which has the form of a Laplacian operator, which characterizes two-point grid cell connectivity over the domain that is to be parameterized.

Note that the basis functions (ϕ_i) are pairwise orthogonal to each other. This orthogonality permits inclusion of additional fine scale variation into the multiplier field.

Initially, all basis coefficients except first have zero value from **Eq. 4.10**. So, first basis vector contributes to calibrating field average and others to local distributions.

$$v = \phi^T m_G \tag{4.10}$$

where spatial parameter (grid properties) $\boldsymbol{m_G}$ is the $n \times 1$ vector depicting the spatial property at n grid cells, $\boldsymbol{\phi}$ is the $n \times m$ GCT basis where the number of basis vectors $m << n$ and v is the m × 1 vector of GCT coefficients that are the calibration parameters. Because the basis vectors (ϕ_i) are pairwise orthogonal to each other, a refinement of the parameterization by the addition of higher-frequency basis vectors (or by the addition of finer-scale variation into the field) is achieved simply by appending the corresponding (ϕ_i) to $\boldsymbol{\phi}$. After updating of the components of v during each iterate of the sensitivity-based minimization, described next, the pairwise orthogonality of $\boldsymbol{\phi}$ also enables an efficient transformation of the GCT coefficient back to the spatial domain as;

$$m_G = \phi v \tag{4.11}$$

This step is required to apply the updated field in simulation. Finally, it is reiterated that we elect not to parameterize and calibrate a fracture property field itself, but rather to apply a parameterized multiplier field so that the prior information at its initial high-resolution will not be degraded (Bhark et al. 2011b). Notating this prior model as $m_{G,0}$, the parameterization is posed as;

$$m_G = m_{G,0} \circ \phi v \tag{4.12}$$

where the multiplication operator ($\circ$) is the entry wise product of each component. That is, the fracture heterogeneity field applied in simulation is computed as the entry wise product of the prior model ($m_{G,0}$) and the calibrated multiplier field (ϕv).

In the local-scale scale calibration workflow in **Fig. 4.2**, the GCT is applied in a multiscale workflow where the parameterized fracture heterogeneity is sequentially refined. Between iterations of a sensitivity-based data misfit minimization algorithm, the additional higher modal frequency basis vectors are added to the parameterization. At the first step of the multiscale workflow, only a small number of the lowest-frequency basis vectors are used to parameterize the fracture heterogeneity in the GCT domain then add more high resolution, corresponds to high frequency basis vector, if require (multi-scale iteration loop).

4.4.5 Sensitivity Calculation

Within each multiscale iterate of the local-scale calibration workflow, the GCT coefficient sensitivity is required for the LQSR-based data misfit minimization (Bhark et al. 2011a). The streamline-based generalized travel time (GTT) sensitivity (Vasco et al. 1999; Wu and Datta-Gupta 2002) is used to efficiently accomplish this. The GTT sensitivity is analytically calculated along the trajectory with single streamline tracing. So, the computation is extremely cheaper and faster than numerical perturbation and applicable to any complex geometry like non-neighbor connection (NNC) model or fracture system. The 'General Travel Time (GTT)' inversion seeks the optimal time shift Δt at each well to minimize the production data misfit at each well. The optimal shift will minimize the misfit function.

$$J = \sum_{i=1}^{N_d} \left[y^{obs}(t_i + \Delta t) - y^{sim}(t_i) \right]^2 \tag{4.13}$$

or, maximize the correlation coefficient defined by

$$R^2(\Delta t) = 1 - \frac{\sum \left[y^{obs}(t_i + \Delta t) - y^{sim}(t_i) \right]^2}{\sum \left[y^{obs}(t_i) - y^{sim}(t_i) \right]^2} \tag{4.14}$$

In the dual-porosity system, the fluid flow is assumed to occur primarily through the high permeability fracture network system and matrixes are acting as storages. So, the streamline sensitivities are calculated by the streamline tracing along the fracture system (Al-Harbi et al. 2005). The water cut arrival time (t) or streamline time of flight (τ) sensitivity with respect to the fracture permeability will be calculated by

$$\frac{\partial t}{\partial m_G} = \left(\frac{\partial \tau}{\partial m_G}\right) / \left(\frac{\partial f_w}{\partial S_w}\right) = -\int_{\sum} \frac{s(x)}{m_G} dx / \left(\frac{\partial f_w}{\partial S_w}\right) \tag{4.15}$$

Here, $s(x)$ is 'slowness' which is reciprocal of interstitial velocity and integral are evaluated along the trajectory (Vasco et al. 1999). The model parameter m_G is linear combination of coefficient weighted basis function and from basis orthogonality;

$$\frac{\partial m_G}{\partial v_i} = \frac{\partial(\phi v)}{\partial v_i} = \phi_i \tag{4.16}$$

or by using multiplier field from **Eq. 4.12**;

$$\frac{\partial m_G}{\partial v_i} = \frac{\partial(m_{G,0} \circ \phi v)}{\partial v_i} = m_{G,0} \circ \phi_i \tag{4.17}$$

The calculated streamline GTT sensitivity is utilized for the basis coefficient sensitivity from expansion;

$$\frac{\partial t}{\partial v_i} = \frac{\partial t}{\partial m_G}\frac{\partial m_G}{\partial v_i} = \left(\frac{\partial t}{\partial m_G}\right)\phi_i \quad \text{or} \quad \frac{\partial t}{\partial v_i} = \left(\frac{\partial t}{\partial m_G}\right) m_{G,0} \circ \phi_i \tag{4.18}$$

Simply, the basis coefficient sensitive is derived from streamline general travel time (GTT) sensitivity by multiplying basis vector as in **Eq. 4.18**. Also, adjoint sensitivity

also easily integrated with the same formulation if available (Bhark and Jafarpour, 2011).

4.4.6 Model Update in the Parameterized Domain

Reconciling high resolution geological models to low resolution field production data involves the under-determined inverse problem (He et al. 2001). Updating in the transformed domain helps to reduce this non-linearity by reducing number of unknown parameters. Then, we minimize the penalized misfit function.

$$\left\|\Delta\tilde{t} - S\delta v\right\| + \beta_1\left\|\delta v\right\| \tag{4.19}$$

Compared to the misfit function by several papers (Al-Harbi et al. 2005; He et al. 2001) as **Eq. 4.20**, we don't add smoothness penalized term. Paramerization will do preserving 'smoothness' during the dimension condensation.

$$\left\|\Delta\tilde{t} - S\delta R\right\| + \beta_1\left\|\delta R\right\| + \beta_2\left\|\hat{L}\delta R\right\| \tag{4.20}$$

The minimum in **Eq. 4.19** can be obtained by an iterative least square solution in the following linear system. An iterative sparse matrix solver, LSQR, is used for solving under-determined inverse problem.

4.5 Field Application: San Pedro Reservoir

In this section the proposed history matching workflow is demonstrated using a field application which a models a faulted and fractured (dual porosity, single permeability) reservoir. After a description of the field geology and reservoir model calibration parameters, each component of the hierarchical workflow is presented in chronological sequence.

4.5.1 Field Descriptions

The San Pedro reservoir sits offshore Peru within a complex structure of normally faulted Paleozoic quartzite and argillites in the Sechura basin. The reservoir is 6,500 ft below sea level and discovered in 2005; 6 years production history up to date. The daily production at the initial is 3,200 BOPD and 1,700 BWPD with 33˚ API on average is shown on previous work by Meza et al. (2010). The dip of the basin structure is approximately 40 degrees to the northeast. The structural geology in **Fig. 4.4**, there is two main faults in the middle of the reservoir. The first one is East-West (EW) directional and a type of strike-slip fault. Second$^{(2)}$ on the north side of reservoir in **Fig. 4.4** is a normal fault. The first fault$^{(1)}$ in **Fig. 4.4** with EW is currently prevailing and influences the distribution of open fractures. A thin post-Paleozoic layer is actively producing but has variations in thickness and productivity. Hence, fracture identification is very important because producible fractures are on those layers whose rock types of main layers are quartzite, phillyte, slate, argillite.

Velez et al. (2010) studied the origin of faults and fractures in the Sechura basin and constructed an initial geologic model using seismic and well log data. They explained how the initial discrete fracture network model is constructed from image logging in this field. From a pre-existing stress analysis (Meza et al. 2010) and image logging (Velez et al. 2010), main strike-slip faults and open fractures were identified and had generated parallel to the predominant stress field.

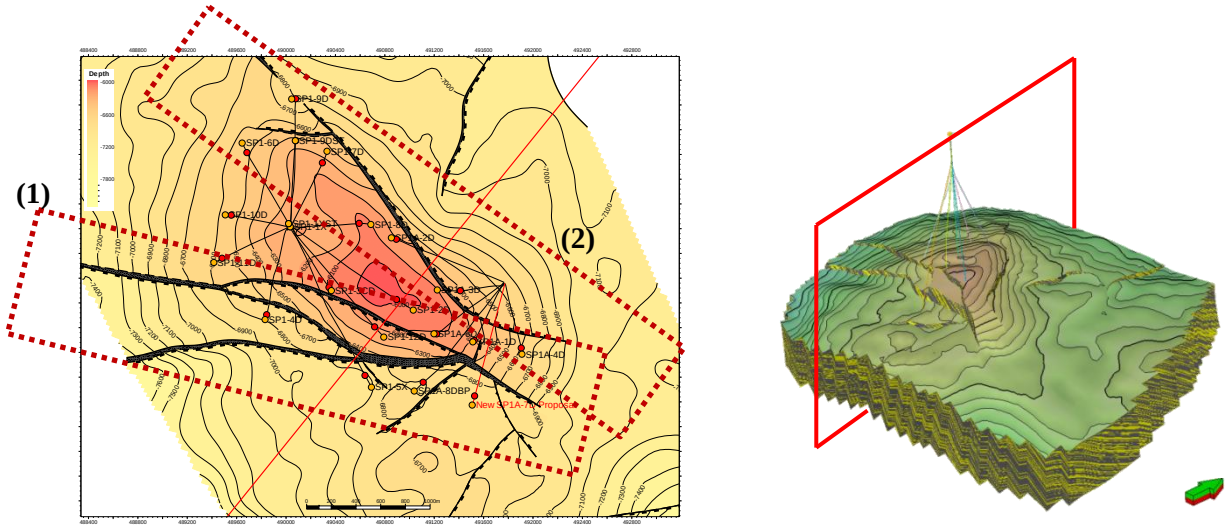

Figure 4.4. (a) Configuration of well and faults (b) geological Model

From a seismic survey, the oil-water contact (OWC) is defined at 7,174 ft and the gas-water contact (GWC) at 6,460 ft as shown in **Fig. 4.5**. Strong aquifer support from the base of reservoir is inferred from pressure observations, although the size and strength of the aquifer are highly uncertain. Initial pressure at the reservoir top level is 2,983 psi and average pressure gradient is 0.35 psi/ft. The estimated bubble point pressure is 3,012 psi from the PVT lab test.

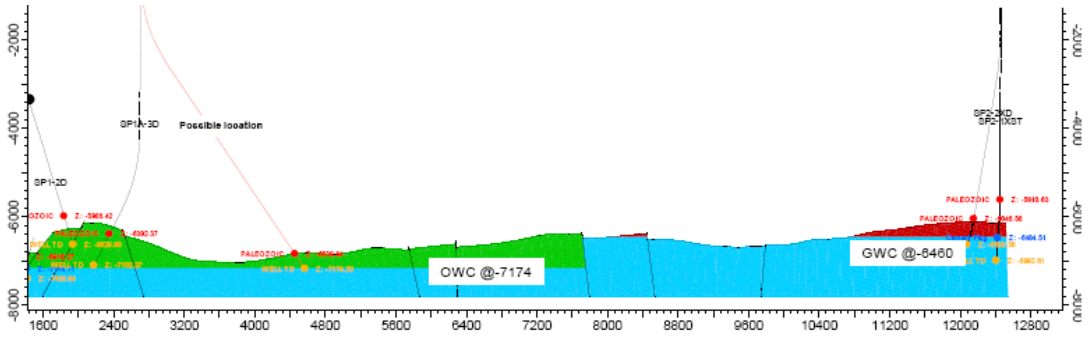

Figure 4.5. Typical Well Section and OWC / GWC level

The San Pedro field has 18 production wells and 1 gas injection well are tied back to two platforms up to date. Meza et al. (2010) determined that the well productivity

indexes are related to average fracture direction and orientation and that the main source of production is primarily from the fractures. They addressed the importance of accurately characterizing reservoir fracture properties. The average reservoir matrix porosity, estimated using the Bortex method, is 3% in the previous study.

In the naturally fractured reservoirs like San Pedro, fluids exist in two systems. The rock matrix provides the storage of fluids and the fracture network provide main route for flow dynamics. If the fractures (or equivalent matrixes) are only considered to provide the main path and storage for flow, this type of system is a single porosity single permeability (SPSP: most common). Otherwise, the main flow exists in the fracture, while the matrixes are only connected to the fracture network in the dual porosity and single permeability (DPSP). The flux interchange between the matrix and fracture are defined with transfer function (Kazemi et al. 1976). Hence, two fracture properties (fracture permeability and porosity) and transfer function factor (σ) are the most important but uncertain parameter in dual porosity models.

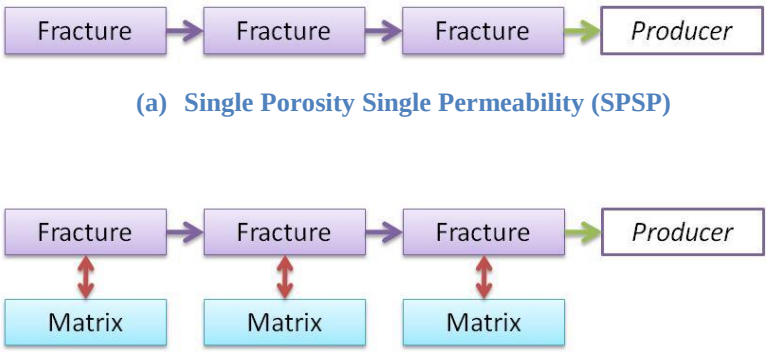

(a) Single Porosity Single Permeability (SPSP)

(b) Dual Porosity Single Permeability (DPSP)

Figure 4.6. Schematics of the Fracture-Matrix Flow Mechanism

4.5.2 Initial Fracture Network (DFN) Model

As shown in **Fig. 4.7**, open fractures are observed in reservoir quality rocks within the basin. Three types of fractures are reported from the geological data. The first corresponds to sedimentary features and are manifest at bed boundaries and in cross-

beds. The second type corresponds to regional joints which are perpendicular to each other. The last is associated with faults, vary locally and have a large uncertainty but closely relate to productivity.

Figure 4.7. Observed Fractures from San Pedro Field

Fracture properties are measured in the field using a Formation Micro Imager (FMI), shown in **Fig. 4.18**. The FMI measures properties including density, dip angle, dip magnitude and azimuth.

Figure 4.8. Image Logging Tool

The stereonet and strike rosset plots (also called *rose plot*) in **Fig. 4.9** show a high dispersion of the fractures with an average dip azimuth in the Paleozoic section of 33˚ / 35 ˚.

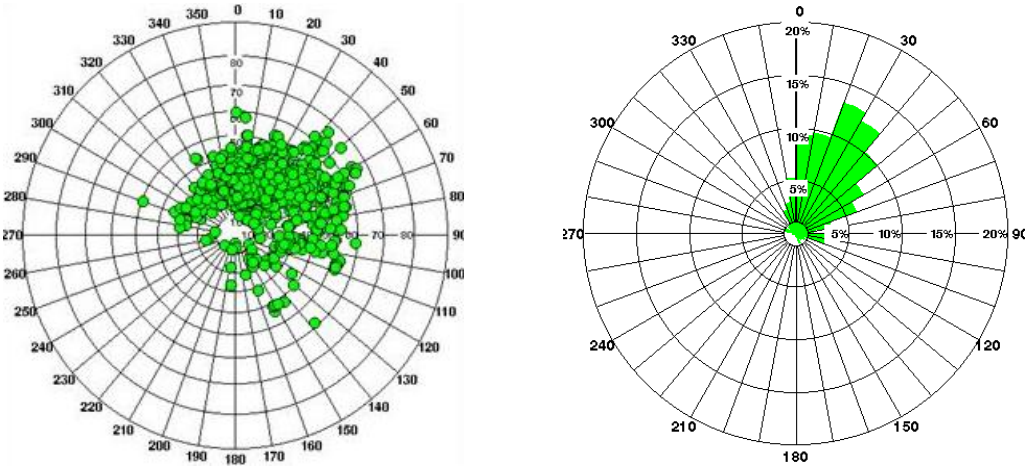

Figure 4.9. Example of Steronet and Strike Rosette of all Conductive open Fractures Interpreted on the Images (FMI)

A detailed structural analysis is obtained from the interpreted bedding planes as in **Fig. 4.10**. Fracture properties derived from logging include density, aperture, permeability and porosity, all of which are incorporated into the prior geologic model. In the first track in **Fig. 4.10**, fracture porosity is computed from the FMI-interpreted fractures to the right. The second track shows the fracture aperture as estimated from a resistivity log; open fractures are shown as blue points and partial or discontinuous fractures as yellow points. The third track depicts the lithology with depth, and the fourth through sixth tracks the dynamic and static formation micro scanner (FMS) images, together with the corresponding fracture orientation at their right. The final track plots the fracture density (fractures per foot). **Table 4.1** lists each of the fracture property distributions as applied for population of the initial geological model. The corresponding Discrete Fracture Network (DFN) model is illustrated in **Fig. 4.11**. The high average fracture permeability, aperture distribution and length indicate a well-connected flow network.

To map the high-resolution DFN properties to the flow simulation grid we use the Oda-based upscaling algorithm which upscales fracture permeability, aperture and length relative to the total area of fractures in each cell (Oda 1985). The Oda approach solves for the upscaled values independent of fluid flux of dynamic information and, therefore, does not account for fracture connectivity or length (Correia et al. 2011). For this reason it is necessary to characterize the upscaled fracture properties of equivalent simulation grids through history matching process.

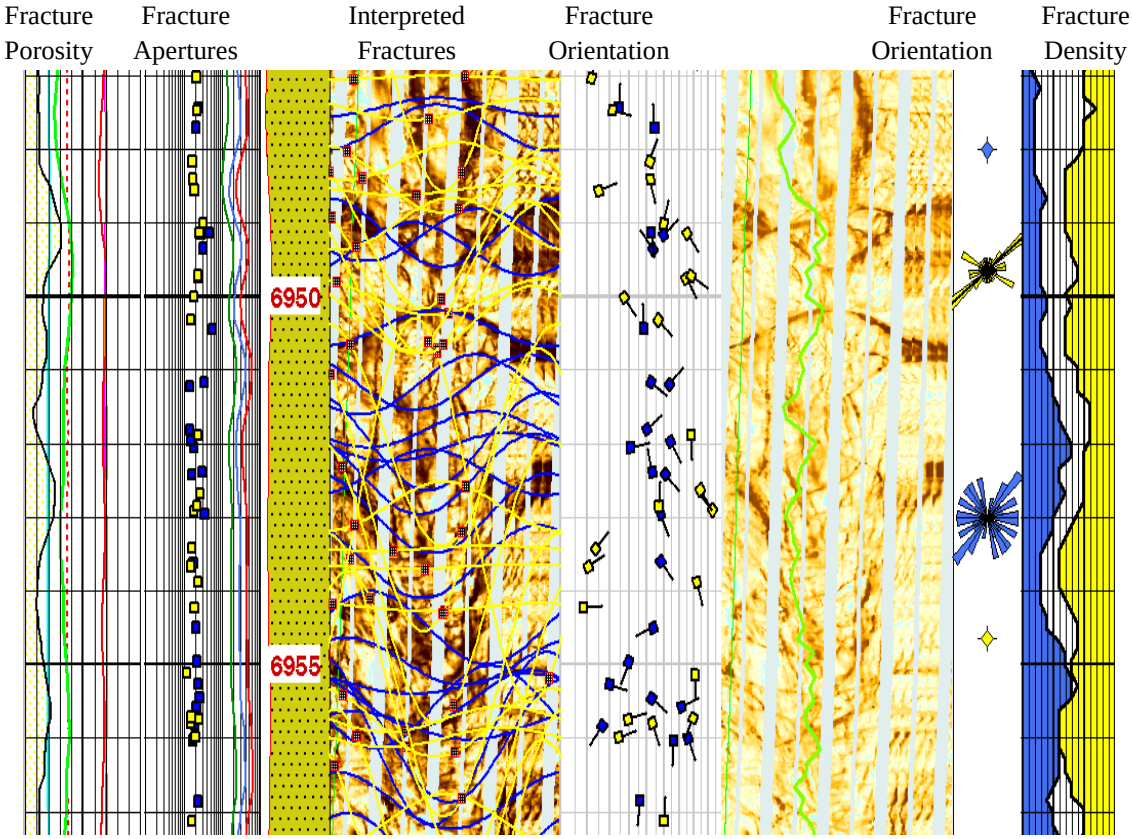

Figure 4.10. Example of the Fracture Interpretation in the geologic data

The distribution of fracture properties from initial geological model, are summarized in **Table. 4.1**. The initial Discrete Fracture Network (DFN) model is illustrated in **Fig. 4.21**.

Table 4.1. Fracture Properties

Fracture Properties	Unit	Min	Max	Mean	Standard Deviation
Permeability	*md*	33.3	1.74E+7	2.19E+6	3.5E+6
Aperture	*ft.*	2.07E-6	1.50E-3	3.98E-4	3.5E-4
Length	*ft.*	5.47	5.0E+2	2.21E+2	1.2E+2
Surface Area	ft^2	6.01	1.25E+5	2.78E+4	2.8E+4
Dip	*deg*	1.73	90.0	56.2	14.3
Dip azimuth	*deg*	0	360	242	99

The high average fracture permeability, aperture distribution and its length show the strong flow network. This fracture network is described in the geologic model then upscaled to equivalent initial simulation model.

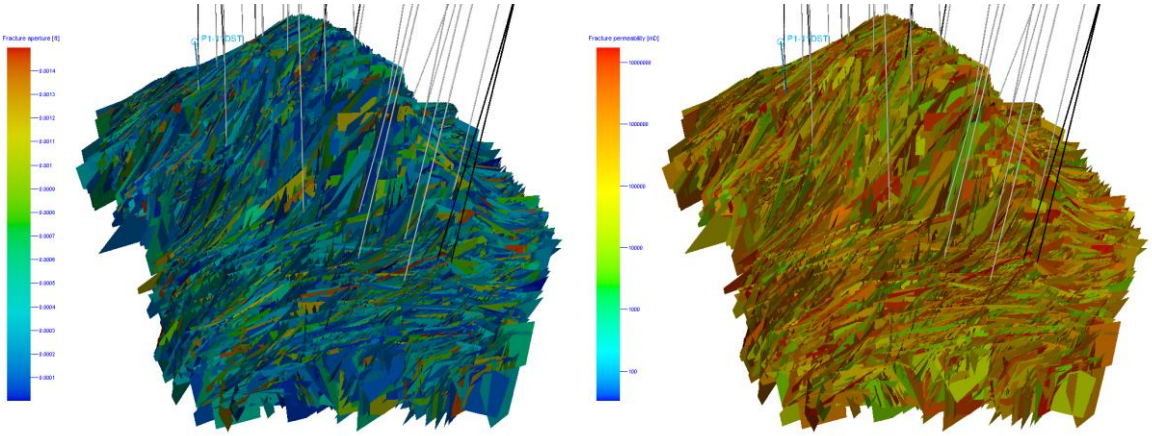

Figure 4.11. Fracture Aperture and Permeability in initial Discrete Fracture Network (DFN) model

For upscaling DFN properties into the simulation grid, we use Oda-based upscaling algorithm in the geologic software package, Petrel, which upscale the fracture permeability based on the total area of fractures in each cell (Oda 1985). This method is fast because it solves upscaling problems without flow simulation, but it cannot account for fracture connectivity and its length (Correia et al. 2011). Now, we have an initial simulation grid for history matching from geologic data.

4.5.3 Global History Match: Initial Model and Parameter Sensitivity Analysis

Throughout the whole History matching process, we focus on the characterizing Aquifer and fracture network properties. From the sensitivity analysis and response surface, we choose the "heavier hitter" with big uncertainties as in **Table. 4.2** from fractures and aquifer parameters.

Table 4.2. Sensitivity Analysis

Global Parameter	Initial	Min	Max	Sensitive	Update Parameter
WOC	7,175	7,060	7,175	YES	NO
GOC	3,275	3,100	3,275	YES	NO
Sigma Multiplier	1	E-4	1	YES	YES
Fracture Porosity Multiplier	1	0.8	1.5	YES	YES
Fracture Transmissibility Multiplier	1	0.8	3	YES	YES
Matrix Porosity Multiplier	1	0.8	1.5	NO	NO
Matrix Transmissibility Multiplier	1	0.8	3	NO	NO
Aquifer Depth	7,300	7,100	7,300	YES	YES

From parameter sensitivity analysis, we select fracture property multipliers (Sigma, fracture porosity and permeability) and aquifer depth as calibrating parameters. Selected multiplier is at first updated with genetic algorithm. In this global stage, we find optimal zonal fracture properties multipliers; fracture porosity and sigma, which are segmented by spectral clustering based on spectral theory as illustrated in next section.

4.5.4 Spectral Clustering: Model Segmentation

The new proposing spectral segmentation technique has been applied for global history matching stage. The affinity Laplacian is constructed based on mesh connectivity based matrix (Zhang et al. 2010) from **Eq. 4.5**.

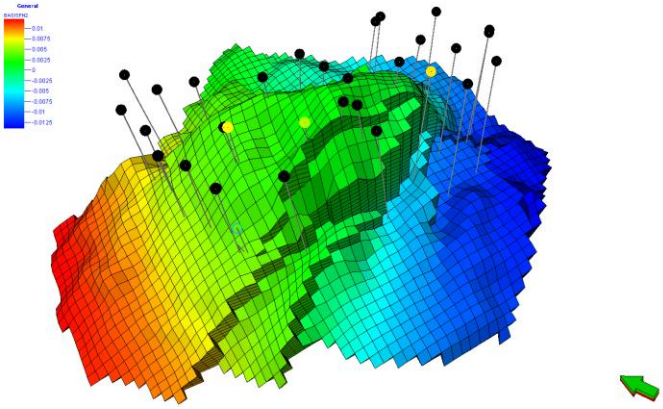

Figure 4.12. The Second Eigen Vector

The second eigenvector of connectivity Laplacian, shown in **Fig. 4.12**, provides the optimal spectral clustering criteria. Using this second eigenvector is the way in spectral clustering, to optimally divide the domain into regions with minimal effort (Shi and Malik 2000). The segmented zones are illustrated in **Fig. 4.13**. Selecting number of segments in the global matching is tradeoff between computation costs and degree of freedom. Hence, selection process is a heuristic approach and need some experience. In this San Pedro model, we selected 20 segments for genetic algorithm calibrating parameters (middle in **Fig. 4.13**). Note that using connectivity Laplacian is efficient than weighting by prior when more than one history matching parameters with different distribution or magnitude involve with clustering. In this stage, we update the fracture sigma and fracture porosity, totally 40 variables plus aquifer depth for GA.

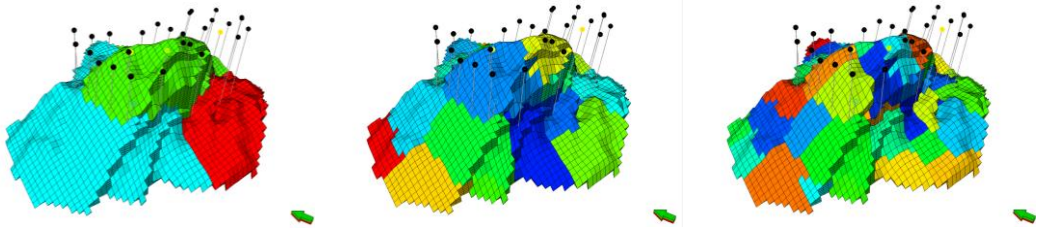

Figure 4.13. Segmented Model (3, 20, 50 Segments from left)

4.5.5 Genetic Algorithm Model Update

In the global stage history matching, we applied the genetic algorithm with proxy. The target dynamic response to match is water production rate in this stage. The reservoir has oil production rate controls and there are some observed pressure data in the tubing head (THP) of key wells. So, we construct our objective function, targeting to minimize as shown in **Eq. 4.1**, combined with water, gas production Total and tubing head pressure misfits between observed data and calculated values from finite difference simulator, which is minimized during first global stage.

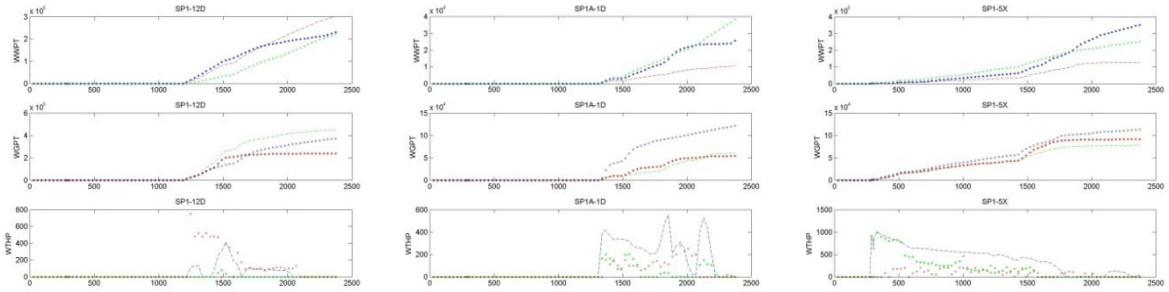

SP1A-12D SP1A-1D SP1-5X

Figure 4.14. Results from Global Stage History Matching (Water and Gas Production Total and Tubing Head Pressure)

We illustrated the some key wells' improved response during the global history matching process in **Fig. 4.14**, where round dots (◦) are observed data, bar dots (-) are initial model response and stars (∗) are GA generate realizations.

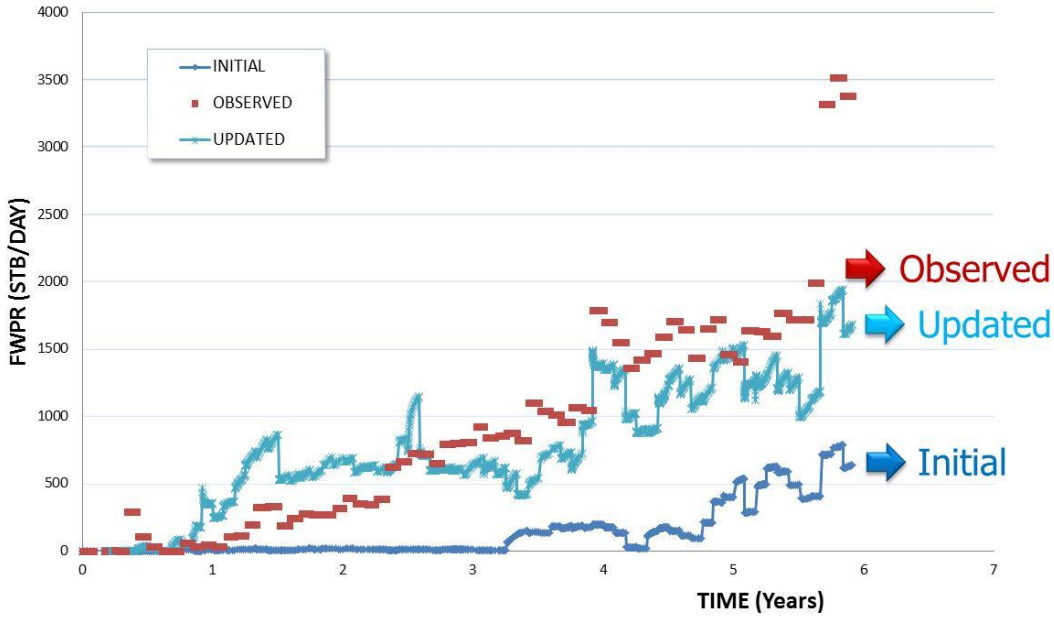

Figure 4.15. Field Water Production Rate (FWPR) after Global Update

Note that in the global matching stage, we updated fracture properties multiplier; porosity and sigma plus aquifer depth to match field wise energy balance. **Fig. 4.15** shows the updated water production rate from one of best GA realizations after global stage. It is clear that overall reservoir energy calibrated after global stage history matching.

4.5.6 Local Parameter Calibration: Parameterization

In the local stage model calibration, we applied the Grid Connectivity based parameterization (GCT). The basis vector in **Fig. 4.16** is generated from grid connectivity Laplacian in **Eq. 4.5**. The transformation between fine grid (u) and transformed domain (v) is easily converted by matrix multiplication. This is important property of reparametrization when we using fine grid sensitivity for updating basis coefficients. Recall that we used the 'second' eigenvector for spectral clustering in

global stage and will use 'leading eigenvectors' for reparameterization in local calibration from the same Laplacian.

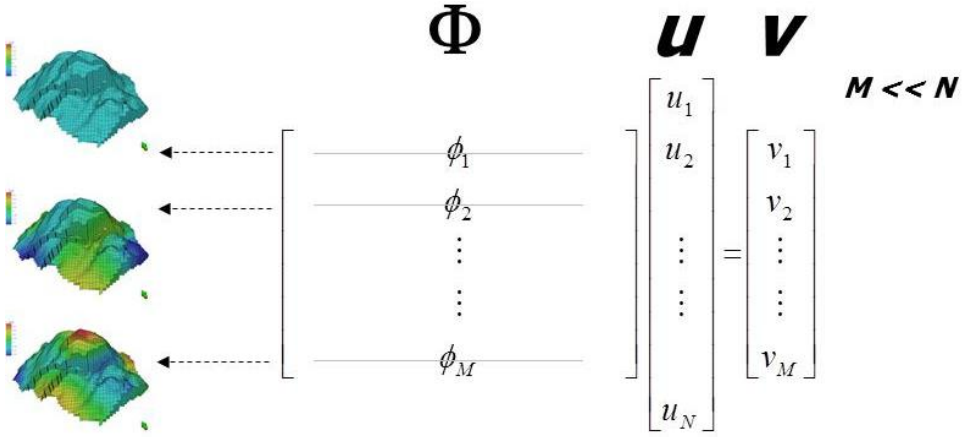

Figure 4.16. Parameterization with Grid Connectivity

4.5.7 Identifying Water Source and Sensitivity Calculation with Streamline

One and efficient way to analyze our problem is viewing local energy source with visualization. Water phase streamline provide a clear movement of water from source. We illustrate the water movement in **Fig. 4.17** and this help us to analysis the source of data misfit.

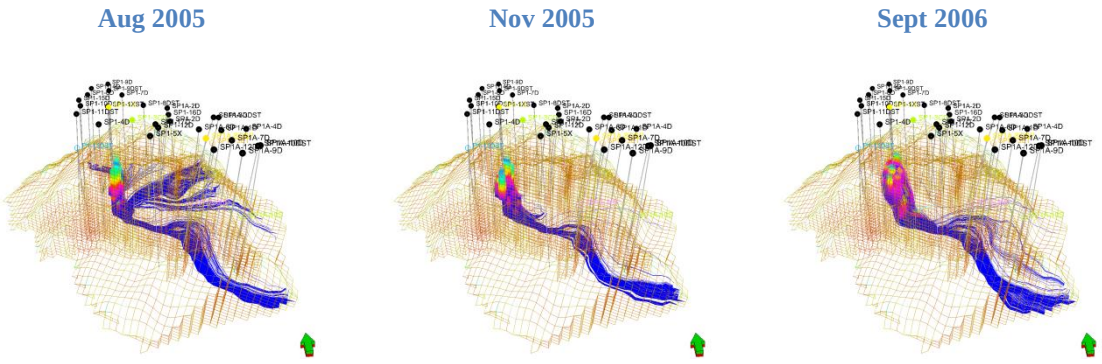

(a) Initial Model Water Influx before History Matching

Figure 4.17. Illustration of Single Water Phase Streamline at SP1-1X Well

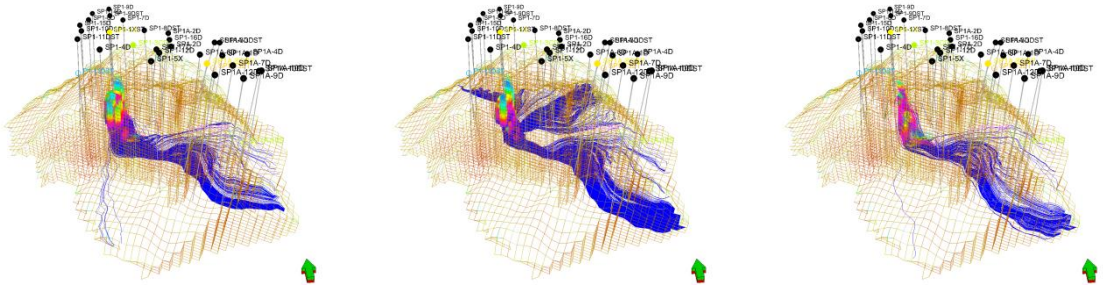

(b) Final Model Water Influx after History Matching

Figure 4.17. Continued

As we mentioned in mathematical section (**Eq. 4.13** to **4.18**), we integrated the streamline Generalized Travel Time (GTT) sensitivity for calculating basis coefficient sensitivity. The benefit of sensitivity based optimization is its fast convergence and cheaper computation time compared to gradient based method. In that sense, calculating basis coefficient (v) sensitivity is fast and attractive in field scale history matching. The streamline sensitivities are calculated by single finite difference calculation and streamline calculation (Cheng et al. 2005). Hence, utilizing this information does provide fast convergence. Updating in the transformed domain also spreads out local fine scale sensitivities to fieldwise scale; hence, we can update grid parameters not just along the streamline trajectory but for the entire reservoir domain.

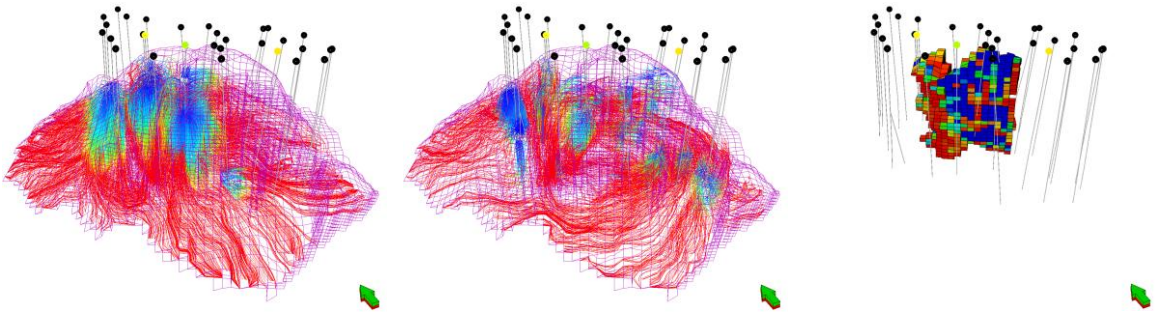

Figure 4.18. 3 Phase Streamline Tracing at Aug 2006 (Left), Oct 2011 (Middle) and Calculated Well Sensitivity (Right, SP1-2D)

Once the streamline sensitivity is calculated, we transform to the basis coefficient sensitivity as in **Eq. 4.18**. In this second local stage update, we used the 50 to 100 basis functions for history matching (see multi-scale iteration in **Fig. 4.2**). Integrating streamline sensitivity make multiscale approach more feasible in large field model, which can be computationally expensive using gradient based approach (Bhark et al. 2011a). At the same time, we update whole the reservoir grid property by updating in the transformed domain instead of calibrating along the streamline trajectory. This fast domain transform enables us to apply multiscale update more effective even to fine scale streamline sensitivity inversion. Finally, we calculate the required basis coefficient change (δv) by using Least Square Iteration Solver (LSQR).

4.5.8 Local Update Results

We illustrate the well by well improved response between the stages in **Fig. 4.19**. After first stage GA history matching, we can match most of reservoir energy in **Fig. 4.15**. From there, we calibrate local production balance with grid connectivity parameterization (GCT) in **Fig. 4.16**. **Fig. 4.19** shows how the two different steps work for reducing mismatch in water producing rate. At the initial stage, there is no water production in those two wells from finite difference simulator unlike the observation data.

The two stage hierarchical approach expedites the overall history matching speed and its quality. The multiscale-loop in **Fig. 4.2** helps to escape local minima and easily can add more resolution. Utilizing streamline sensitivity provides visual inspection of flow dynamics and fast computation for model update.

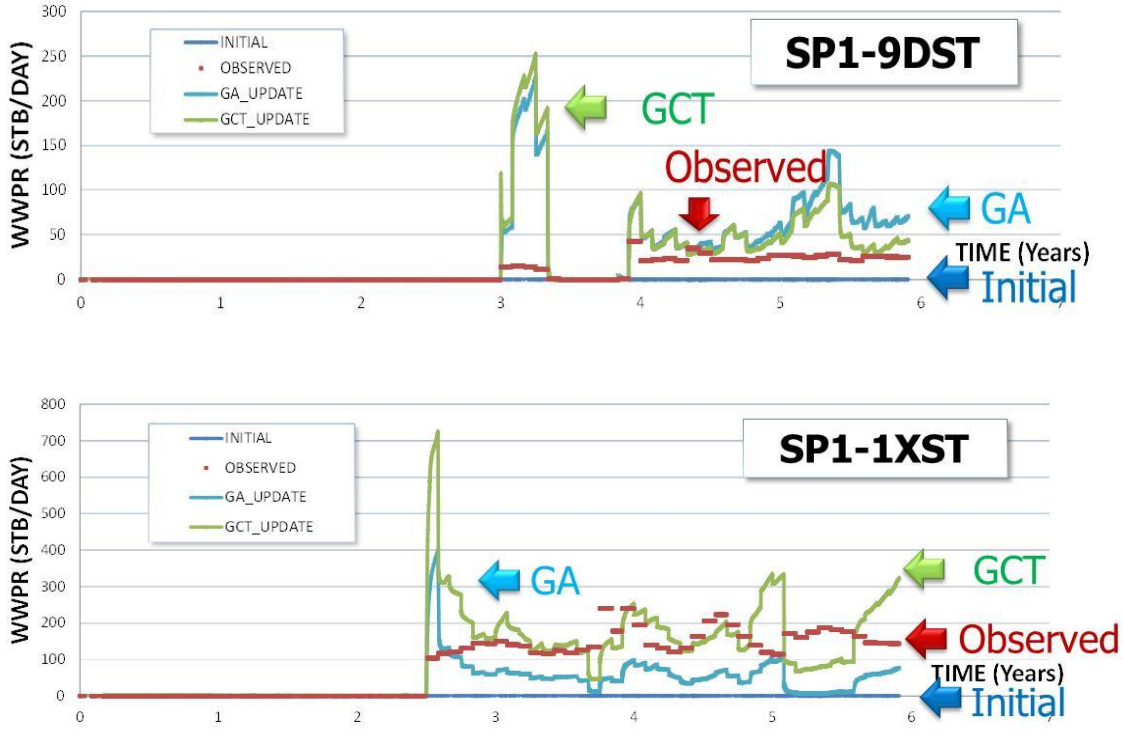

Figure 4.19. Well Water Production Rate (WWPR) Response

The final results are compared in **Fig. 4.20**; Well water production rate (WWPR), gas production rate (WGPR) and tubing head pressure (WTHP) are illustrate in sequence. Most of producing wells have big improvement (minimized data misfit) compared to initial dynamic response.

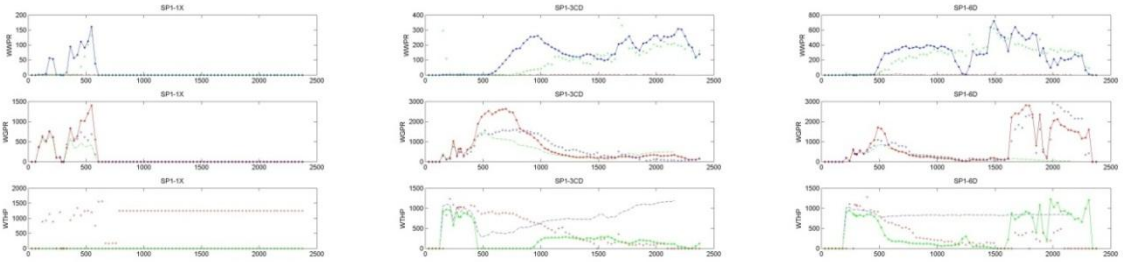

SP1-1X **SP1-3CD** **SP1-6D**

Figure 4.20. Final History Matching Results in All Producers
(round dot (○): observed, line (-): initial and star (⁎): updated)

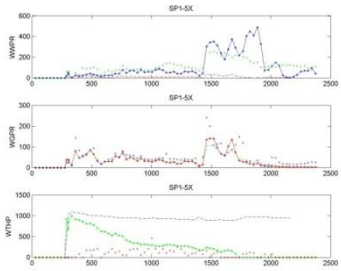

SP1-5X

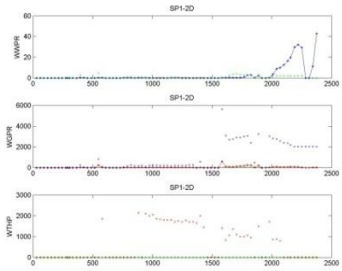

SP1-2D

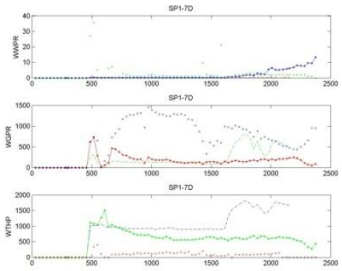

SP1-7D

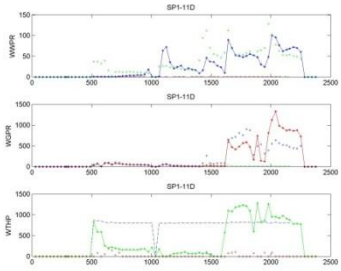

SP1-11D

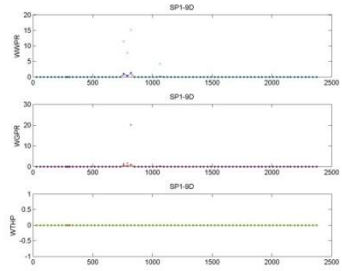

SP1-9D

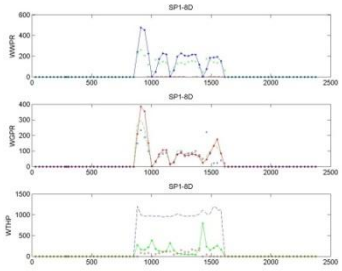

SP1-8D

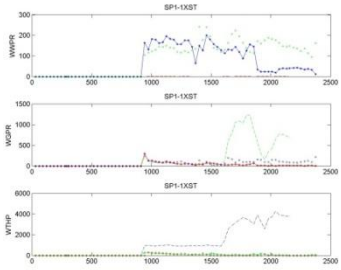

SP1-1XST

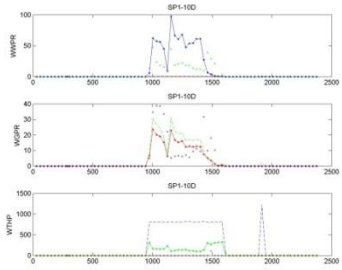

SP1-10D

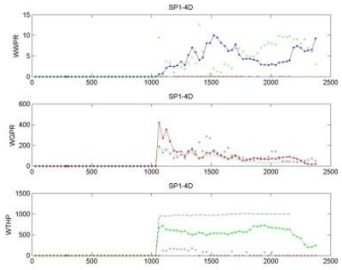

SP1-4D

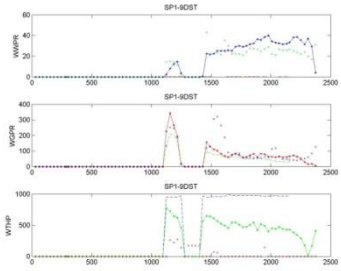

SP1-9DST

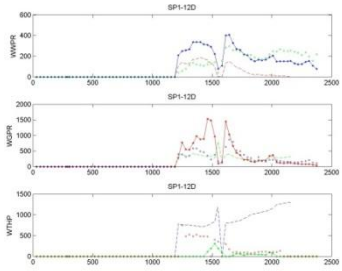

SP1-12D

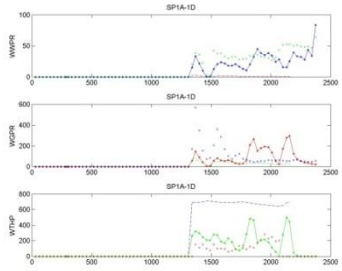

SP1A-1D

Figure 4.20. Continued

4.6 Summary and Conclusions

We propose a hierarchical history matching for complex geometry and highly fractured reservoir model. Our structured approach is successfully applied in the field example. We characterize the most uncertain model parameters in fractured reservoirs, fracture properties (fracture porosity, permeability and sigma) and aquifer depth. We can summarize our results as following,

1. We have proposed a hierarchical history matching process and simplified our problem into two stages in a highly fractured reservoir. Our approach starts from global parameter update with zonal multiplier from spectral clustering (or segmentation). We then calibrate local parameter with GCT parameterization. This hierarchical or structured history match corresponds with many industry experience but we suggest automatic history matching workflows both global and local stage.

2. In the global scale updating, we have updated a few heavy hitters such as fracture shape factor (σ) and fracture porosity multipliers, in addition to aquifer property. This small size of global parameters and zonation approach can significantly expedite field scale reservoir energy balance after minimal runs.

3. The spectral clustering using 'Normalized cut' from Connectivity Laplacian, which provides a good zonation measure. This is not an arbitrary cut but based on spectral theories. The algorithm proposes a fast and reasonable multiplicative zones based on the flow dynamic connectivity and/or model heterogeneity.

4. Model reduction into parameterized domain with Grid Connectivity Transformation increases the convergence speed through a significant reduction in the parameter space. The updating in the parameter domain prevents the

trapping in the local minima and helps to preserve initial model heterogeneity by introducing multiplier field.

5. Integrating streamline sensitivity or adjoint sensitivity can save expensive computation costs compared to gradient based methods. With single reservoir simulation and streamline tracing, we can determine basis coefficient sensitivity. This sensitivity can be utilized for updating model with Least Square Iteration Solver (LSQR). Model is updated not just along the streamline but at the entire reservoir scale. The integration approach provides an easy multiscale updating from coarse scale to finest.

6. We have validated our approach with a field example. The applicability for the real problem has been demonstrated by a highly fractured field with complex geometry, San Pedro in the Offshore Peru. For a complex example, initial model analysis and a structured hierarchical history matching approach are essential in addition to the assisted history matching algorithm.

CHAPTER V
CONCLUSION AND RECOMMENDATION

In this research, we focused on aspects of closed loop reservoir management, especially for highly fractured reservoirs. The proposed new methodologies are tested in simple synthetic and field examples. In the first part (**Chapter 2**), we introduce the generalized drainage volume calculations with streamline diffusive time of flight. The depth of investigation is calculated along the streamline trajectory from the diffusivity equation. This approach can be applicable to unconventional tight and shale gas reservoir under general and changing field operator conditions. The identified drainage region can help optimize new infill well locations. We expand the drainage volume calculations to propose optimal fracture stages in the horizontal wells. We also proposed a novel reservoir model segmentation technique for global scale model update using history matching and for field scale optimization in **Chapter 3**. Our proposed algorithm provides decision criteria for model partitioning, multiplicative zones, in the global scale model update.

Finally in **Chapter 4**, we apply a hierarchical history matching approach to a structurally complex fractured reservoir. We suggest a systematic history matching approach for fractured reservoirs with genetic algorithm (GA) and model segmentation for global change and grid connectivity transformation (GCT) for local update.

5.1 Drainage Volume Calculation, Well Placement and Hydraulic Fracture Stages Optimization

We have presented a systematic approach to well placement in naturally fractured tight gas reservoirs based on the well drainage volumes computed from dual porosity numerical simulation. Specifically, we have extended the radius of investigation concept (Lee 1982) to arbitrary heterogeneity and well conditions by utilizing the gas streamlines derived from dual porosity numerical simulation. This allows us to visualize the undrained regions and optimize infill well placement based on a single flow simulation.

The results have been shown to be consistent with well placement optimization through exhaustive flow simulations. Some specific conclusions from this study are as follows.

1. Using a high frequency asymptotic solution of the diffusivity equation, the concept of radius of drainage (Lee 1982) has been generalized to arbitrary heterogeneous medium and general flow conditions by examining the propagation of a 'pressure front' corresponding to an impulse (instantaneous) source along gas streamlines. The gas streamlines can be traced from the flux field of a finite-difference flow simulation.

2. Visualizing the well drainage is a physical and intuitive way of examining the influence of existing wells and their mutual interference. By summing up the grid cells intersected by the streamlines originating from a producing well, we can quantitatively estimate the well drainage volume, its evolution with time and potential interference from wells in the vicinity.

3. We have used a discrete fracture network model to examine the role of natural fractures in the well drainage volumes. As expected, the results show that the presence of natural fractures tends to enhance the well drainage volumes and accelerate production depending upon the distribution and orientation of fractures.

4. Based on the undrained reservoir volumes and reservoir static and dynamic properties, we have defined a 'depletion capacity' map for rapid identification and optimization of infill locations in tight gas reservoirs. The power and utility of the method has been demonstrated using both synthetic and field applications.

5. We have demonstrated the use of drainage volume concept in optimizing number of fracture stages in the Cotton Valley formation. The incremental drainage

volumes with the number of fracture stages seem to reach a diminishing return. Eight to ten hydraulic fracture stages indicate the most optimal completion strategy for the horizontal well studied from the field example.

6. The optimization based on the drainage volume was found to be consistent with the performance forecasting based on the rate profiles generated from the simulator. Besides quantitative analysis, drainage volume calculations provide the added benefits of flow visualization with no additional simulation.

5.2 Model Segmentation from Spectral Clustering

We propose a new model segmentation technique from spectral clustering theory. The suggested zonal approach is verified with both synthetic and Brugge SPE benchmark model. The new zonation algorithm provides rigorous criteria for history matching compared to old industry practice of using box multiplier.

Our proposed procedure is: (1) construct adjacency based Laplacian to capture spatial variability in subsurface properties (2) use graph partitioning techniques to create zonation and find cutting edge (3) apply partitioning with history matching algorithm. The graphic cut from the model geometry and/or heterogeneity is not arbitrary and is derived from optimization with graphic cutting metric.

1. The proposed zonation algorithm can preserve the major features of the prior model after history matching because the generated zonation is based on the model heterogeneity and/or connectivity information. We illustrate that spectral clustering approach can potentially capture different facies in the reservoir.

2. We propose three different Affinity Laplacian constructions and four different graph cutting algorithms. Basically, there is no ground truth in spectral clustering. So, it is not possible to say which one is the best or the worst. But we can arrive at some general conclusions from image clustering problems:

'normalized' cut is more statistically stable than 'ratio' cut. Also, 'Cheeger' cut shows at least as good or better performance than 'standard' cut. Hence, 'Normalized Cheeger Cut' is a good starting point for segmentation.

3. The spectral clustering problem is a NP-hard and heuristic approach. As we demonstrated, we can generate different cutting with combinations of Laplacian and cutting algorithms. Even wider choices are available with free parameter and cutting range. We inherited these properties in our proposed segmentation. Hence, we require some initial experiments and experience with different combination of cutting algorithms and Laplacian. Also, the two free parameters and cut off range heavily impact the clustering.

4. Through human interventions and heuristics, the spectral clustering provides a good guideline for automatic zonation criteria. This is more attractive when we do hierarchical history matching; which is essential for history matching problems for full-field model with decades of production history. We can adapt this zonal concept for global stage history matching and then further calibrate with fine scale approach.

5.3 A Hierarchal Multiscale Model Calibration with Spectral Domain Parameterization and its Application

We propose a hierarchical history matching for complex geometry and highly fractured reservoir model. Our structured approach is successfully applied in the field example. We characterize the most uncertain model parameters in fractured reservoirs, fracture properties (fracture porosity, permeability and sigma) and aquifer depth. We can summarize our results as following,

1. We have proposed a hierarchical history matching process and simplified our problem into two stages in a highly fractured reservoir. Our approach starts from

global parameter update with zonal multiplier from spectral clustering (or segmentation). We then calibrate local parameter with GCT parameterization. This hierarchical or structured history match corresponds with many industry experience but we suggest automatic history matching workflows both global and local stage.

2. In the global scale updating, we have updated a few heavy hitters such as fracture shape factor (σ) and fracture porosity multipliers, in addition to aquifer property. This small size of global parameters and zonation approach can significantly expedite field scale reservoir energy balance after minimal runs.

3. The spectral clustering using 'Normalized cut' from Connectivity Laplacian, which provides a good zonation measure. This is not an arbitrary cut but based on spectral theories. The algorithm proposes a fast and reasonable multiplicative zones based on the flow dynamic connectivity and/or model heterogeneity.

4. Model reduction into parameterized domain with Grid Connectivity Transformation increases the convergence speed through a significant reduction in the parameter space. The updating in the parameter domain prevents the trapping in the local minima and helps to preserve initial model heterogeneity by introducing multiplier field.

5. Integrating streamline sensitivity or adjoint sensitivity can save expensive computation costs compared to gradient based methods. With single reservoir simulation and streamline tracing, we can determine basis coefficient sensitivity. This sensitivity can be utilized for updating model with Least Square Iteration Solver (LSQR). Model is updated not just along the streamline but at the entire reservoir scale. The integration approach provides an easy multiscale updating from coarse scale to finest.

6. We have validated our approach with a field example. The applicability for the real problem has been demonstrated by a highly fractured field with complex geometry, San Pedro in the Offshore Peru. For a complex example, initial model analysis and a structured hierarchical history matching approach are essential in addition to the assisted history matching algorithm.

5.4 Recommendation

1. Drainage Volume Calculation with Streamline Diffusive Time of Flight
    1) Application to Dual Porosity and Dual Permeability (DPDP) Model.
    2) Well Spacing Optimization
    3) Compare with Decline Curve Analysis
    4) History Matching with Pressure Transient Analysis

2. Spectral Clustering
    1) Clustering with Dynamic Data
    2) Include Producers and Injector Information in the Clustering
    3) Co-Clustering Algorithm
    4) K-Means Clustering
    5) Grouping of Realizations in the Solution Space

3. Hierarchical History Matching
    1) Reparameterization with Prior-weighted Connectivity Transformation
    2) Fine scale Fracture Porosity and Sigma Sensitivity Calculation with Streamline and Inversion
    3) History Matching with DPDP Model

NOMENCLATURE

a_{ij}	Adjacency between cell *i* and *j*
A	Adjacency matrix
A_k	Real functions of amplitude of wave
α	Diffusivity
β_1	The strength of preserving prior model
β_2	The strength of change model smooth
C	Cluster
$\overline{C}$	Complement of Cluster *C*
$\|C\|$	Number of Vertices
cut	Objective for graph partitioning
d_i	Degree of connectivity of cell *i*
D	Degree of connection matrix
DC	Depletion capacity
$(\circ)$	Entrywise product operator
δR	Change in the reservoir property to be made
$\Delta\tilde{t}$	The vector of generalized travel time shift at the wells
δv	The vector of basis coefficient change to be made
ε	A Negligible Value
f_i	Grid Property of cell *i*
f_k	k^{th} natural vibration frequency of a system
f_n	Natural vibration frequency
f_w	Water fractional flow
ij	Grid block position *i, j*
J	Objective function for local stage
k	Number of basis used for domain transform
k	Permeability

L	Grid Laplacian matrix
L_s	String length
$\hat{L}$	A second spatial difference operator
λ_i	i^{th} Eigenvalue
m	Vector of parameters for GA update
m	Matrix
m_G	Local model parameter for local update
μ	Linear density of string
$Ncut$	Normalized cut
N_d	Number of observation points
n	Number of connected grid points
n_m	Harmonic mode
$\| \cdot \|$	Norm
O	Objective function
Obs	Observed data
P	Probability of model
$p(x,t)$	Pressure at time t
p_i	Grid property of cell i
ϕ_i	Basis function or vector
$\phi(\mathbf{x})$	porosity
ψ	Streamline
r	Euclidean distance cut off limit
$\boldsymbol{R^2}$	Correlation Coefficient
$Rcut$	Ratio cut
$s(x)$	Slowness of streamline
S	The basis coefficient sensitivity matrix
Sim	Simulated response
S_w	Water saturation

t	Time, t
t_{max}	Time of maximum pressure change
T_n	Temperature like parameter
τ	Streamline time of flight
$\tau(x)$	Diffusive time of flight
$\hat{\tau}(x)$	Streamline time of flight
u	Fine Grid property
μ	Fluid viscosity
v	Basis coefficient
$v(x)$	Interstitial velocity of a neutral tracer
V_{porv}	Pore volume
$vol(C)$	Summation over the Weights of all edges attached to Vertices
w_{ij}	Connectivity weight between grids i and j
W	Connectivity weight Matrix
ω	Wave frequency
w	Connectivity Weight between Two Points
$\mathbf{x}$	Location of grid block
x	Location in a String
x_f	Length of hydraulic fracture (one wing)
x_i	Grid centroid coordinate of cell i
ζ	Distance along the streamline
y	Magnitude of Vibration

REFERENCES

Adalsteinsson, D. and Sethian, J. 1995. A Fast Level Set Method for Propagating Interfaces. *Journal of Computational Physics* **118** (2): 269 - 277. USA

Aguilera, R. 2008. Role of Natural Fractures and Slot Porosity on Tight Gas Sands. Paper SPE-114174-MS presented at the SPE Unconventional Reservoirs Conference, Keystone, Colorado, USA, 02/10/2008.

Agunwoke, G.O., Egbele, E., and Onyekonwu, M. 2004. A Statistical Approach to Reservoir Zonation. Paper SPE-88962 presented at the Nigeria Annual International Conference and Exhibition, Abuja, Nigeria, 01/01/2004. DOI: 10.2118/88962-ms.

Al-Harbi, M.H., Cheng, H., He, Z. et al. 2005. Streamline-Based Production Data Integration in Naturally Fractured Reservoirs. *SPE Journal* **10** (4): 426 - 439 DOI: 10.2118/89914-pa

Al-Hussainy, R., Jr., H.J.R., and Crawford, P.B. 1966. The Flow of Real Gases through Porous Media, *Journal of Petroleum Technology* **18**. DOI: 10.2118/1243-A-PA.

Al-Huthali, A.H. and Datta-Gupta, A. 2004. Streamline Simulation of Water Injection in Naturally Fractured Reservoirs. Paper SPE-89443 presented at the SPE/DOE Symposium on Improved Oil Recovery, Tulsa, Oklahoma, 01/01/2004. DOI: 10.2118/89443-ms.

Al-madani, H.S. and Holditch, S.A. 2011. A Methodology to Determine Both the Technically Recoverable Resource and the Economically Recoverable Resource in an Unconventional Gas Play. Paper SPE-141368-MS presented at the SPE Middle East Oil and Gas Show and Conference, Manama, Bahrain, 01/01/2011. DOI: 10.2118/141368-ms.

Alhuthali, A.H. 2009. Optimal Waterflood Management under Geologic Uncertainty Using Rate Control: Theory and Field Applications. Paper SPE-129511-STU presented at Annual Technical Conference and Exhibition, 10/04/2009, New Orleans, Louisiana, USA. DOI 10.2118/129511-STU.

Amghibech, S. 2003. Eigenvalues of the Discrete P-Laplacian for Graphs. *Ars Combinatoria* **67**: 283-302.

Baihly, J.D., Coolidge, A.W., Dutcher, S.D. et al. 2007. Optimizing the Completion of a Multilayer Cotton Valley Sand Using Hydraulic-Fracture Monitoring and

Integrated Engineering. Paper SPE-110068-MS presented at the SPE Annual Technical Conference and Exhibition, Anaheim, California, U.S.A., 01/01/2007. DOI: 10.2118/110068-ms.

Bear, J. 1972. *Dynamics of Fluids in Porous Media*. New York: American Elsevier Pub. Co. The University of California. CA, USA.

Bhark, E.W., Datta-gupta, A., and Jafarpour, B. 2011a. History Matching with a Multiscale Parameterization Based on Grid Connectivity and Adaptive to Prior Information. Paper SPE-147372 presented at the SPE Annual Technical Conference and Exhibition, Denver, Colorado, USA, 01/01/2011. DOI: 10.2118/147372-ms.

Bhark, E.W., Jafarpour, B., and Datta-Gupta, A. 2011b. A Generalized Grid Connectivity Based Parameterization for Subsurface Flow Model Calibration. *Water Resour. Res.* **47** (6): W06517. DOI: 10.1029/2010wr009982

Bhark, E.W., Rey, A., Datta-gupta, A. et al. 2011c. Multiscale Parameterization and History Matching in Structured and Unstructured Grid Geometries. Paper SPE-141764 presented at the SPE Reservoir Simulation Symposium, The Woodlands, Texas, USA, 01/01/2011. DOI: 10.2118/141764-ms.

Blasingame, T.A. and Rushing, J.A. 2005. A Production-Based Method for Direct Estimation of Gas-in-Place and Reserves. Paper SPE-98042 presented at the SPE Eastern Regional Meeting, Morgantown, West Virginia, 09/14/. DOI.

Bogatkov, D.S. and Babadagli, T. 2008. Integrated Modeling and Statistical Analysis of 3-D Fracture Network of the Midale Field. Paper SPE-12165 presented at the International Petroleum Technology Conference, Kuala Lumpur, Malaysia, 01/01/2008. DOI: 10.2523/12165-ms.

Britt, L.K. and Smith, M.B. 2009. Horizontal Well Completion, Stimulation Optimization, and Risk Mitigation. Paper SPE-125526-MS presented at the SPE Eastern Regional Meeting, Charleston, West Virginia, USA, 01/01/2009. DOI: 10.2118/125526-ms.

Brun, B., Gosselin, O., and Barker, J.W. 2004. Use of Prior Information in Gradient-Based History Matching. *SPE Journal* **9** (1). DOI: 10.2118/87680-pa

Bubeck, S., Meila, M., and Von Luxburg, U. 2009. How the Initialization Affects the Stability of the K-Means Algorithm. *Arxiv preprint arXiv:0907.5494*. Cornell University Library.

Buhler, T. and Hein, M. 2009. Spectral Clustering Based on the Graph P-Laplacian. Paper presented at the Proceedings of the 26th Annual International Conference on Machine Learning, Montreal, Quebec, Canada. DOI: 10.1145/ 1553374. 1553385.

Červený, V. 2005. *Seismic Ray Theory*. Cambridge University Press.

Cheeger, J. 1970. A Lower Bound for the Smallest Eigenvalue of the Laplacian. *Problems Anal*: 195.

Chen, Y. and Oliver, D.S. 2010. Ensemble-Based Closed-Loop Optimization Applied to Brugge Field. *SPE Reservoir Evaluation & Engineering* **13** (1): 56 - 71. DOI: 10.2118/118926-pa

Cheng, H., Dehghani, K., and Billiter, T.C. 2008. A Structured Approach for Probabilistic-Assisted History Matching Using Evolutionary Algorithms: Tengiz Field Applications. Paper SPE-116212 presented at the SPE Annual Technical Conference and Exhibition, Denver, Colorado, USA, 01/01/2008. DOI: 10.2118/116212-ms.

Cheng, H., Kharghoria, A., He, Z. et al. 2005. Fast History Matching of Finite-Difference Models Using Streamline-Derived Sensitivities. *SPE Reservoir Evaluation & Engineering* **10**. DOI: 10.2118/89447-pa

Cipolla, C.L., Lewis, R.E., Maxwell, S.C. et al. 2011. Appraising Unconventional Resource Plays: Separating Reservoir Quality from Completion Effectiveness. Paper SPE-14677 presented at the International Petroleum Technology Conference, Bangkok, Thailand, 01/01/2011. DOI: 10.2523/14677-ms.

Cipolla, C.L., Lolon, E., Erdle, J. et al. 2009a. Modeling Well Performance in Shale-Gas Reservoirs. Paper SPE-125532 presented at the SPE/EAGE Reservoir Characterization and Simulation Conference, Abu Dhabi, UAE, 01/01/2009. DOI: 10.2118/125532-ms.

Cipolla, C.L., Lolon, E., Mayerhofer, M.J. et al. 2009b. Fracture Design Considerations in Horizontal Wells Drilled in Unconventional Gas Reservoirs. Paper SPE-119366-MS presented at the SPE Hydraulic Fracturing Technology Conference, The Woodlands, Texas, 01/19/2009.

Cipolla, C.L. and Mayerhofer, M. 1998. Understanding Fracture Performance by Integrating Well Testing & Fracture Modeling. Paper SPE-00049044 presented at the SPE Annual Technical Conference and Exhibition, New Orleans, Louisiana, 01/01/1998. DOI: 10.2118/49044-ms.

Cominelli, A., Ferdinandi, F., Montleau, P.C.d. et al. 2007. Using Gradients to Refine Parameterization in Field-Case History-Matching Projects. *SPE Reservoir Evaluation & Engineering* 10 (3): pp. 233-240. DOI: 10.2118/93599-pa

Correia, M., Maschio, C., Schiozer, D.J. et al. 2011. Upscaling Technique Applied to Naturally Fractured Carbonate Reservoirs. Paper SPE-143150 presented at the Brasil Offshore Conference, Brazil, 01/01/2011. DOI: 10.2118/143150-ms.

Cox, S.A., Gilbert, J.V., Sutton, R.P. et al. 2002. Reserve Analysis for Tight Gas. Paper SPE-78695-MS presented at the SPE Eastern Regional Meeting, Lexington, Kentucky, 10/23/2002.

D'Windt, A. 2007. Reservoir Zonation and Permeability Estimation:A Bayesian Approach. Paper 2007_UUU presented at the 48th Annual Logging Symposium, Austin, Texas, 01/01/2007.

Datta-Gupta, Kulkarni, A., Yoon, K.N. et al. 2001. Streamlines, Ray Tracing and Production Tomography: Generalization to Compressible Flow. *Petroleum Geoscience* **7**: 75-86.

Datta-Gupta, A. and King, M.J.M.J. 2007. *Streamline Simulation :Theory and Practice*. Spe Textbook Series. Richardson, TX: Society of Petroleum Engineers.

Dhillon, I.S., Mallela, S., and Modha, D.S. 2003. Information-Theoretic Co-Clustering. Paper presented at the Proceedings of the Ninth ACM SIGKDD International Conference on Knowledge Discovery and Data Mining, Washington, D.C. DOI: 10.1145/956750.956764.

Dyman, T.S. and Condon, S.M. 2006. Assessment of Undiscovered Conventional Oil and Gas Resources – Upper Jurassic – Lower Cretaceous Cotton Valley Group, Jurassic Smackover Interior Salt Basins Total Petroleum System, in the East Texas Basin and Louisiana – Mississippi Salt Basins Provinces. *Geological Survey Digital Data Series*. USGS. http://pubs.usgs.gov/dds/dds-069/dds-069-e/chapters.html. Downloaded 20 Aug 2011.

ElRafie, E.A. and Wattenbarger, R.A. 1997. Comprehensive Evaluation of Horizontal Wells with Transverse Hydraulic Fractures in the Upper Bahariyia Reservoirs. Paper SPE-00037759 presented at the Middle East Oil Show and Conference, Bahrain, 01/01/1997. DOI: 10.2118/37759-ms.

Fetkovich, M.J. 1980. Decline Curve Analysis Using Type Curves. *SPE Journal of Petroleum Technology* **32** (6): 1065-1077. DOI: 10.2118/4629-pa

Fiedler, M. 1973. Algebraic Connectivity of Graphs. *Czechoslovak Mathematical Journal* **23**: 298-305.

Fiedler, M. 1975. A Property of Eigenvectors of Nonnegative Symmetric Matrices and Its Application to Graph Theory. *Czechoslovak Mathematical Journal* **25** (4): 619-633.

Fischer, I. and Poland, J. 2004. *New Methods for Spectral Clustering*. Technical Report No. IDSIA-12-04. June. School of Computer Science and Engineering. Hebrew University, Jerusalem 91904, Israel

Gale, J.F.W. and Holder, J. 2008. Natural Fractures in the Barnett Shale: Constraints on Spatial Organization and Tensile Strength with Implications for Hydraulic Fracture Treatment in Shale-Gas Reservoirs. Paper 08-096 presented at the 42nd U.S. Rock Mechanics Symposium (USRMS), San Francisco, CA, 01/01/2008.

Gildin, E. and Lopez, T. 2011. Closed-Loop Reservoir Management: Do We Need Complex Models? Paper SPE-144336-MS presented at the SPE Digital Energy Conference and Exhibition, The Woodlands, Texas, USA, 01/01/2011. DOI: 10.2118/144336-ms.

Gringarten, E. and Deutsch, C.V. 1999. Methodology for Variogram Interpretation and Modeling for Improved Reservoir Characterization. Paper SPE-00056654 presented at the SPE Annual Technical Conference and Exhibition, Houston, Texas, 01/01/1999. DOI: 10.2118/56654-ms.

Hagen, L. and Kahng, A.B. 1992. New Spectral Methods for Ratio Cut Partitioning and Clustering. *Computer-Aided Design of Integrated Circuits and Systems, IEEE Transactions on* **11** (9): 1074-1085. DOI: 10.1109/43.159993

Hareland, G., Rampersad, P., Dharaphop, J. et al. 1993. Hydraulic Fracturing Design Optimization. Paper SPE-00026950 presented at the SPE Eastern Regional Meeting, Pittsburgh, Pennsylvania, 01/01/1993. DOI: 10.2118/26950-ms.

Hatzignatiou, D.G. and McKoy, M.L. 2000. Probabilistic Evaluation of Horizontal Wells in Stochastic Naturally Fractured Gas Reservoirs. Paper SPE-65459 presented at the SPE/CIM International Conference on Horizontal Well Technology, Calgary, Alberta, Canada, 11/06/2000.

He, Z., Datta-Gupta, A., and Yoon, S. 2001. Streamline-Based Production Data Integration under Changing Field Conditions. Paper SPE-71333 presented at the SPE Annual Technical Conference and Exhibition, New Orleans, Louisiana, 01/01/2001. DOI: 10.2118/71333-ms.

He, Z., Parikh, H., Datta-Gupta, A. et al. 2002. Identifying Reservoir Compartmentalization and Flow Barriers Using Primary Production: A Streamline Approach. Paper SPE-77589 presented at the SPE Annual Technical Conference and Exhibition, San Antonio, Texas, 01/01/2002. DOI: 10.2118/77589-ms.

Hein, M. and Büuhler, T. 2010. An Inverse Power Method for Nonlinear Eigenproblems with Applications in 1-Spectral Clustering and Sparse PCA. DOI: citeulike-article-id:10384511

Holditch, S.A. and Tschirhart, N. 2005. Optimal Stimulation Treatments in Tight Gas Sands. Paper SPE-96104-MS presented at the SPE Annual Technical Conference and Exhibition, Dallas, Texas, 10/09/2005.

Huang, X., Bentley, L.R., and Laflamme, C. 2001. Integration of Production History and Time-Lapse Seismic Data Guided by Seismic Attribute Zonation. Paper SPE-68819 presented at the SPE Western Regional Meeting, Bakersfield, California, 01/01/2001. DOI: 10.2118/68819-ms.

Huffman, C.H., Harkrider, J.D., and Thompson, R.S. 1996. Fracture Stimulation Treatment Design Optimization: What Can the Npv Vs Xf Plot Tell Us? Paper SPE-00036575 presented at the SPE Annual Technical Conference and Exhibition, Denver, Colorado, 01/01/1996. DOI: 10.2118/36575-ms.

Hur, A., Elisseeff, A., and Guyon, I. 2002. A Stability Based Method for Discovering Structure in Clustered Data. In *Pacific Symposium on Biocomputing*: 6-17.

Igor, F. and Jan, P. 2004. New Methods for Spectral Clustering. In. Galleria 2, 6928 Manno, Switzerland: IDSIA / USI-SUPSI, Dalle Molle Institute for Artificial Intelligence.

Jabbari, H. and Zeng, Z. 2011. A Three-Parameter Dual Porosity Model for Naturally Fractured Reservoirs. Paper SPE-144560 presented at the SPE Western North American Region Meeting, Anchorage, Alaska, USA, 01/01/2011. DOI: 10.2118/144560-ms.

Jimenez, E., Datta-Gupta, A., and King, M.J. 2008. Full Field Streamline Tracing in Complex Faulted Systems with Non-Neighbor Connections. Paper SPE-113425 presented at the SPE/DOE Symposium on Improved Oil Recovery, Tulsa, Oklahoma, USA, 01/01/2008. DOI: 10.2118/113425-ms.

Kang, S., Datta-gupta, A., and Lee, W.J.J. 2011. Impact of Natural Fractures in Drainage Volume Calculations and Optimal Well Placement in Tight Gas Reservoirs. Paper SPE-144338 presented at the North American Unconventional Gas

Conference and Exhibition, The Woodlands, Texas, USA, 01/01/2011. DOI: 10.2118/144338-ms.

Kazemi, H., Merrill Jr., L.S., Porterfield, K.L. et al. 1976. Numerical Simulation of Water-Oil Flow in Naturally Fractured Reservoirs *SPE Journal* **6**: 317-326. DOI: 10.2118/5719-pa

Kim, J.U., Datta-Gupta, A., Brouwer, R. et al. 2009. Calibration of High-Resolution Reservoir Models Using Transient Pressure Data. Paper SPE-124834 presented at the SPE Annual Technical Conference and Exhibition, New Orleans, Louisiana, 01/01/2009. DOI: 10.2118/124834-ms.

Kline, M. and Kay, I.W. 1965. *Electromagnetic Theory and Geometrical Optics*. New York: Interscience Publishers.

Kulkarni, K.N., Datta-Gupta, A., and Vasco, D.W. 2001. A Streamline Approach for Integrating Transient Pressure Data into High-Resolution Reservoir Models. *SPE Journal* **6** (3). DOI: 10.2118/74135-pa

Lee, J., Rollins, J.B., and Spivey, J.P. 2003. *Pressure Transient Testing*. Ed Engineers, S.o.P. Spe Textbook Series: Richardson, Texas.

Lee, W.J. 1982. *Well Testing*. New York: Society of Petroleum Engineers of AIME.

Lee, W.J. and Hopkins, C.W. 1994. Characterization of Tight Reservoirs. *SPE Journal of Petroleum Technology* **46** (11): 956-964. DOI: 10.2118/29091-pa

Lolon, E., Archer, R.A., Ilk, D. et al. 2008. New Semi-Analytical Solutions for Multilayer Reservoirs. Paper SPE-114946-MS presented at the CIPC/SPE Gas Technology Symposium 2008 Joint Conference, Calgary, Alberta, Canada, 06/16/2008.

Lolon, E.P., McVay, D.A., and Schubarth, S.K. 2003. Effect of Fracture Conductivity on Effective Fracture Length. Paper SPE-84311-MS presented at the SPE Annual Technical Conference and Exhibition, Denver, Colorado, 10/05/2003.

Massonnat, G., Viszkok, J., and Vrignon, M. 2002. Hierarchical Organization of Flow Network in Fractured Carbonate Reservoirs: Identification and Characterization of Key Parameters. Paper SPE-77488 presented at the SPE Annual Technical Conference and Exhibition, San Antonio, Texas, 01/01/2002. DOI: 10.2118/ 77488-ms.

Meyer, B.R., Bazan, L.W., Jacot, R.H. et al. 2010. Optimization of Multiple Transverse Hydraulic Fractures in Horizontal Wellbores. Paper SPE-131732 presented at the

SPE Unconventional Gas Conference, Pittsburgh, Pennsylvania, USA, 01/01/ 2010. DOI: 10.2118/131732-ms.

Meza, O., Gandulias, V.P., and cordova, E.n.e. 2010. Influence of Stress Field in the Productivity of Naturally Fractured Reservoirs in Metamorphic Basement: A Case Study of the San Pedro Field, Amotape Group. Paper SPE-138946 presented at the SPE Latin American and Caribbean Petroleum Engineering Conference, Lima, Peru, 01/01/2010. DOI: 10.2118/138946-ms.

Oda, M. 1985. Permeability Tensor for Discontinuous Rock Masses. *Géotechnique* **35**. DOI 10.1680/geot.1985.35.4.483.

Olson, J.E. 2008. Multi-Fracture Propagation Modeling: Applications to Hydraulic Fracturing in Shales and Tight Gas Sands. Paper 08-327 presented at the The 42nd U.S. Rock Mechanics Symposium (USRMS), San Francisco, CA, 01/01/2008.

Olson, J.E. and Taleghani, A.D. 2009. Modeling Simultaneous Growth of Multiple Hydraulic Fractures and Their Interaction with Natural Fractures. Paper SPE-119739 presented at the SPE Hydraulic Fracturing Technology Conference, The Woodlands, Texas, 01/01/2009. DOI: 10.2118/119739-ms.

Pearson, C.M., Bond, A.J., Eck, M.E. et al. 1992. Optimal Fracture Stimulation of a Moderate-Permeability Reservoir - Kuparuk River Unit, Alaska. *SPE Production Engineering* **7** (3): 259-266. DOI: 10.2118/20707-pa

Peters, L., Arts, R., Brouwer, G. et al. 2010. Results of the Brugge Benchmark Study for Flooding Optimization and History Matching. *SPE Reservoir Evaluation & Engineering* **13** (3): 391-405. DOI: 10.2118/119094-pa

Pothen, A., Simon, H.D., and Liou, K.-P. 1990. Partitioning Sparse Matrices with Eigenvectors of Graphs. *SIAM Journal on Matrix Analysis and Applications* **11** (3): 430-452.

Raghavan, R., Chen, C.C., and Agarwal, B. 1994. An Analysis of Horizontal Wells Intercepted by Multiple Fractures. Paper PETSOC-HWC-94-39 presented at the SPE/CIM/CANMET International Conference on Recent Advances in Horizontal Well Applications, Calgary, Canada, 01/01/1994. DOI: 10.2118/hwc-94-39.

Richardson, M. 2000. A New and Practical Method for Fracture Design and Optimization. Paper SPE-00059736 presented at the SPE/CERI Gas Technology Symposium, Calgary, Alberta, Canada, 01/01/2000. DOI: 10.2118/59736-ms.

Rushing, J.A., Newsham, K.E., Perego, A.D. et al. 2007. Beyond Decline Curves: Life-Cycle Reserves Appraisal Using an Integrated Work-Flow Process for Tight Gas Sands. Paper SPE-109836-MS presented at the SPE Annual Technical Conference and Exhibition, Anaheim, California, U.S.A., 11/11/2007. DOI.

Schulze-Riegert, R.W., Axmann, J.K., Haase, O. et al. 2002. Evolutionary Algorithms Applied to History Matching of Complex Reservoirs. *SPE Reservoir Evaluation & Engineering* **5** (2): 163-173. DOI: 10.2118/77301-pa

Sen, M.K., Datta-Gupta, A., Stoffa, P.L. et al. 1995. Stochastic Reservoir Modeling Using Simulated Annealing and Genetic Algorithms. *SPE Formation Evaluation* **10** (1). DOI: 10.2118/24754-pa

Sethian, J.A. 1999a. Fast Marching Methods. *SIAM Review* **41**: 199-235. DOI: citeulike-article-id:3102246

Sethian, J.A. 1999b. *Level Set Methods and Fast Marching Methods*: Cambridge University Press.

Shi, J. and Malik, J. 2000. Normalized Cuts and Image Segmentation. *Pattern Analysis and Machine Intelligence, IEEE Transactions on* **22** (8): 888-905. DOI: 10.1109/34.868688

Still, S. and Bialek, W. 2003. How Many Clusters? An Information Theoretic Perspective. *Neural Comput.* **16** (12 (December 2004)): 2483-2506. DOI: 10.1162/0899766042321751

Szu-Hao, H., Yi-Hong, C., Shang-Hong, L. et al. 2009. Learning-Based Vertebra Detection and Iterative Normalized-Cut Segmentation for Spinal Mri. *Medical Imaging, IEEE Transactions on* **28** (10): 1595-1605. DOI: 10.1109/tmi.2009.2023362

Thompson, R.R. and Blumer, D.J. 1991. Economic Optimization of Fracture Stimulations Using Mixed Integer-Linear Programming. Paper SPE-00021648 presented at the SPE Production Operations Symposium, Oklahoma City, Oklahoma, 01/01/1991. DOI: 10.2118/21648-ms.

Tibshirani, R., Walther, G., and Hastie, T. 2001. Estimating the Number of Clusters in a Dataset Via the Gap Statistic. Journal of the Royal Statistical Society: Series B (Statistical Methodology) **63** (2): 411 - 423. London, U.K

Vallhs, B. and Naevdal, G. 2009. Revisiting Brugge Case Study Using a Hierarchical Ensemble Kalman Filter. Paper IPTC-14074-MS presented at the International

Petroleum Technology Conference, Doha, Qatar, 01/01/2009. DOI: 10.2523/14074-ms.

Vasco, D.W. and Finsterle, S. 2004. Subsurface Hydrology - W01507. Numerical Trajectory Calculations for the Efficient Inversion of Transient Flow and Tracer Observations (Doi 10.1029/2003wr002362). *Water resources research.* **40** (1): n.p.

Vasco, D.W., Keers, H., and Karasaki, K. 2000. Estimation of Reservoir Properties Using Transient Pressure Data: An Asymptotic Approach. *Water Resour. Res.* **36** (12): 3447-3465. DOI: 10.1029/2000wr900179

Vasco, D.W., Yoon, S., and Datta-Gupta, A. 1999. Integrating Dynamic Data into High-Resolution Reservoir Models Using Streamline-Based Analytic Sensitivity Coefficients. SPE *Journal* **4** (4). DOI: 10.2118/59253-pa

Velez, E.I., Vasquez, J., Frydman, M. et al. 2010. Novel Approach for Fracture Characterization in a Metamorphic Reservoir. Paper SPE-138965 presented at the SPE Latin American and Caribbean Petroleum Engineering Conference, Lima, Peru, 01/01/2010. DOI: 10.2118/138965-ms.

Virieux, J., Flores-Luna, C., and Gibert, D. 1994. Asymptotic Theory for Diffusive Electromagnetic Imaging. *Geophysical Journal International* **119** (3): 857-868. DOI: 10.1111/j.1365-246X.1994.tb04022.x

von Luxburg, U. 2007. A Tutorial on Spectral Clustering. *Statistics and Computing* **17** (4): 395-416. DOI: citeulike-article-id:1856674

Von Luxburg, U. 2010. Clustering Stability. *Foundations and Trends in Machine Learning* **2** (3) : 235 - 274. DOI: 10.1561/2200000008

von Luxburg, U., Williamson, R.C., and Guyon, I. 2011. Clustering: Science or Art?. NIPS Workshop, December 11

Wang, S. and Siskind, J.M. 2003. Image Segmentation with Ratio Cut. *Pattern Analysis and Machine Intelligence, IEEE Transactions on* **25** (6): 675-690.

Warren, J.E. and Root, P.J. 1963. *The Behavior of Naturally Fractured Reservoirs*. SPE *Journal* **3** (3): 245-255.

Weiss, G. 1960. The Theory of Matrices. Vol. 1 and Vol. 2. F. R. Gantmacher. Chelsea Publishing Company, New York 68, 1959. Vol. 1: X + 374 Pp. Vol. 2: X + 277 Pp. . *Science* **131** (3408): 1216. DOI: 10.1126/science.131.3408.1216-a

Weiss, Y. 1999. Segmentation Using Eigenvectors: A Unifying View. In *Computer Vision, 1999. The Proceedings of the Seventh IEEE International Conference on* **972**, 2:975-982.

Wem, J., Jiang, H., and Wang, Y. 2010. Normalized Cut as Basic Tool for Remote Sensing Image. In *Intelligent Computing and Integrated Systems (ICISS), 2010 International Conference on* 247-249.

Weng, X., Kresse, O., Cohen, C.-E. et al. 2011. Modeling of Hydraulic-Fracture-Network Propagation in a Naturally Fractured Formation. *SPE Production & Operations* **26** (11). DOI: 10.2118/140253-pa

Wu, C.W. 2005. Algebraic Connectivity of Directed Graphs. *Linear and Multilinear Algebra* **53** (3): 203-223. DOI: 10.1080/03081080500054810

Wu, Z. and Datta-Gupta, A. 2002. Rapid History Matching Using a Generalized Travel-Time Inversion Method. *SPE Journal* **26** (4). DOI: 10.2118/78359-pa

Yin, J., Park, H., Datta-Gupta, A. et al. 2010. A Hierarchical Streamline-Assisted History Matching Approach with Global and Local Parameter Updates. Paper SPE-132642 presented at the SPE Western Regional Meeting, Anaheim, California, USA, 01/01/2010. DOI: 10.2118/132642-ms.

Zhang, H., Van Kaick, O., and Dyer, R. 2010. Spectral Mesh Processing. *Computer Graphics Forum* **29** (6): 1865-1894. DOI: 10.1111/j.1467-8659.2010.01655.x

APPENDIX A
A PETREL PLUG-IN FOR STREAMLINE TRACING, RESERVOIR MANAGEMENT & HISTORY MATCHING

A.1 Introduction

Reconciling high-resolution geologic models to dynamic data such as transient pressure, tracer and multiphase production history or time-lapse seismic data is by far the most time-consuming aspect of the workflow for geoscientists and engineers. Although significant advancements have been made in this area over the last decade, current industry practice still largely involves iterative trial and error methods and property multipliers that often result in local discontinuities and loss of geologic realism. Manual history matching is time-consuming, manpower intensive and highly subjective.

The DESTINY plug-in is designed for fast calibration of high resolution geologic models to dynamic data based on the research at the Texas A&M University. There are additional functionalities in DESTINY that allow for flow visualization, reservoir management and optimization through identification of well drainage and swept volumes and selection of optimal well locations for infill drilling. DESTINY can be used with both finite difference as well as streamline simulators. This extends its application from slightly compressible flow situations (for example, waterflood about bubble point pressure) to highly compressible flow such as gas reservoirs. DESTINY utilizes unique information gleaned from streamlines and a novel generalized travel time inversion of production data to update geologic models. Streamline-based sensitivities can be used to quickly identify the discrepancies between the geologic model and reservoir dynamic response. The sensitivities can be used in conjunction with the inversion algorithm to make targeted changes to geologic models while preserving geologic realism. In particular, the sensitivities can be obtained in a single forward simulation because it utilizes an analytic approach that involves 1-D integral along streamlines. The

DESTINY can also be used for assisted history matching aided by the streamline-derived sensitivities.

The DESTINY plug-in utilizes Ocean and PETREL technology extensively. It is composed of three sequential workflows: streamline tracing, parameter sensitivity calculation and history matching. The users can choose to turn on or off any of these functionalities. The inversion output provides complete information on the status of the history matching during execution. The plug-in has functions to monitor the sensitivity of each well, the updated geological model and its production response, and the production data misfit during the inversion process. Descriptive statistics can be generated on a field-wide or on a facies-by-facies basis with using the PETREL embedded functions. The synergy between PETREL and Ocean technology is fully utilized by the plug-in.

A.2 Streamline Applications Using DESTINY

Streamlines provide several benefits for reservoir characterization and management. The streamline trajectories and time of flight are useful for visualizing reservoir flow dynamics. Using streamlines, we can easily identify the drainage volumes and swept volumes associated with producers and injectors, respectively. This provides us with a natural way to identify potential infill producer and injector locations during water flooding. Streamlines can also be used to identify and visualize the connectivity and communication among wells or between wells and the aquifer. This allows us to identify the source of and also allocate fluid volumes associated with individual producers and injectors. This information can be utilized for pattern balancing and flood optimization.

A powerful application of streamlines is in waterflood management and optimization. The streamline time of flight provides us with a dynamic picture of the flood front evolution. By adjusting the injection and production rates at the wells, we can manage

the movement of the flood front to maximize waterflood sweep efficiency. This gives us an efficient approach to optimal waterflood management through rate control.

A commonly held misconception about the application of streamlines is that the technology is limited to incompressible flow and requires injectors and producers. In reality, the streamlines are simply a representation of the velocity field and streamlines exist whenever there is an underlying velocity field. This allows us to take advantage of the streamline technology in conjunction with finite difference simulation. For example, we can apply streamlines to compute and visualize the drainage volumes in tight gas reservoirs using the flux field generated from the finite difference simulation. The drainage volumes of existing wells can then be used to optimize infill locations based on undrained parts of the reservoir.

Streamlines are particularly useful for history matching. Streamlines can be used to identify and target changes during history matching. In particular, streamlines can be used to efficiently compute the sensitivity of the production response to reservoir parameters such as porosity and permeability. These sensitivities can then be used to facilitate manual history matching or can be used in conjunction with inversion algorithms to suggest updates to the geologic models. Reconciling high-resolution geologic models to production history is a very time-consuming aspect in reservoir modeling. Current practice still involves a tedious and manual history-matching process that is highly subjective and often employs ad-hoc property multipliers that can lead to loss of geologic realism. Streamline can aid during history matching in terms of (i) efficiency in workflow, (ii) obtaining geologic insight (iii) understanding reservoir dynamics and, (iv) preserving geologic realism.

A.3 DESTINY Process and Workflow

Fig. A.1 shows the general process of DESTINY. First, it runs the forward simulator and reads the output of the simulator. The forward simulator can be either a finite

difference or a streamline simulator. The current options for simulators are: ECLIPSE, VIP and FRONTSIM. For finite difference simulators, DESTINY utilizes the flux field to compute streamlines and time of flight. This information can then be used to visualize swept volumes and drainage volumes of existing wells during water flooding and also for gas reservoirs to locate potential locations for infill producers or injectors. The flux associated with streamlines can also be used to optimize injection and production rates of the wells to maximize flood performance. DESTINY is particularly useful for streamline-assisted history matching. Using DESTINY, we can visualize the sensitivities of production data with respect to reservoir properties. These sensitivities depict the region of the geologic model impacting the production data. Guided by these sensitivities, we can either manually update the geologic model to match the production data or use inverse modeling techniques for suggested updates to the model.

Figure A.1. General DESITNY Process

Fig. A.2 shows the overall work flow of streamline tracing and production history matching.

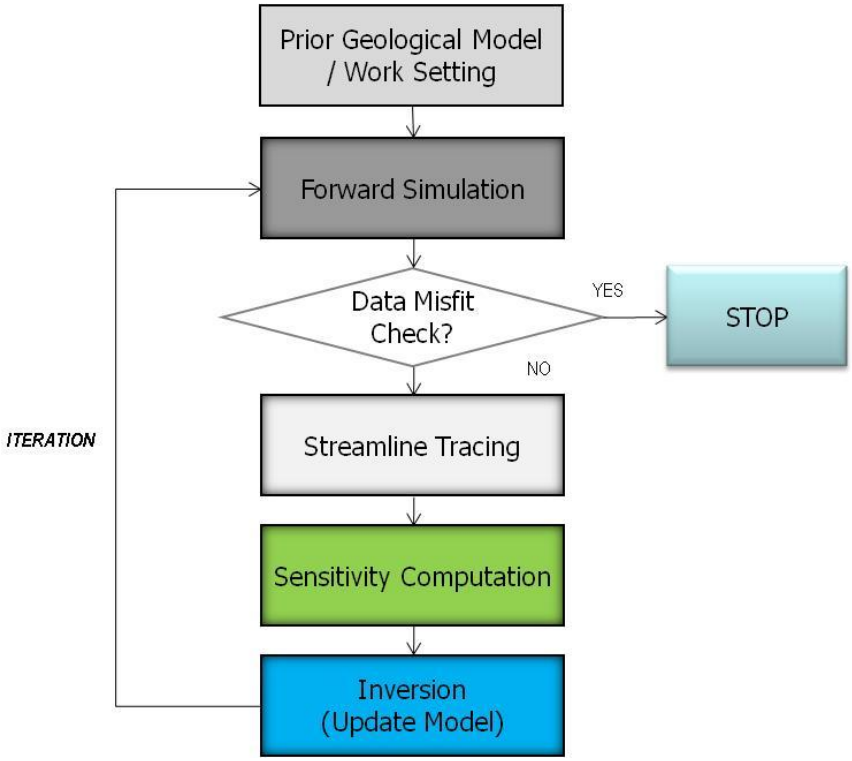

Figure A.2. Destiny Work Flow

The use of commercial simulators in DESTINY provides a great deal of flexibility in terms of grid geometry, well conditions and process simulations. However, because of the multiple options offered by commercial simulators and the resulting variations in setting up the simulation deck, instead of scanning the input deck made by the users, DESTINY scans output files from simulator to obtain the necessary data to trace streamlines and compute time of flight. It enables users to fully utilize flexibility for describing the flow simulation model and leads to robust streamline tracing without failure because of the fixed simulation output file format.

A.4 Installation and Getting Started

The installation package consists of two files named "setup.exe" and "DestinyModuleInstaller.msi" as shown in **Fig. A.3**. Users can easily install DESTINY plug-in for PETREL with just a few clicks on "setup.exe". For successful installation, users need installation authority on that machine and proper version of PETREL the as **Fig. A.3** right. We provide several versions of installation package, which depend on installed PETREL version in the user's machine. This is because the Ocean technology allows different version of plug-in for different versions of PETREL. Members can download the latest version of the plug-in from our MCERI website (http://www.pe.tamu.edu/mceri/) with member's log-in or can ask us to make a new plug-in for your particular version of PETREL.

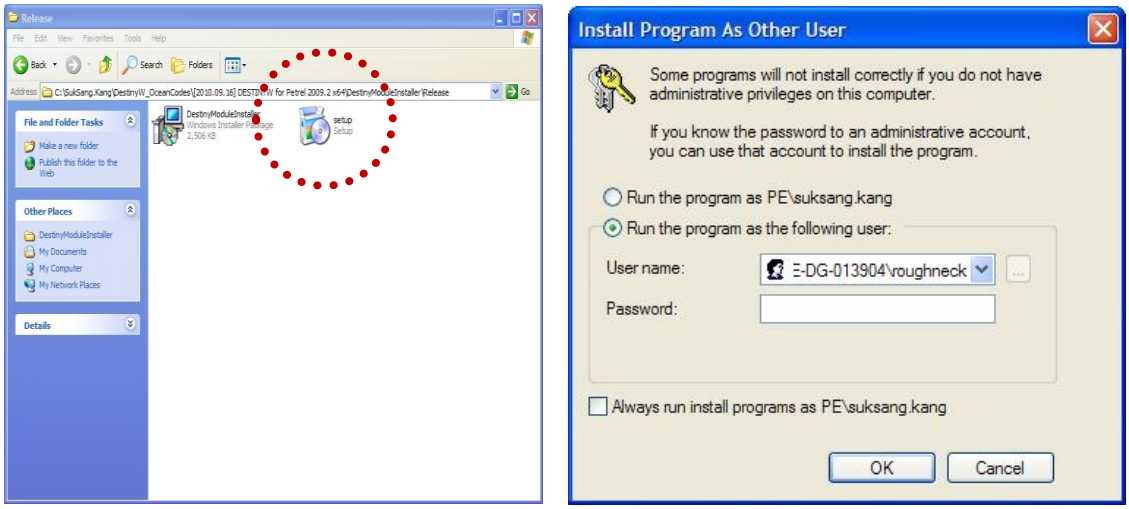

Figure A.3. Installation Package

This installed plug-in is shown at PETREL "Process window" as in **Fig. A.4** and users can start DESTINY workflow by double clicking this icon. Note that PETREL allows just one process window at a time. Sometimes, different process windows may manipulate one data set at the same time and this causes undesired results to occur.

If your model will take too long for history matching, we also provide the option to run DESTINY as an independent process. This allows you to release the PETREL license. This functionality enables the user to work on other jobs during DESTINY computation as a background process.

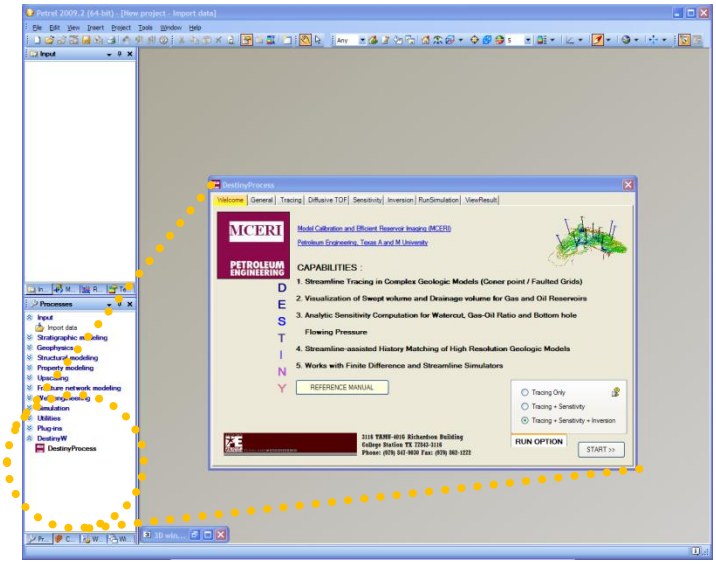

Figure A.4. DESTINY in PETREL Process

A.5 User Interface

DESTINY module consists of 8 different tab windows. After starting DESTINY, users can move each tab by clicking the tab name on the title or next/previous button at the bottom right. Also in each option, DESTINY provides default values to choose for user's convenience. If you are not sure about those options, default values will work in many cases.

A.5.1 Welcome

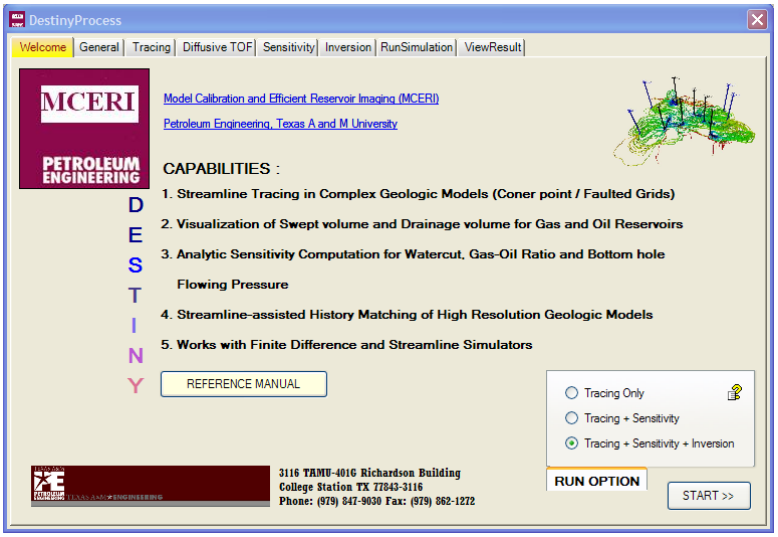

Users can open the manual by clicking “REFERENCE MANUAL” button. There are also quick pop-up help balloons if the user moves the mouse over a question mark beside each option box. Note that the description in this manual is mainly based on the ECLIPSE100 developed by Schlumberger although DESTINY has been interfaced with several commercial simulators such as FRONTSIM and VIP.

In the first tab, users can choose between 3 main work branches in “RUN OPTION”. If you choose “Tracing Only” option, then the “Sensitivity” and “Inversion” setting tabs disappear to keep the process simple and transparent. Alternatively, if you want to run “Tracing and Sensitivity”, then you will not see “Inversion” setting tab. Otherwise, users can change every setting for running DESTINY.

The main module of DESTINY is structured as in **Fig. A.5**. It consists of three main modules which are encapsulated with object oriented program language.

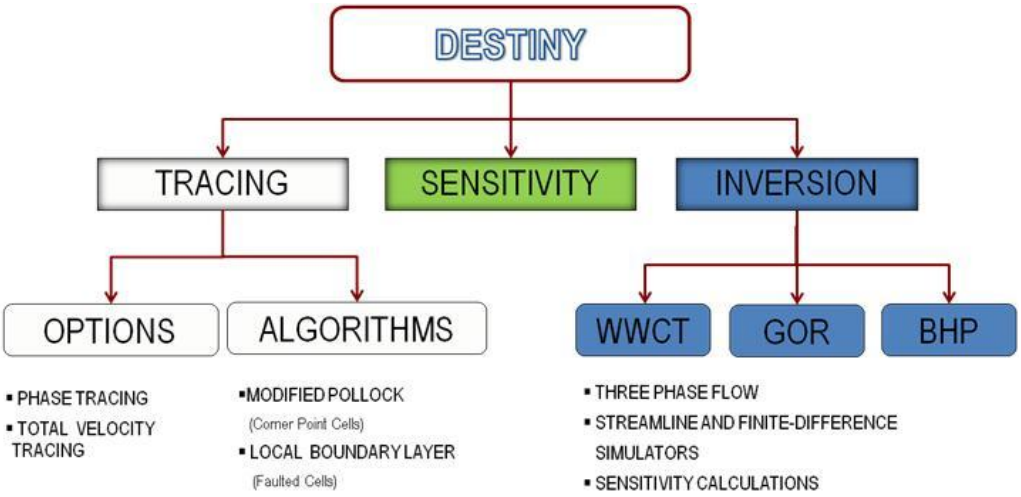

Figure A.5. DESTINY Main Module

A.5.2 General

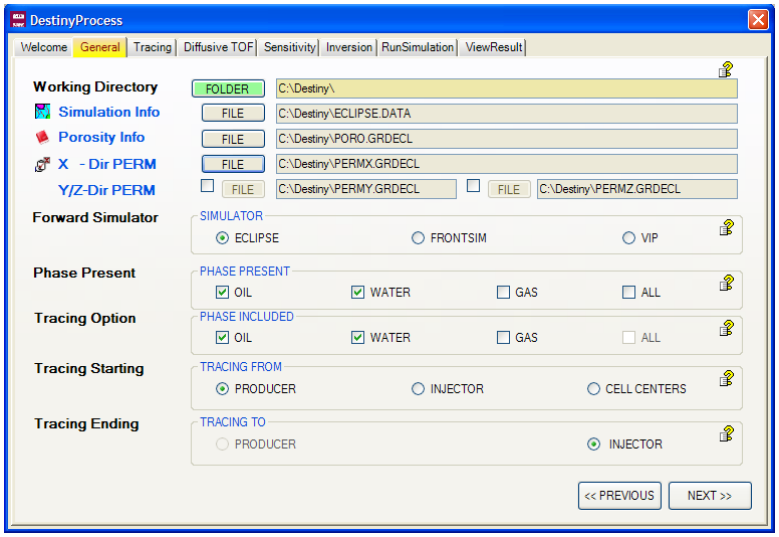

In the "General" setting tab, users need to define the basic simulation settings. As mentioned earlier, DESTINY reads simulation output and does its own computation. Therefore, we strongly recommend verifying that the forward simulation deck runs without error before the DESTINY computation.

Working Directory Defines the location of existing Forward simulation data deck. This requires information for 3 files. "Simulation Info: main simulation data file name", "Porosity Info: Porosity file name" and "PERM: Permeability file name". If users don't have these porosity and permeability with different files, users should make as separate files with "INCLUDE" keyword for iterative model update. Users also can consider Y and Z directional permeability to preserve the original relationship between these directions. It can be activated by checking the appropriate box.

Please, note that DESTINY requires a few keywords in the simulation deck to make sure that the simulation output contains all the information for DESTINY to carry out its computations. These are discussed later in the manual under 'TEST CASES' in Example 1.

Forward Simulator Defines which simulator will be used for tracing and inversion calculations. Current DESTINY is interfaced to work with *ECLIPSE /FRONTSIM/VIP*.

Phase Present Defines model phases for calculation. Users can check this simulation phase from forward simulator setting.

Tracing Option Defines phases to be traced for streamline calculation. These tracing phases should also be marked in "Phase Present".

Tracing Starting Defines the starting points of streamline tracing. Streamlines can start from the injector, producer or cell center based on the user's visualization or computation purpose.

Tracing Ending Define the ending points of streamline tracing. This button becomes active / inactive based on "Tracing Starting" setting. If the user traces from producers to injectors, the streamlines will depict the drained area. If the tracing is from injectors to producers, swept area will be visualized. Tracing from cell centers to producers / injector will visualize the relation between grid cells and wells and will be used to visualize the flood front location at different times.

A.5.3 Tracing

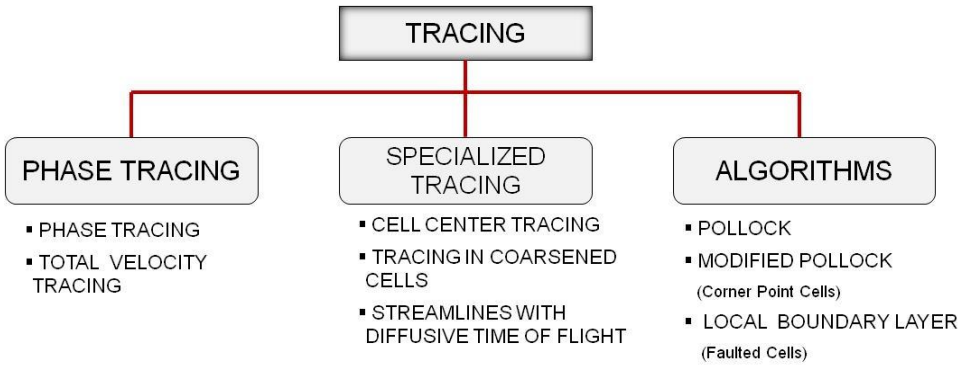

Figure A.6. Detail of Tracing Module

In "Tracing" tab, users can set up streamline tracing options. DESTINY uses flux information for streamline generation.

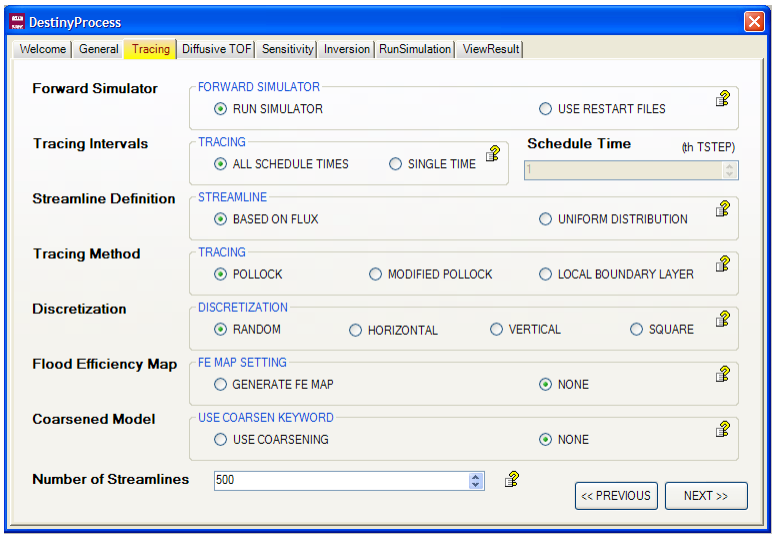

Forward Simulator Defines if we want to *RUN* the forward simulator or not. If *USE RESTART FILES* is selected, then there must be an available set of restart files for use by DESTINY.

Tracing Intervals Defines if tracing is to be done at *ALL* schedule dates or at a *SINGLE* date. If the user chooses "Single Time", the "**Schedule Time**" will be activated and the user can choose the time step for tracing.

Streamline definition Specifies if the originating streamlines per completion is defined based on flux or should be uniformly distributed.

Tracing Method Defines tracing schemes near faults and non-neighbor connections (NNC). This option provides a consistent representation for streamlines and velocities near faults and non-neighbor connections. ***(Reference paper: SPE-113425)***

Discretization Defines the location of the streamline starting point at the boundary of the starting grid block. Based on the user

choice, streamlines start from those points and then tracing continues.

Flood Efficiency Map Defines the use of Flood Efficiency MAP visualization. Users can generate intuitive connections between injection and production wells. DESTINY provides two methods for MAP, based on flux and time of flight. ***(Reference paper: SPE-132642)***

Coarsened Model Defines the use of COARSEN keyword in Finite Difference simulator. This option saves a lot of simulation time for large field model and gives good approximated result. DESTINY can trace streamline under coarsened geometry, calculate sensitivities and calibrate model under coarsened scale and finally update fine geological model.

Number of SLN Defines the total number of streamline for tracing. If you choose tracing from cell centers, this option will be ignored and try to generate from the entire grid block.

A.5.4 Diffusive TOF (Time of Flight)

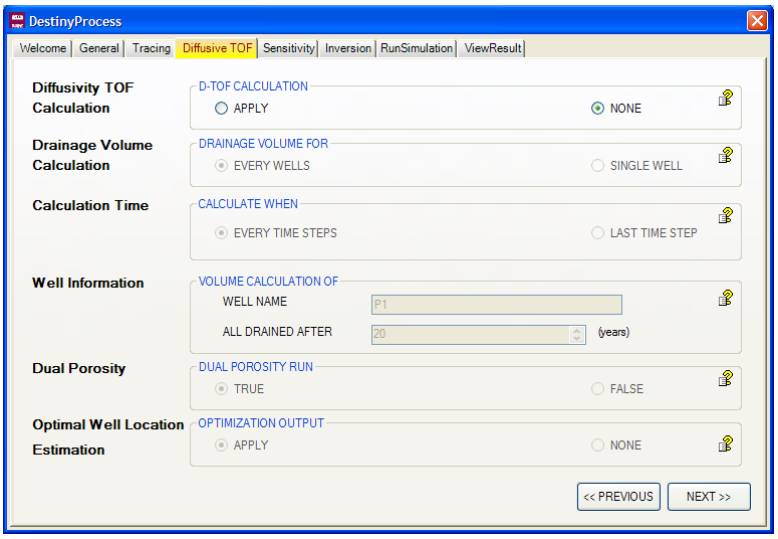

In "Diffusive TOF" tab, 'diffusive' time of flight can be used to define the drainage radius and infill well optimization in case of primary recovery or compressible flow such as gas reservoirs.

Diffusive TOF — Select if the user wants to trace using Diffusive Time of Flight. This option is activated if the user chooses "Tracing Only" in the "Welcome" tab. This diffusive time of flight will trace from cell center to producer as a default. ***(Reference paper: SPE-88802)***

Drainage Volume — Defines the well for which the user wants to calculate the drainage volume. If the user wants to calculate for a single well, then "Well Name" will be activated.

Calculation Time — Defines if the user wants to calculate the well drainage volume in every time step or at the last time step.

Well Information Defines the well name for single well drainage volume calculations and the threshold time to visualize the drainage volume (year).

Dual Porosity Can use dual porosity model which is common in unconventional oil/gas models. DESTINY can generate streamlines along the natural and/or hydraulic fracture networks.

Optimal well Can visualize the next infill well location. Users can easily visualize the most optimal regions for potential infill well placement.

A.5.5 Sensitivity

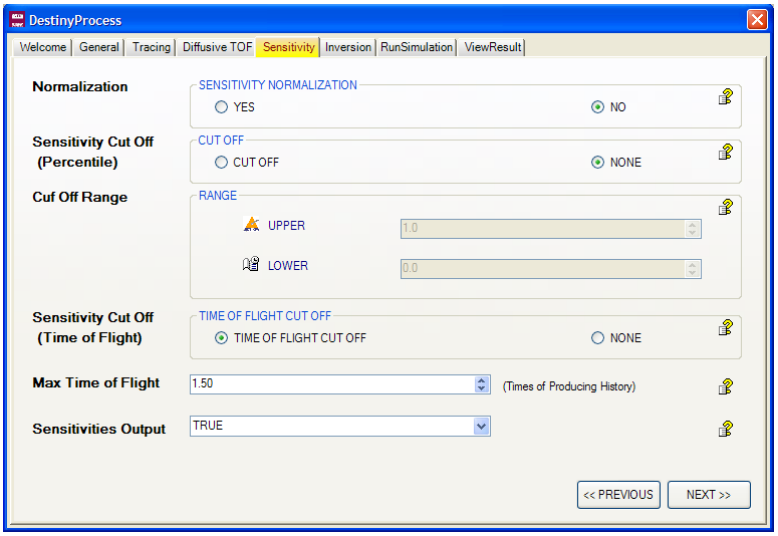

In "Sensitivity" tab, the user can define calculation options for grid block sensitivity computations. For mathematical background for sensitivity calculations, the user can

refer to chapter 10 of the SPE streamline textbook or papers. (Reference paper: SPE-99465)

Normalization	When checked, the sensitivities are normalized. The normalization facilitates convergence of the inversion algorithm when different data are involved.
Sensitivity Cut off	Defines a percentile based cutoff that will be applied to water cut sensitivities on a well-basis. It is used to reduce unusually high and low sensitivity values.
Cut off Range	Defines the upper and lower percentile for the water cut sensitivity cut-off.
Sensitivity cut off	Defines a time of flight based cut off that will be applied to water cut sensitivities on a well-basis. This is used to eliminate the sensitivities in stagnation regions which may cause poor inversion performance.
Maximum TOF	Defines the threshold of the time of flight for the water cut sensitivity cut-off. This Maximum Time of Flight cut off value is automatically calculated by multiplication of actual producing time period with input multiplier value.
Sensitivities Output	Define whether the user wants to generate sensitivity outputs or not. This sensitivity output can be used as reference data for manual history matching. Sensitivity files will be found at working folder with well name and no extension.

A.5.6 Inversion

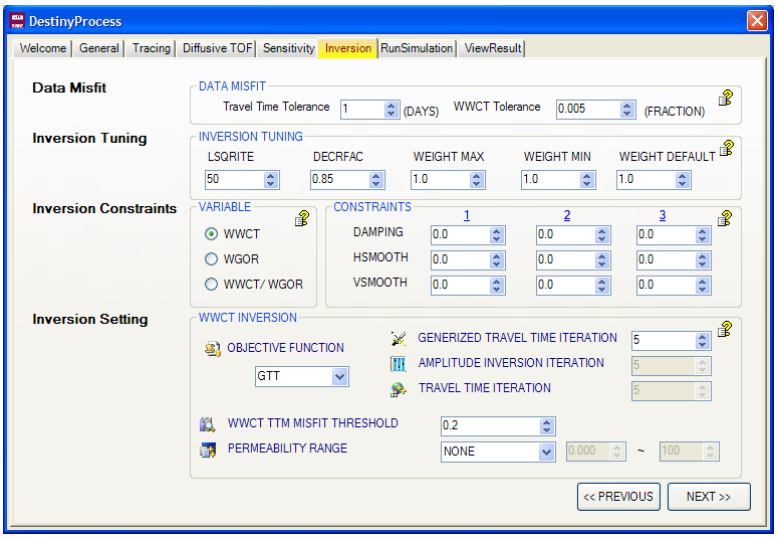

In the "Inversion" tab, users can change several options for improved inversion results. These settings also improve the calculation speed and help maintain geologic continuity and geologic realism during history matching.

Data Misfit — Travel Time Tolerance will define overall travel time misfit for all wells and water cut (WWCT) misfit tolerance defines the overall amplitude misfit defined for all wells. These values will be used to stop the inversion whenever the specified tolerance is satisfied.

Inversion Tuning

LSQRITE — Number of LSQR iterations for non-linear solution

DECRFAC Decrease factor to be applied to the norm and smoothing constraints through iterations.

Weight MAX Defines maximum weight given to permeability changes in the each iteration.

Weight MIN Defines minimum weight given to permeability changes in the each iteration.

Weight default Defines default weight given to permeability changes in the each iteration.

Inversion Constraints

Variables to integrate production well water cut (WWCT) and well gas oil ratio (WGOR). Users can also use both water-cut and gas oil ratios.

Constraints *DAMPING* Norm constraint. A large value of the norm constraint minimizes changes to the prior model. This will lead to poor quality data match. We can then gradually lower the norm constraint to get an acceptable compromise between changes to the prior model and quality of the data match.

HSMOOTH Horizontal smoothing constraint. A large value of this parameter leads to more continuity of the estimated property in the horizontal direction.

VSMOOTH Vertical smoothing constraint. A large value of this parameter will lead to more continuity of the estimated parameter in the vertical direction.

The inversion constraints on this version of DESTINY are only meant to update permeability. Only the first values on each line will be considered during the minimization of the objective function. The other values are reserved for further development when integrating additional reservoir parameters.

Inversion Setting

Objective functions that are targeted for minimization. DESTINY can utilize three options for choice of objective function (1) "Generalized Travel Time", (2) "Amplitude" and (3) "Travel Time". The travel time inversion mainly focuses on matching the breakthrough time whereas the generalized travel time matches both breakthrough and amplitude response (recommended). The amplitude match focuses on matching the production amplitude. If user changes the objective function option, corresponding iteration number box is activated and others are kept inactive.

Threshold This is the water cut value selected for travel time misfit evaluation. At every producing well, whenever the water cut reaches this value, both simulated and observed times will be extracted and used for misfit and sensitivity calculations.

Permeability range enables users to set updating permeability range during history match. By default, initial permeability field range is used.

A.5.7 Run Simulation

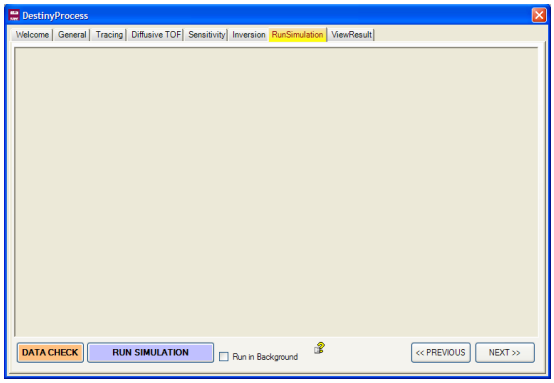

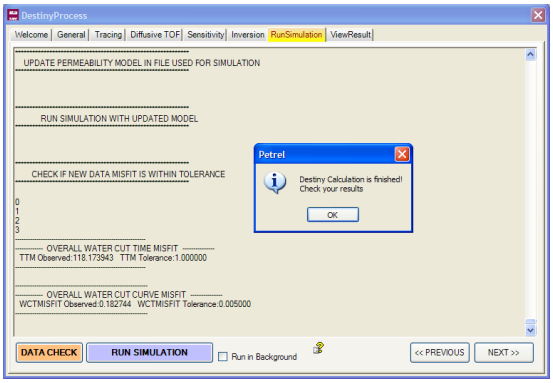

After finishing DESTINY setting, users can easily check the compatibility between DESTINY setting and Finite Difference Simulator. At the left bottom of this page has a "DATA CHECK" button, which provides this compatibility report and user can get advice for successful simulation.

Now, DESTINY is ready to run for streamline tracing, sensitivity calculation and model calibration depending on your choice. The DESTINY calculation simply starts by clicking "Run Simulation" button at the bottom. Users can see the run time comments at this tab and also can find it recorded in the file "DESTINY.PRT" under the working directory after the computation. Another choice is "Run in Background" for running DESTINY. If the user checks this box, DESTINY computations will run as an independent process and the PETREL license will not be occupied during the simulation run. The user then can close the DESTINY window and open again after the simulation is finished.

A.5.8 View Result

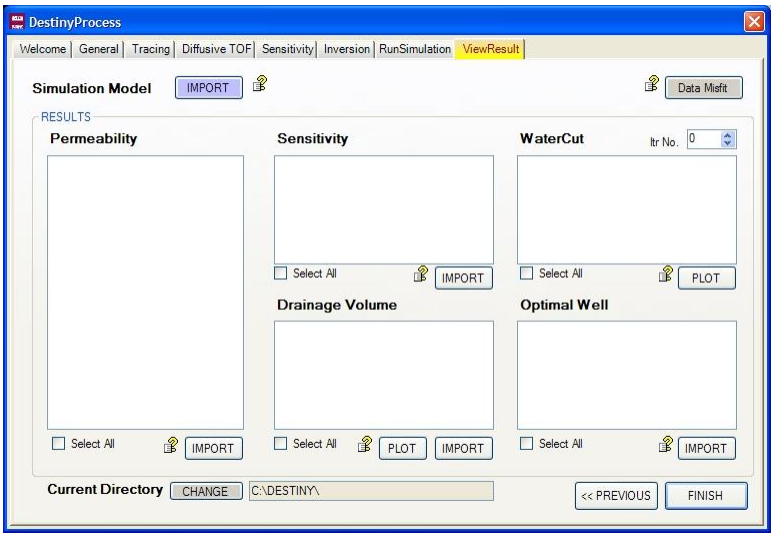

DESTINY provides a lot of outputs which are very useful to monitor the performance of both tracing and inversion. The streamline output is compatible with a wide range of commercial visualization packages. DESTINY generates streamline files which can be loaded directly to PETREL.

Users can import simulation model by clicking “Import” button. Users can see import file window and must designate main simulation file name. Imported model will be placed at PETREL model window. Users have to check current directory name as indicated in the lower part of tab.

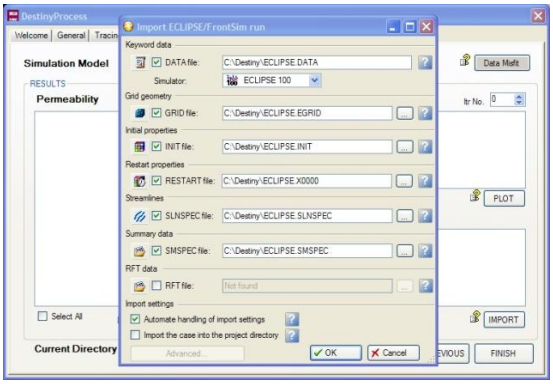

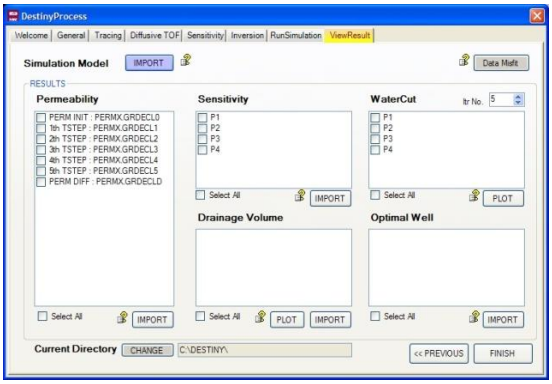

The streamline information is imported together with the model as default. Users can visualize various streamline properties as shown in **Fig. A.7** under the "Streamline folder".

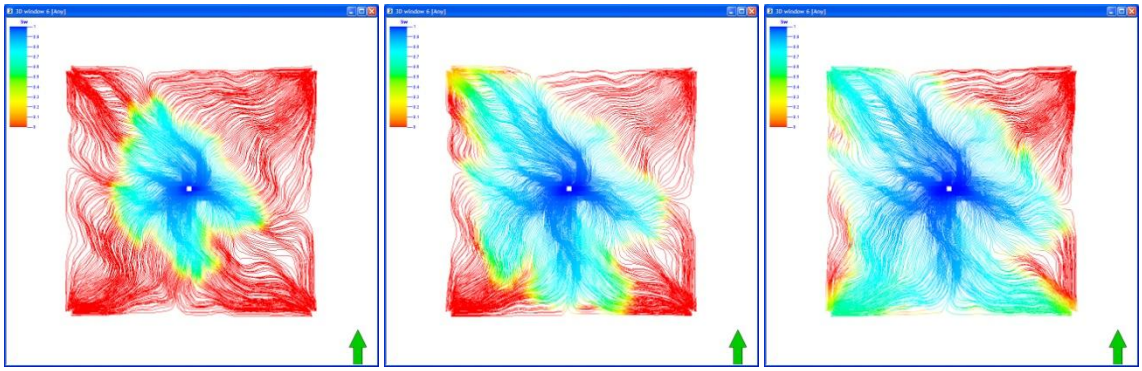

Figure A.7. Streamline (Water Saturation)

To visualize objective function change with iterations, click "Data Misfit" button. Users can see the change in data misfit with respect to iterations as in **Fig. 8** left. The water cut change in each well can be visualized by selecting "Check Well Name" and then clicking "Plot" button. Those graphs are placed under "Input" window and can be modified for color and line thickness for capture at the "Setting option".

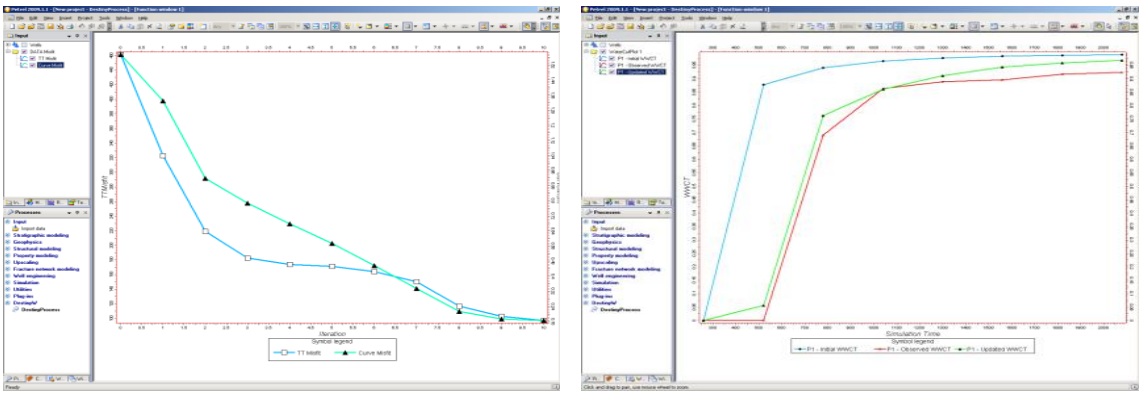

Figure A.8. Data Misfit (Objective Function) and Water Cut Response

To visualize the permeability field, users need to check the permeability file name and import each permeability field. The imported data set will be placed under “Properties”. Note that the permeability data will be in log scale as default. The user needs to turn off this log scale and color range for visualization of permeability difference.

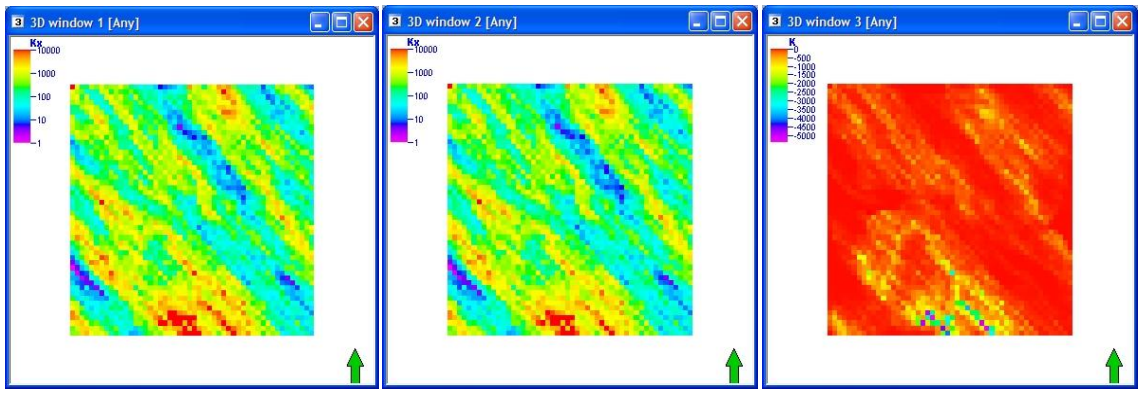

Figure A.9. Initial / Updated / Change of Permeability Field

To visualize the sensitivity of each well, check the well name in the “Sensitivity” list and then import that file from working folder. Note that sensitivity is equal or less than zero, so users also change data value range from “color table”.

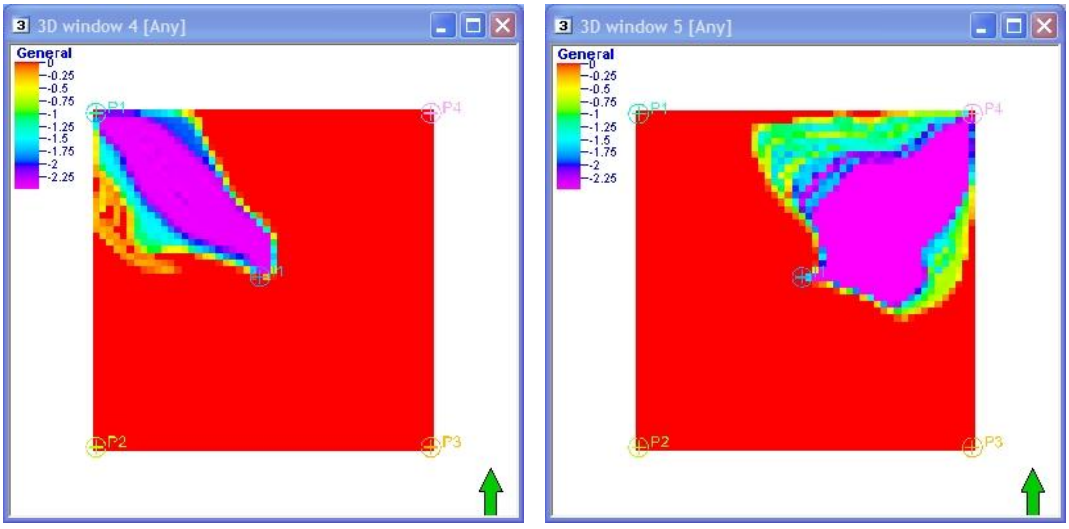

Figure A.10. Streamline Sensitivities of Well P1 and P4

"Drainage Volume" and "Optimal Well" window will be explained at "Diffusive Time of Flight" example.

The inversion output offers information to know the status of the history matching performance at any iteration. DESTINY has implemented functions to monitor the permeability changes during the inversion iterations. Descriptive statistics can be generated to monitor the behavior of statistical moments on a field-wide or on a facie-based basis. A brief summary of the DESTINY output files are presented for advanced users.

A.6 Streamline Output

- ***SLNXXX Files***: When the binary output is selected, DESTINY will generate *.*sln* files for every simulation time step. ECLIPSE users can use the restart files and the *.*sln* files to load the entire simulation workspace to PETREL.

A.7 Inversion Output

- ***Updated permeability files***: After running the first inversion iteration this file will be modified and to the end of the each iteration. The updated permeability will be written out as initial permeability file name (the updated files will have a suffix with the iteration number in which the permeability was updated).
- ***resinv.obj***: This file has the objective function behavior through all iterations. It has two columns representing the travel time and amplitude misfit defined at all producing wells included in the data integration
- ***resInv.wwctX***: It contains the simulated and observed production water cut for all wells included in the project. At the header of each well the travel time misfit will be written out. This file is generated at the end of the each iteration.
- ***dynamic.bin***: Binary files contain the production sensitivities. This file is used by LSQR to perform the objective function minimization.
- ***dynamic.ascii***: An ASCII file contains the production sensitivities. This file is provided for history matching applications where streamline-based sensitivities are used as complementary information.

A.8 Test Cases

We provide 7 different synthetic test cases for DESTINY testing. DESTINY reads the necessary information from the restart file of the forward simulator. Hence, it is important to include some specific keywords in the forward simulator setting for successful DESTINY running. We discuss these keywords in the following examples.

A.8.1 ECLIPSE Model Tracing and History Matching

(1) Eclipse Settings for Tracing

SECTION	EECLIPSE SETTING	REASON
SOLUTION	RPTSOL 'RESTART=2' /	Print output to the Restart files
	REMOVE “UNIFOUT” & “FMTOUT”	Destiny use separate binary file for each time step
SUMMARY	WOPR / WGPR / WWPR /	Read production rate base on tracing phase
SCHEDULE	RPTRST 'BASIC=2' FLOWS PRESSURE ALLPROPS/	Control restart file written data for computation

(2) Eclipse Settings for Inversion (History Matching)

SECTION	EECLIPSE SETTING	REASON
GRID	INCLUDE 'PORO.GRDECL' / INCLUDE 'PERMX.GRDECL' /	Use “INCLUDE” as separate porosity and permeability files for iterative parameter update
SOLUTION	RPTSOL 'RESTART=2' /	Print output to the Restart files
SUMMARY	WOPR / WGPR / WWPR /	Print out production rate base on tracing phase
	WWCT / WWCTH /	Print out water cut data and history for water cut match
	WOPT / WWPT / WGPT / WOPRH / WWPRH / WGPRH /	Print out oil, water and gas production rate
SCHEDULE	RPTRST 'BASIC=2' FLOWS PRESSURE ALLPROPS /	Control restart file written data for computation

	WCONHIST P1 1* LRAT 69.87 559.09 1* / P2 1* LRAT 168.62 460.34 1* / P3 1* LRAT 163.53 465.43 1* / P4 1* LRAT 628.97 0 1* / / WCONINJH I1 WATER 1* 2515.92 / /	Use "WCONHIST" for production target and "WCONINJH" for injection target instead of "WCONPROD" and "WCONINJ" for history match. Two control modes return similar but different results. DESTINY use history target.

Users can test this model by changing "RUN OPTION". All of default settings are based on this test model. All of Eclipse data file is located under "Eclipse_SET" folder.

A.8.2 FRONTSIM Model History Matching

FRONTSIM is a streamline simulator. The FRONTSIM generates its own streamline and DESTINY reads the streamlines for sensitivity calculation and inversion. Hence, DESTINY will not trace streamline for the FRONTSIM option. One nice feature is that FRONTSIM uses almost the same keywords as ECLIPSE and thus the same keyword restrictions apply as in previous "Eclipse setting for Inversion". This data set is located under "FrontSim_SET" folder.

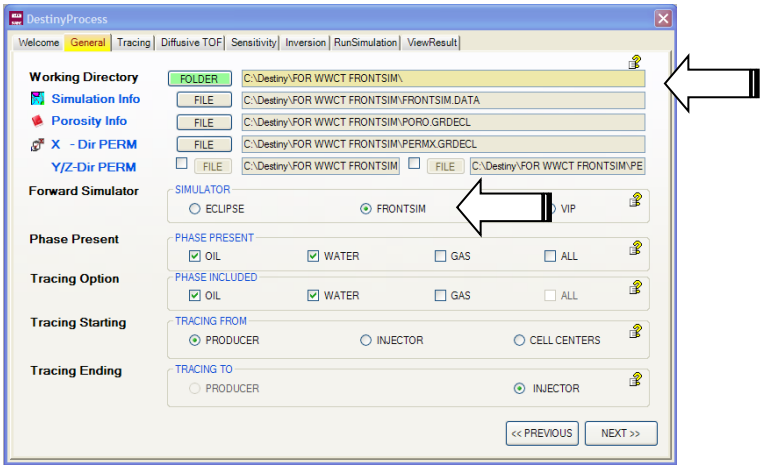

Figure A.11. Setting for FrontSim Test

A.8.3 GOR + Water cut History Matching

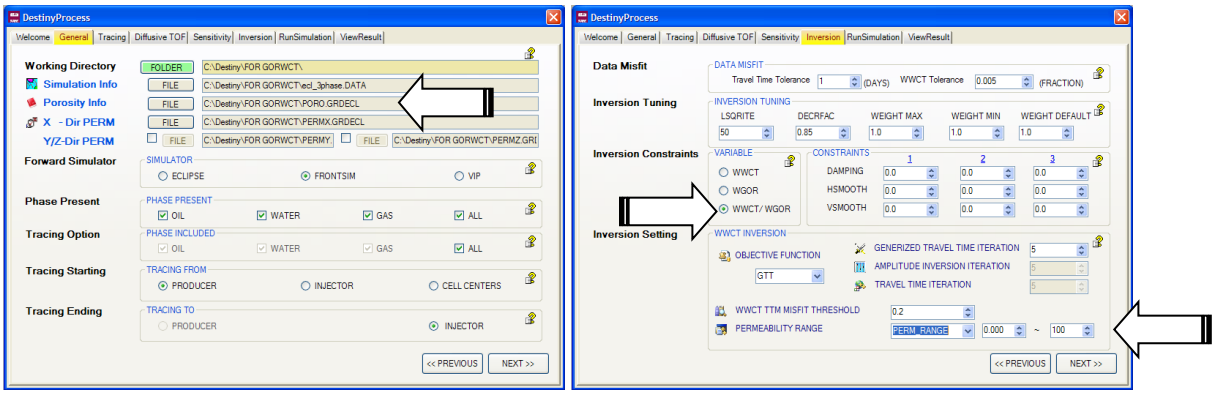

Figure A.12. Setting for GOR/WWCT Model

For testing this GOR/WCT model, users need to change some options in the inversion part. Also for speedy inversion, we recommend to turn on "Permeability Cut Off" as shown in **Fig. A.11**. This data set is located under "GORWCT_SET" folder.

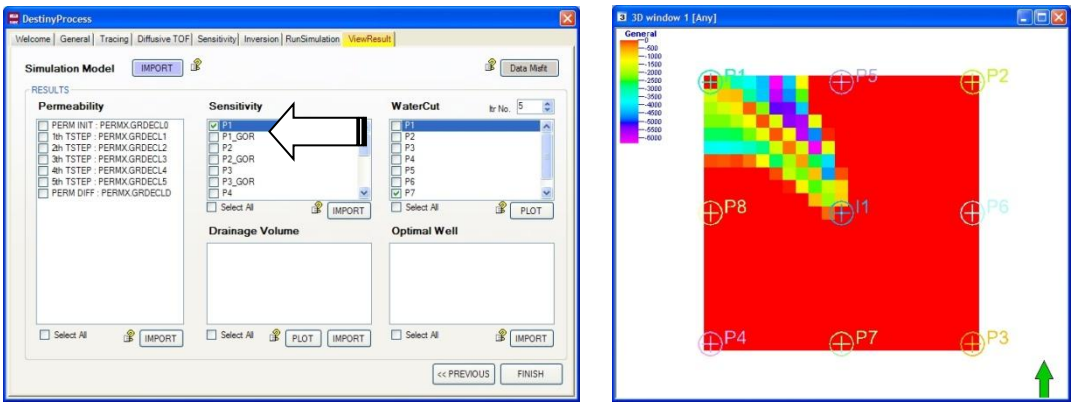

Figure A.13. Results of Simulation Run and Well (P1) GOR Sensitivity

After running DESTINY, simulation data files are imported as shown in **Fig. A.13**. In this model, you can also check GOR sensitivity as shown.

A.8.4 Reservoir Management Examples

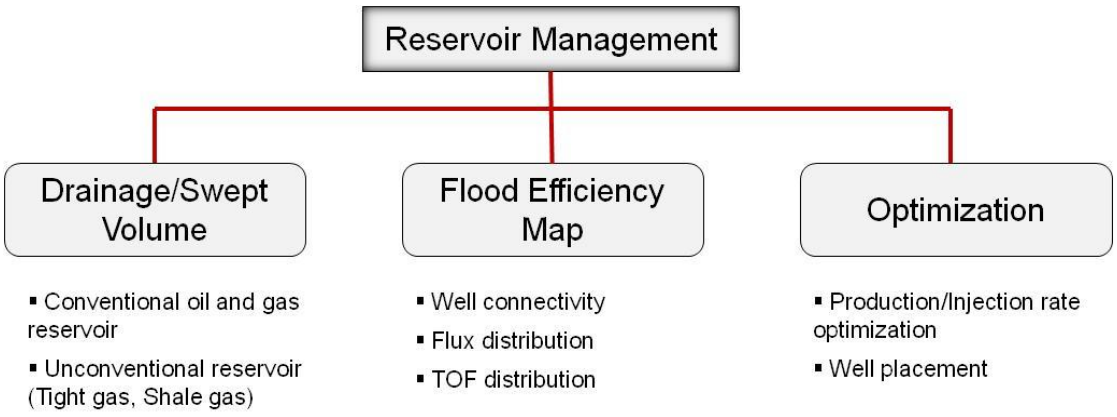

Figure A.14. New Reservoir Management Modules

We added new features for reservoir management purposes. **Fig. A.14** shows the details of the new algorithm and illustrated relevant examples below.

A.8.5 Diffusive Time of Flight

(1) Eclipse Settings for Tracing

SECTION	EECLIPSE SETTING	REASON
SOLUTION	RPTSOL 'RESTART=2' /	Print output to the Restart files
SUMMARY	WOPR / WGPR / WWPR / **WGPT**	Read production rate base on tracing phase
SCHEDULE	RPTRST 'BASIC=2' FLOWS PRESSURE ALLPROPS /	Control restart file written data for computation

This diffusive time of flight is a function of calculating drainage volumes in primary recovery/gas reservoirs and also for well placement optimization in gas reservoirs. So, WGPT keyword is necessary for this computation.

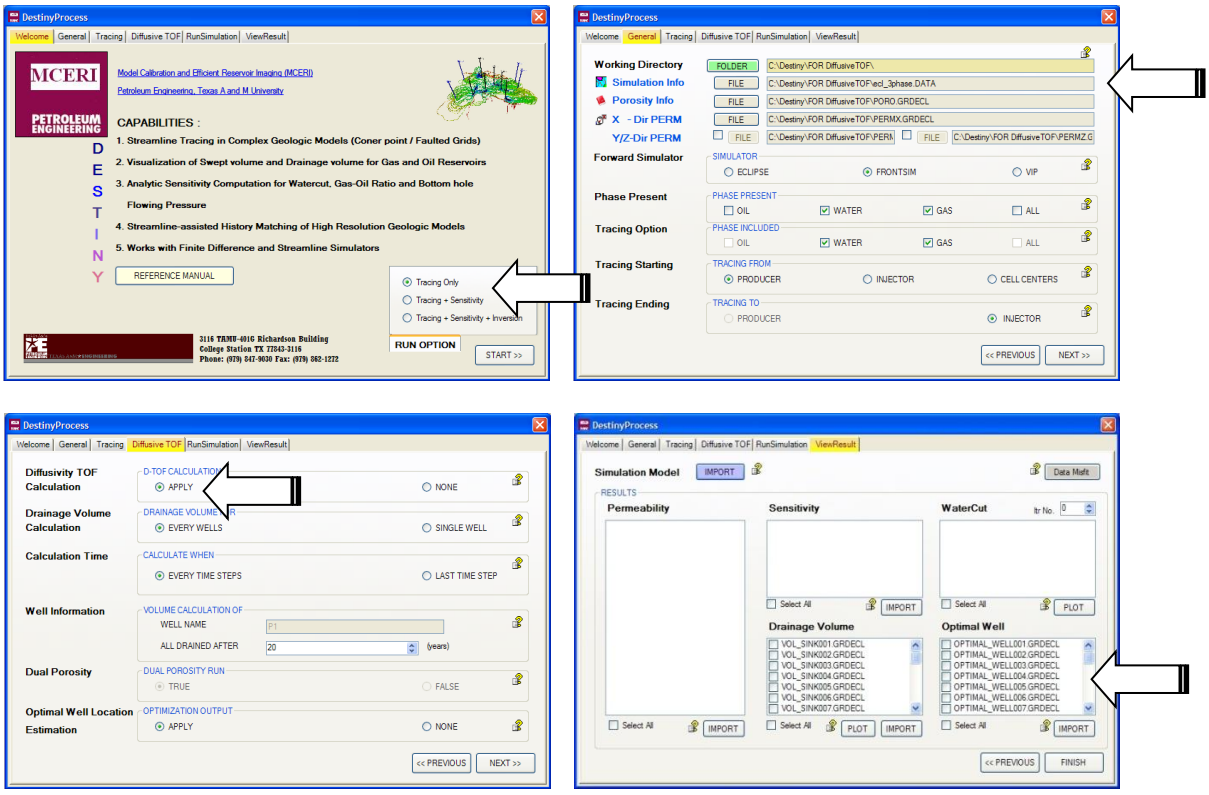

Figure A.15. Setting for Diffusive Time of Flight Calculation

For Diffusive time of flight test case, users need to choose “Tracing Only” at “Run Option” and then follow the next settings as above. There is no file information here under “Permeability”, “Sensitivity” and “WaterCut” which are related to model inversion.

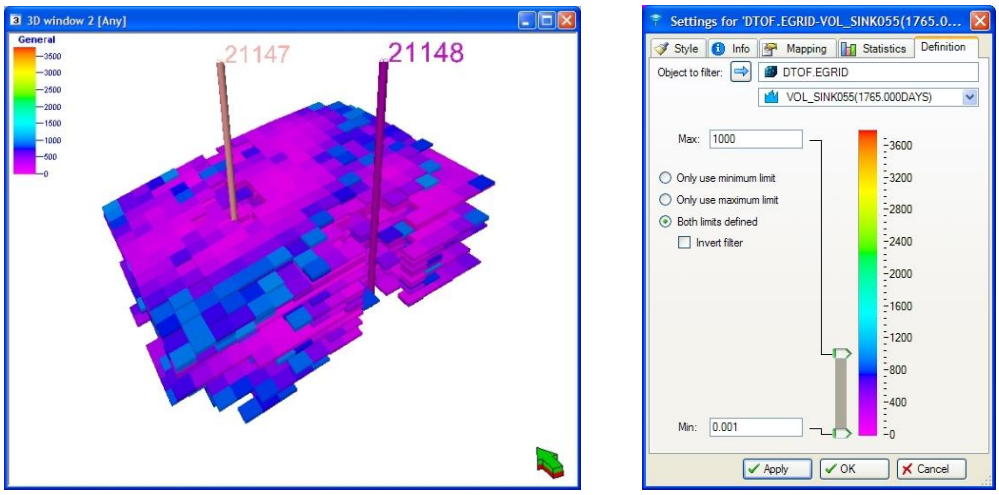

Figure A.16. Drainage Volume Mapping and PETREL filter

Users can visualize drainage volume of each well at certain time step with the embedded PETREL filter function as in **Fig. A.14**. This volume data can be imported by clicking "Import" button.

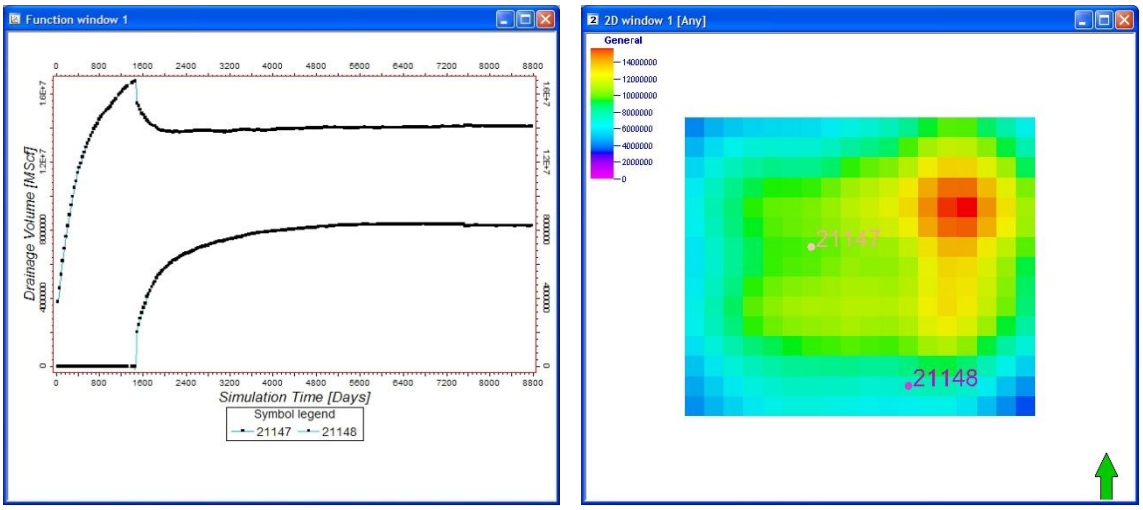

Figure A.17. Drainage Volume Plot of Each Well and Optimal Infill Well Location

Also, users can check the interaction between wells by clicking “PLOT” button at the bottom. The power of this functionality is suggesting next optimal infill well location without additional simulations as shown in **Fig. A.16**.

A.8.6 Flood Efficiency Map

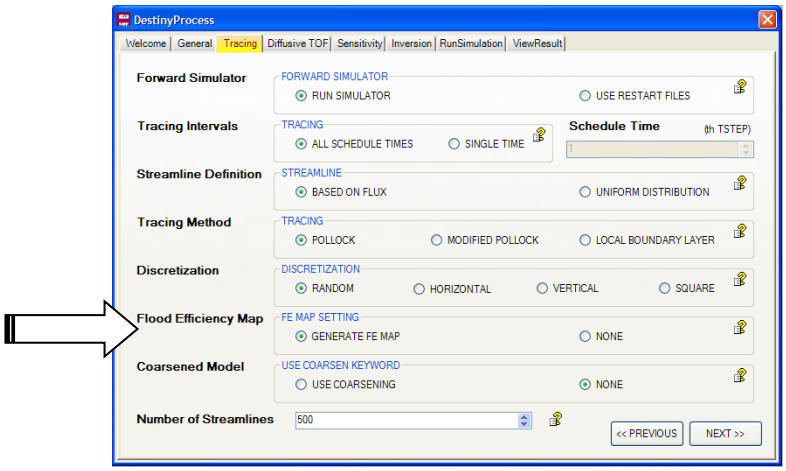

Figure A.18. Setting for Flood Efficiency Map

For tracing with Flood Efficiency maps, the user can choose for calculation “GENERATE FE MAP”. Users can try this function with “FEMAP_SET” for testing and Flood Efficiency map will be generated in addition to normal streamlines. Users can import this result in “Models ➔ Streamlines folder ➔ Import (on selection)”. This option will generate both “Time of Flight” and “Flux Distribution” Flood efficiency map in addition to normal streamlines. So, user can import both results as a sequential manner.

We display the key information related to flow patterns and reservoir sweep with the flood efficiency map. It includes a flux distribution map and an average TOF distribution map that enable us to optimize waterflood management. The streamlines connecting each injector-producer pair is depicted with a single representative streamline and the fastest streamline. The TOF distribution map displays the ‘average TOF’ between the

well pairs. The average TOF is calculated by a simple arithmetic average of time of flight associated with all the streamlines for each connection. The flux distribution map display volumetric flux between connecting wells computed by summing the fluxes carried by the streamlines. The flux distribution map is colored by the total flux connecting the wells while the color in TOF distribution map displays the average TOF. Thus, the flood efficiency map is a compact representation of the reservoir flow pattern and the flood front advancement.

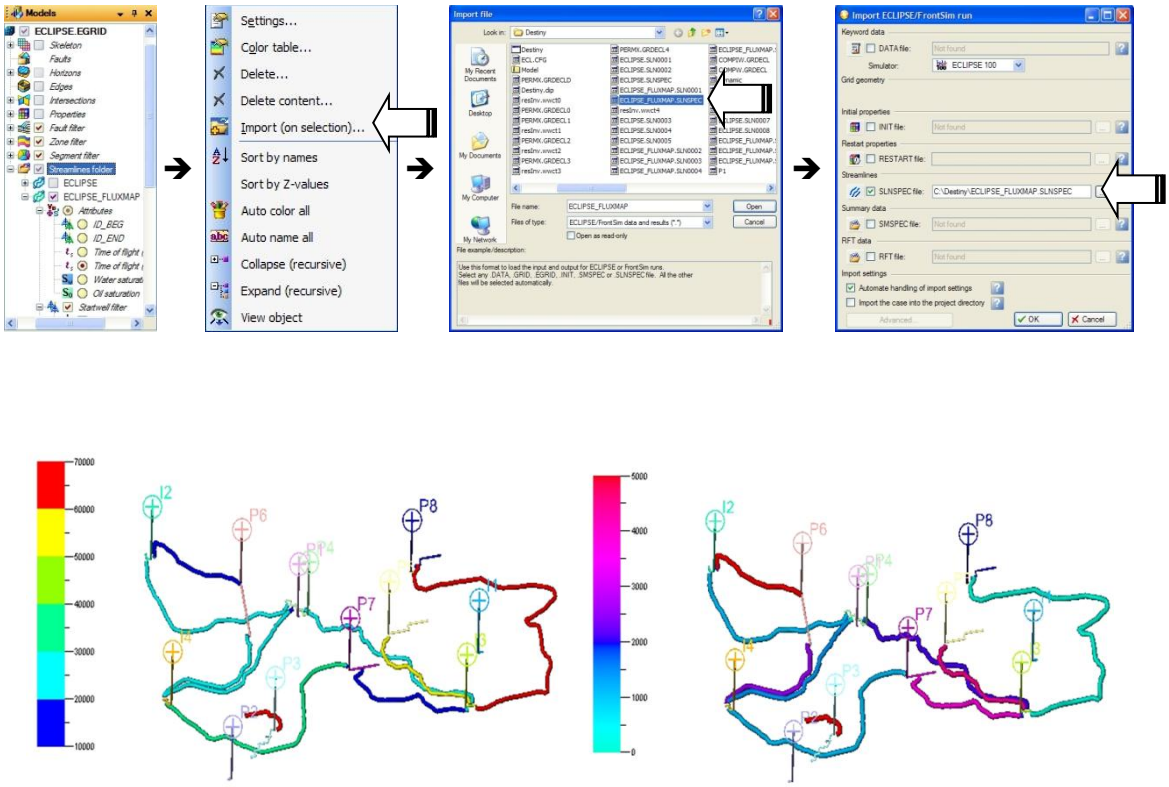

Figure A.19. (a) Time of Flight Distribution Map and (b) Flux Distribution Map

A.8.7 Tracing and Inversion in Coarsened Scale Model

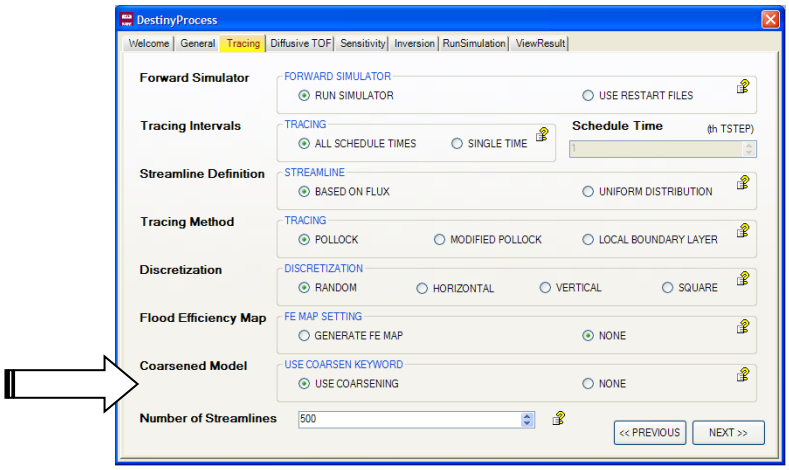

Figure A.20. Setting for Coarsened Model

For tracing and model calibration in Coarsened scaled model, we need to verify that Finite Simulation Model is using "COARSEN" keyword. Then we can trace streamline, calculate sensitivity and calibrate model under the coarsen scale. Finally, DESTINY updates the fine grid model as shown in **Fig. A.20**.

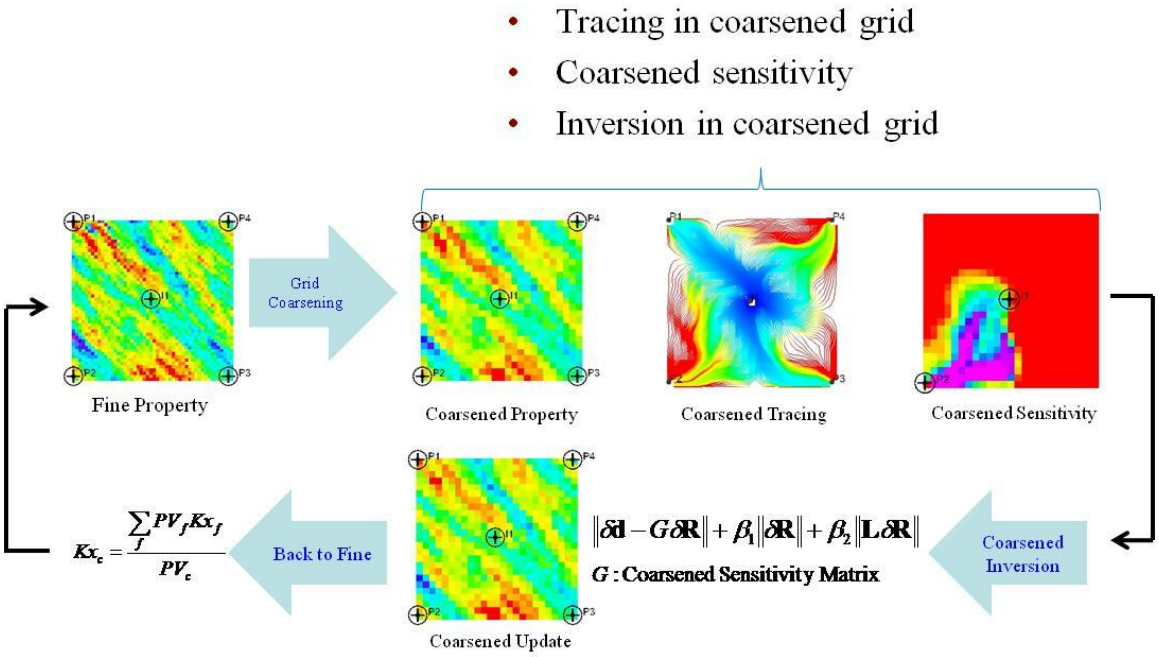

Figure A.21. Inversion Process in Coarsened Mode

APPENDIX B
A STECTRAL CLUSTERING PROGRAM WITH DESCRETE DATA

B.1 Introduction

The clustering or grouping algorithm is defined as “minimize the similarity between groups and maximize the similarity within a group”. A graph partitioning from spectral theory provides a fast way to decompose a domain for local spatial grouping. The spectral clustering has been used in various engineering fields; supercomputing, machine learning, logistics, internet shopping and social network service. Hence, the spectral clustering algorithm has profound theoretical background and is comparatively easy to implement in new area.

The graphic partitioning in the petroleum engineering provide a good decision gauge to segment regions while keeping prior model’s main heterogeneous and/or connectivity features; such as high or low permeable channel and barrier. For this purpose, we have introduced graphical partitioning for reservoir segmentation based on grid properties and/or connectivity on **Chapter 3** and 4. The heterogeneity and connectivity are closely related to flow dynamics of a reservoir.

To understand the Spectral Clustering features is important to get a good segmentation results for history matching. For the purpose, we prepare a simple data clustering program with MATLAB graphic user interface.

B.2 Program Overview

The background theories are explained more details on **Chapter 3**. The provided spectral clustering demonstration program consists of the following steps: (1) Randomly generate Gaussian distribution data clusters (2) Construct affinity Laplacian matrix based on input free parameters and correlation distance (3) Use graph partitioning techniques to create zonation and find groups. The graphic cut from the data location and heterogeneity, is not arbitrary and derived from optimization with graphic cutting metric.

Users can easily test the correlations of initial data distribution, free parameters, correlation distance and cutting algorithms, which are input parameters in the program.

B.3 The Graphic User Interface (GUI)

The GUI illustrated in **Fig. B.1** follows this procedure as (1) generate data set (2) construct affinity Laplacian and calculate the second eigenvector (3) apply cutting algorithm.

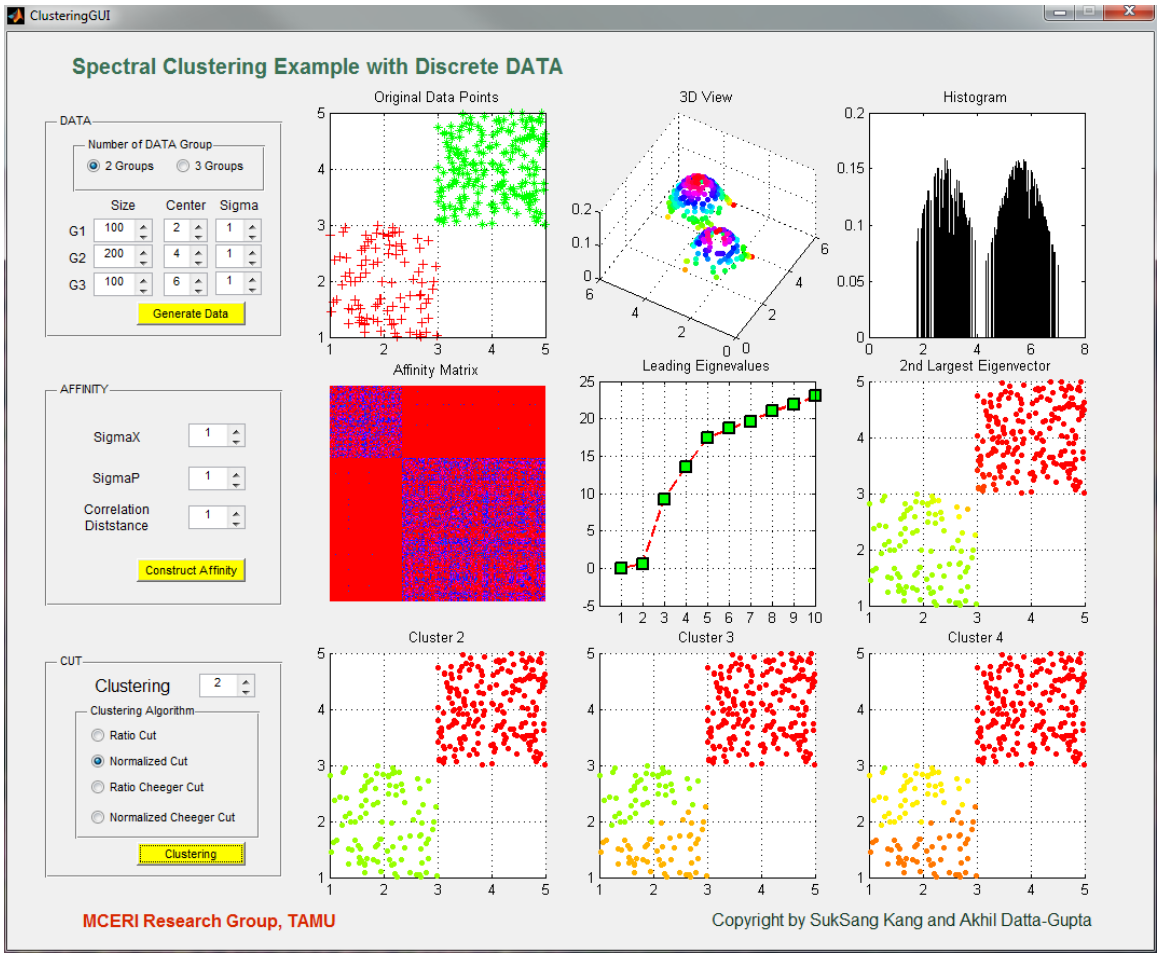

Figure B.1. Graphic User Interface for Clustering

- ***Generate Data Set*** We generate data sets based on input setting: number of group, size, center point and standard deviation. If user selects two groups, G3 row input data will be ignored. Randomly generated Gaussian data sets will be displayed with 2D, 3D plots and histogram.

- ***Construct Affinity Laplacian and Calculate Eigenvectors*** We construct affinity ($\boldsymbol{a_{ij}}$) Laplacian (L) from the data location ($\boldsymbol{x_i, x_i}$) and data value ($\boldsymbol{f_i, f_j}$) from below formulation, which is corresponding to grid block and heterogeneity of a reservoir model. Calculation details are explained at **Section 4.5.1**. From eigenvalue decomposition of the computed affinity matrix, the leading eigenvectors can be attained. The 'second' eigenvector, more exactly 'eigenvector corresponding to smallest positive eigenvalue', will be used for spectral clustering. The reason of using 'second' vector is described more details in **Section 4.5.3**. In the below formulation, three input parameters can be tried: SigmaX ($\boldsymbol{\sigma_I}$), SigmaP ($\boldsymbol{\sigma_P}$) and Correlation Distance (r).

$$a_{ij} = \exp\left(\frac{-\left\| f_i - f_j \right\|_2^2}{\sigma_P}\right) \times \begin{cases} \exp\left(\dfrac{-\left\| x_i - x_j \right\|_2^2}{\sigma_I}\right) & if \left\| x_i - x_j \right\|_2 < r \\ 0 & else \end{cases}$$

- ***Spectral Clustering with Cutting Algorithm*** In the demo program, we provide 4 different spectral clustering algorithms: '*Ratio Cut*', '*Normalized Cut*', '*Ratio Cheeger Cut*' and '*Normalized Cheeger Cut*'. Details of each algorithm are explained in **Section 3.5.2.**

B.4 Experiments

B.4.1 DATA: Equally Distributed Two Groups

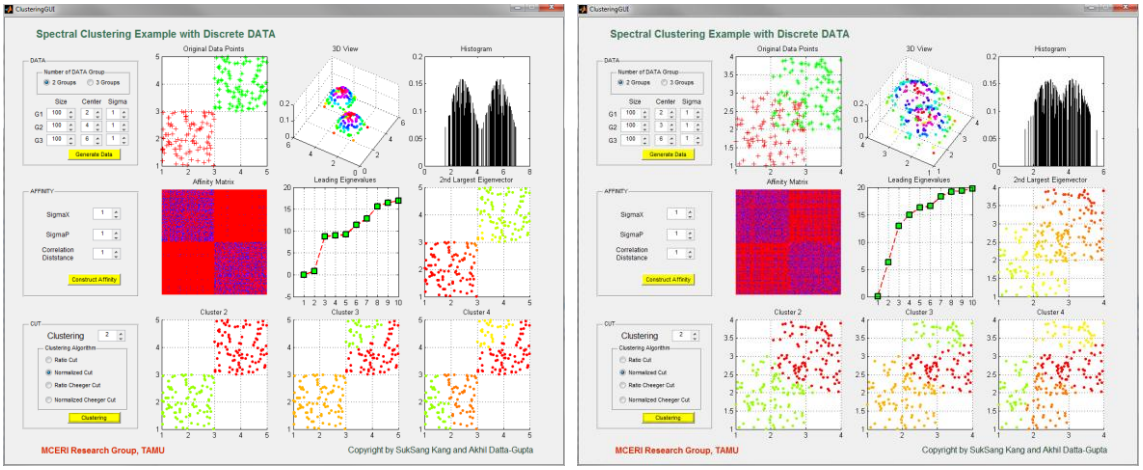

Figure B.2. DATA Part

Above two figures show the effect of distance between two groups. Second group moves to left by shifting center location at right figure. The computed affinity matrix has more connectivity and second eigenvalue has bigger value in right figure, as observed in well-connected graph *G*.

B.4.2 AFFINITY: Three Groups with Overlap

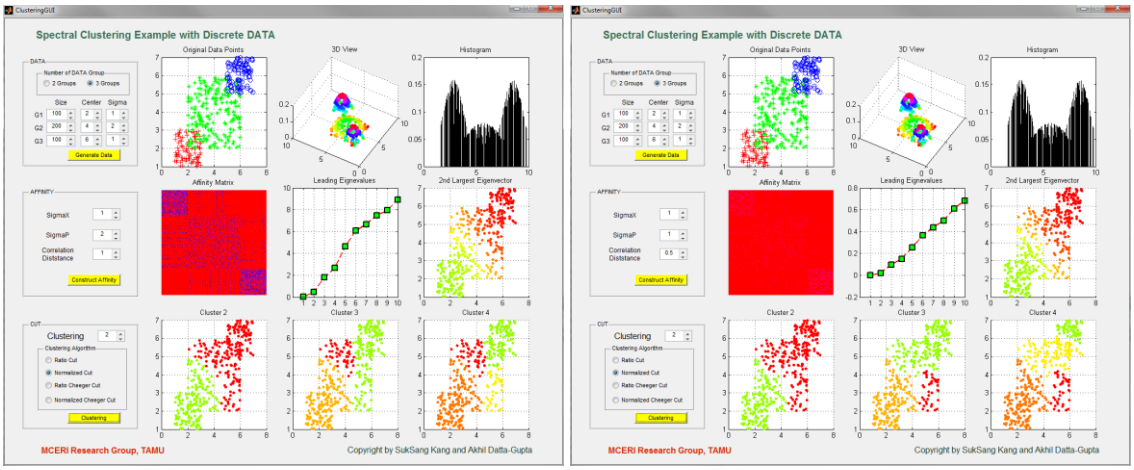

Figure B.3. AFFINITY Part

The correlation distance effect is tested above two figures. In the right of **Fig. B.3**, The affinity is sparse and the range of eigenvalue is small, which means 'not well-connected' graph. But the clustering results shows similar in both cases.

B.4.3 CUT: Three Groups Clustering Results

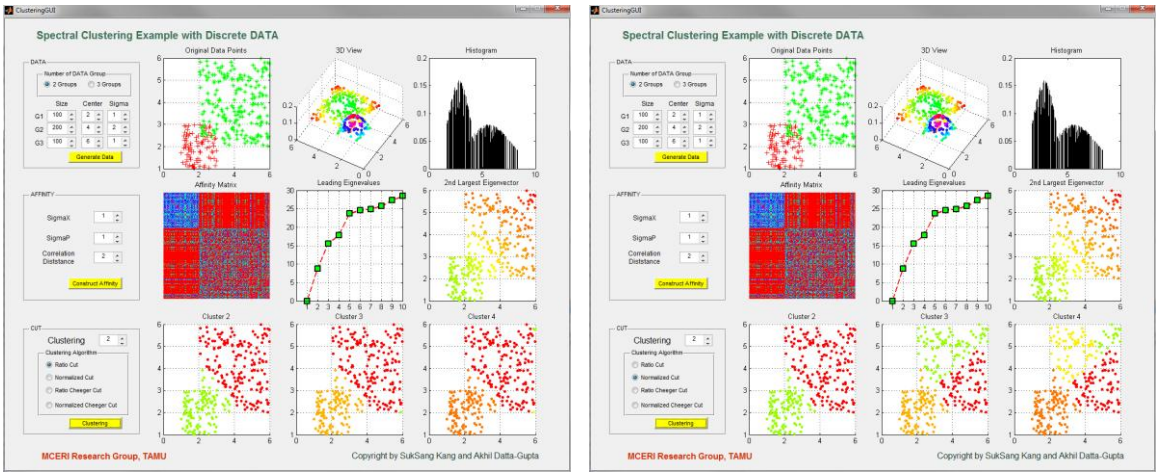

Ratio Cut **Normalized Cut**

Figure B.4. CUT Part

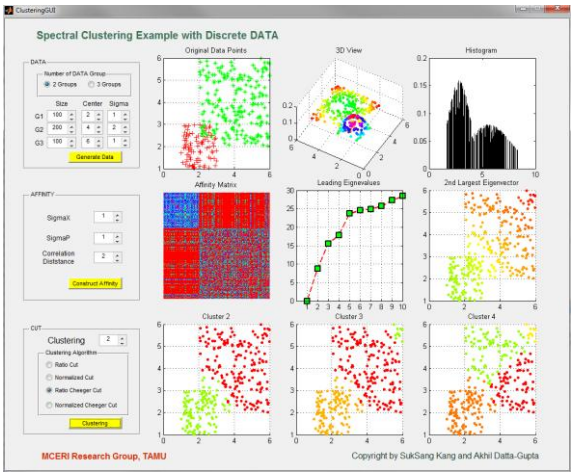

Ratio Cheeger Cut

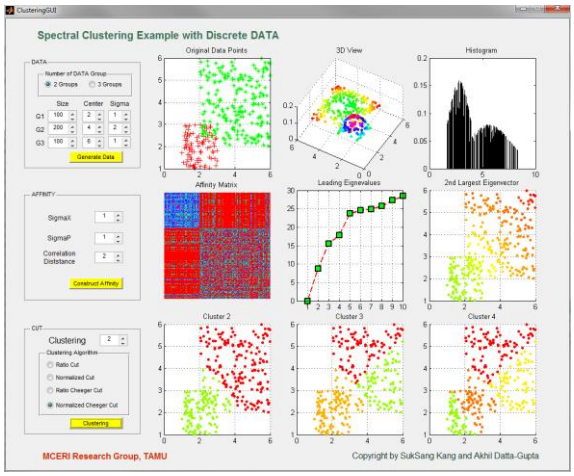

Normalized Cheeger Cut

Figure B.5. Continued

Different cutting algorithms return different grouping results in **Fig. B.4**. Normalized cut shows statistically stable cut, if we compare right two figures to left figures. Cheeger cut appears to be better than standard cuts. It is still complex problem to choose single best one, but 'Normalized Cheeger Cut' is a good starting point for segmentation as explained in **Chapter 3**.

B.5 Summary

The spectral clustering problem is basically a NP-hard and heuristic approach. As we explored, we can generate different cutting results from combinations of Affinity Laplacian and cutting algorithms. Even we have wider choice of free parameters and correlation distance, which are heavy impact factors for clustering. We inherited these spectral clustering properties in our model segmentation. Hence, we require some experiments and experience with different combination of cutting algorithms and constructing Affinity Laplacian. This simple clustering Program with handy Graphic User Interface provides intuitive experiments to users.